

ADVANCEMENTS IN INSTRUMENTATION FOR FOURIER  
TRANSFORM MICROWAVE SPECTROSCOPY

Christopher Thomas Dewberry, B.S.

Dissertation Prepared for the Degree of

DOCTOR OF PHILOSOPHY

UNIVERSITY OF NORTH TEXAS

August 2011

APPROVED:

Stephen A. Cooke, Major Professor  
Paul Marshall, Committee Member  
Guido Verbeck, Committee Member  
Michael Richmond, Committee Member  
William Acree, Chair of the Department of  
Chemistry  
James D. Meernik, Acting Dean of the  
Toulouse Graduate School

Dewberry, Christopher Thomas. *Advancements in Instrumentation for Fourier Transform Microwave Spectroscopy*. Doctor of Philosophy (Chemistry-Physical Chemistry), August 2011, 122 pp., 29 tables, 35 illustrations, references, 65 titles.

The efforts of my research have led to the successful construction of several instruments that have helped expand the field of microwave spectroscopy. The classic Balle-Flygare spectrometer has been modified to include two different sets of antenna to operate in the frequency ranges 6-18 GHz and 18-26 GHz, allowing it to function for a large range without having to break vacuum. This modified FTMW instrument houses two low noise amplifiers in the vacuum chamber to allow for the LNAs to be as close to the antenna as physically possible, improving sensitivity. A new innovative Balle-Flygare type spectrometer, the efficient low frequency FTMW, was conceived and built to operate at frequencies as low as 500 MHz through the use of highly curved mirrors. This is new for FTMW techniques that normally operate at 4 GHz or higher with only a few exceptions around 2 GHz. The chirped pulse FTMW spectrometer uses horn antennas to observe spectra that span 2 GHz versus the standard 1 MHz of a cavity technique. This instrument decreases the amount of time to obtain a large spectral region of relative correct intensity molecular transitions. A Nd:YAG laser ablation apparatus was attached to the classic Balle-Flygare and chirped pulse FTMW spectrometers. This allowed the study of heavy metal containing compounds. The instruments I constructed and the techniques I used have allowed the discovery of further insights into molecular chemistry. I have seen the effects of fluorinating an alkyl halide by determining the geometry of the carbon backbone of trans-1-iodoperfluoropropane and observing a  $\Delta J = 3$  forbidden transition caused by a strong quadrupole coupling constant on this heavy molecule. The quadrupole coupling tensors of butyronitrile, a molecule observed in space, have been improved. The nuclear quadrupole

coupling tensor of difluoroiodomethane was added to a list of variably fluorinated methyl halides upholding a trend for the magnitude of  $\chi_{zz}$ . The study of SrS led to the determination of the Born-Oppenheimer breakdown terms and improving the precision of the SrS internuclear distance. I have also conducted the first pure rotational spectroscopic investigation on an actinide containing molecule, ThO.

Copyright 2011

By

Christopher Thomas Dewberry

## ACKNOWLEDGEMENTS

I would like to start by thanking the Department of Chemistry at the University of North Texas and the National Science Foundation (NSF) for financial support during my time as a graduate student. Also, funding for the equipment that I used for my research could not have been achieved without the support of the University of North Texas in its provision of startup funds for Dr. Steve Cooke and the National Science Foundation's Research Grant. I must also mention Dr. Jens Grabow, for letting our lab use his spectroscopy software and helping with trouble shooting during the lab's initial setup. Special thanks to Dr. Mike Gerry for donating a vacuum chamber and various other supplies to our lab. I would also like to thank Dr. Steve Cooke for all his guidance and mentoring as he patiently encouraged me and fostered ideas for my research.

## TABLE OF CONTENTS

ACKNOWLEDGEMENTS .....	iii
INTRODUCTION .....	1
History.....	1
Premise.....	1
Purpose.....	2
INSTRUMENTATION.....	4
Cavity Instrument .....	4
Balle-Flygare Type Spectrometers	
The Fabry-Pérot Cavity	
Pulsed Supersonic Nozzle	
Pulsed Microwave Fourier Transform Method	
Wave Theory	
Modes	
Electromagnetic Field Regions	
Q Factor	
Classic Balle-Flygare FTMW Spectrometer	
Resonator	
Vacuum System	
Circuit	
Efficient Low Frequency FTMW Spectrometer	
Interest	
Past Work	
Premise	
Resonator	
Vacuum System	
Circuit	
Broadband Instrument.....	33
Chirped Pulse FTMW Spectrometer	
Chirped Pulse Region	
Vacuum System	
Circuit	
Laser Ablation .....	38
Nd:YAG Laser	
Walker-Gerry Nozzle	
Rod Building	
CASE STUDIES.....	41
Theory .....	41
Rotational Constants	
Geometry	

Observed Rotational Transitions	
Centrifugal Distortion	
Nuclear Quadrupole Coupling	
Spectral Analysis .....	46
Simple Patterns	
Changes To The Simple Pattern	
Parameters	
Experimental Practice .....	52
Basic Outline of Experiment	
Preparation of Gas	
Observing Rotational Transitions	
Fitting	
Trans-1-Iodoperfluoropropane <sup>22</sup> .....	55
Introduction	
Experimental Method	
Results	
Discussion	
Conclusion	
n-Butyronitrile <sup>18</sup> .....	79
Introduction	
Experimental Method	
Results	
Discussion	
Conclusion	
Difluoroiodomethane <sup>35</sup> .....	90
Introduction	
Experimental Method	
Results	
Discussion	
Conclusion	
Strontium Sulfide <sup>47</sup> .....	100
Introduction	
Experimental Method	
Results	
Discussion	
Conclusion	
Thorium Oxide <sup>57</sup> .....	107
Introduction	
Experimental Method	
Results	
Discussion	
Conclusion	

CURRENT WORK.....	112
High Frequency System .....	112
Microwave Region	
Horns	
Nozzle	
Vacuum System	
Circuit	
80-120 GHz	
Microwave Synthesizer	
Oscilloscope	
Results	
Carbonyl Sulfide	
CONCLUSION.....	116
The Classic Balle-Flygare FTMW Spectrometer .....	116
ELF-FTMW Spectrometer .....	116
Chirped Pulse FTMW Spectrometer.....	117
Laser Ablation Apparatus.....	117
Molecules .....	117
WORKS CITED .....	118



## INTRODUCTION

### History

Typically, microwave spectroscopy is synonymous with rotational spectroscopy. However, the first electromagnetic spectrum observed in the microwave region was in fact an inversion in 1933. Claud Cleeton and Neal Williams were able to observe the inversion of  $\text{NH}_3$  at approximately 3000 GHz. Not much was done with microwave spectroscopy until after advancements in microwave technology came about during World War II. Researchers such as Walter Gordy and Bob Curl began making microwave spectroscopy known in the scientific community by determining the structures of molecules observed within a waveguide. Then in 1981, Terry Balle and Willis Flygare used Charles Fabry and Alfred Pérot's cavity design of the Fabry-Pérot interferometer as an essential part in the Balle-Flygare spectrometer to replace room length waveguide experiments with a compact cavity experiment. The Balle Flygare spectrometer is still considered the standard in microwave spectroscopy. Laser ablation of solids to be mixed with gases was introduced in 1989 by Richard Suenram. The most recent substantial innovation in microwave spectroscopy is broadband microwave spectroscopy which was realized by Brooks Pate. Broadband microwave spectroscopy is used to look at large regions of spectra at one time, greatly improving the speed of acquiring new rotational transitions.<sup>1-5</sup>

### Premise

The current methods of microwave spectroscopy discussed in this work proceed on the premise of assuming a Hamiltonian and using rotational transitions that have been observed to solve for the constants within the assumed Hamiltonian. Through studying multiple isotopes, an atom's relative geometry can be deduced. To observe a pure rotational transition, a molecule must have a dipole moment and, typically, adhere to the selection rules shown on Table 1.<sup>6,7</sup>

Table 1. Selection Rules For Microwave Spectroscopy For Different Types of Molecules

Linear Molecules	Example
$(I_a = 0 \ I_b = I_c)$ $\Delta J = 1$	$1 \leftarrow 0$ $\Delta J = +1$
Symmetric Top Molecules	Example
$(I_a = I_b < I_c \text{ or } I_a < I_b = I_c)$ $\Delta J = 0, \pm 1$ Parity: $+ \leftrightarrow -$ $\Delta K = 0, \pm 1$	$5_4 \leftarrow 5_5$ $\Delta J = 0 \ \Delta K = -1$
Asymmetric Top Molecules	Example
$(I_a < I_b < I_c)$ $\Delta J = 0, \pm 1$ Parity: a-type transition: $++ \leftrightarrow +-, -+ \leftrightarrow --$ b-type transition: $++ \leftrightarrow --, +- \leftrightarrow -+$ c-type transition: $++ \leftrightarrow -+, +- \leftrightarrow --$	a-type $3_{22} \leftarrow 4_{23}$ $\Delta J = -1 \ k_{-1}, k_{+1} = \text{even, even} \leftarrow \text{even, odd}$ b-type $3_{22} \leftarrow 4_{11}$ $\Delta J = -1 \ k_{-1}, k_{+1} = \text{even, even} \leftarrow \text{odd, odd}$ c-type $3_{22} \leftarrow 4_{12}$ $\Delta J = -1 \ k_{-1}, k_{+1} = \text{even, even} \leftarrow \text{odd, even}$

$I_a$ ,  $I_b$ , and  $I_c$  are the principal moments of inertia in the a axis, b axis, and c axis respectively. J is the rotational quantum number corresponding to the total angular momentum and K is the rotational quantum number corresponding to the component of J in the direction of the figure axis.  $k_{-1}$  and  $k_{+1}$  are the label for the K quantum number in an asymmetric top for the prolate and oblate limit respectively. “+” represents an “even” integer for K,  $k_{-1}$ , or  $k_{+1}$ . “-” represents an “odd” integer for K,  $k_{-1}$ , or  $k_{+1}$ .

In brief, rotational transitions are observed by pulsing molecules into a cavity; introducing microwaves at a transitional frequency causing the molecules to coherently gyrate; ending the manmade signal; and then observing the field induced by the rotating dipoles of the molecules as decoherence occurs.

### Purpose

The efforts of my research have been to expand the capabilities of microwave spectroscopy. I have done this by building and modifying instruments to allow for increased sensitivity, better resolution, expanded frequency range of operation, improved data acquisition speeds, and alternate types of molecular sampling. Four instruments have been built to address

specific areas of improvement. The functionality of these improvements is presented through studies on selected molecules.

## INSTRUMENTATION

I have built and maintained several instruments during my research at University of North Texas. The instruments discussed convert the time-diminishing, rotational transition data by Fourier transformation into a frequency output, also known as Fourier transform microwave (FTMW) spectroscopy. Two instruments use the advantages that come from cavity techniques of increased resolution. One of these cavity instruments is a classic Balle-Flygare instrument that was designed to have superior resolution and sensitivity compared to other microwave spectrometers. The second cavity instrument, the efficient low frequency FTMW, was my primary research project where a new type of FTMW spectrometer was constructed. This novel instrument can operate at a much lower frequency region than typical FTMW spectrometers due to its unique mirror geometry. I was an integral part in the construction of a broadband instrument which offers the ability to search large regions of spectra at one time using chirped pulses. Also, I have assembled and aligned a laser ablation apparatus that allows heavy metal-containing compounds to be studied with both the classic Balle-Flygare and chirped pulse FTMW spectrometers.

### Cavity Instrument

Cavities work by tuning mirrors to create a standing wave for a given frequency. This allows for the electromagnetic field of the tuned frequency to reflect between the mirrors several hundred times before dissipating. The additional path length from the reflections serves to greatly improve the sensitivity and resolution of the instrument when compared to non-cavity techniques. However, the set distance between the mirrors causes destructive interference for the neighboring frequencies which makes the cavity a band pass filter.

## Balle-Flygare Type Spectrometers

The Balle-Flygare setup consists of a Fabry-Pérot cavity, a pulsed supersonic nozzle, and the use of a pulsed microwave Fourier transform method.<sup>4</sup>

### *The Fabry-Pérot Cavity*

The Fabry-Pérot interferometer has been used to increase sensitivity in spectrometers. A Fabry-Pérot interferometer consists of two reflective surfaces, or mirrors, that are in alignment to reflect electromagnetic waves back and forth. Typically, the mirrors are 600 mm in diameter and 1000 mm in its radius of curvature with a separation of 900 mm apart. This type of spectrometer, which uses resonance techniques over absorption techniques, can greatly increase sensitivity. By creating a standing wave within the Fabry-Pérot interferometer, the cavity serves as a band pass filter by only causing constructive interference for a small range of frequencies, generally a few MHz, and causing deconstructive interference for other frequencies.

### *Pulsed Supersonic Nozzle*

During a pulse duration of  $\sim 900 \mu\text{sec}$ , the pulsed supersonic nozzle allows gas under very high pressure to enter the cavity which is at very low pressure. This process rotationally cools the molecules through adiabatic expansion and conversion of energy into mass flow. Molecules populate the low J states from this cooling and do not experience collisions in the vacuum, allowing the pure rotational spectra of transitions from the lower J states to be observed. Also, the collision free environment allows the study of unstable, transient species.<sup>8</sup>

### *Pulsed Microwave Fourier Transform Method*

An electromagnetic field induces coherent gyration of the molecules being pulsed into the chamber by the nozzle. When the electromagnetic field is removed the decohering, rotating dipoles produce their own time diminishing electromagnetic field which is received as a current

in an antenna. This free induction decay is recorded in the time domain and is Fourier transformed into the frequency domain. Measurements are taken approximately 20  $\mu\text{sec}$  after the microwaves are pulsed into the chamber to avoid reading the induced signal and also to increase sensitivity.

### Wave Theory

There is little information on how the electromagnetic field works in a traditional Fourier transform cavity. To explain general wave theory in regards to Fabry-Pérot Type Resonators, I will discuss modes, electromagnetic field regions, and the Q-factor.

### Modes

A standing wave pattern formed inside a resonator is called a mode. There are two classes of modes, transverse and longitudinal. Transverse modes are broken down into several types based on the direction of propagation for electric and magnetic fields. Typically, the Fabry-Pérot cavity operates using transverse electromagnetic, TEM, modes. TEM modes have curved wave fronts and are Gaussian in nature. Figure 1 shows a depiction of a Gaussian beam.

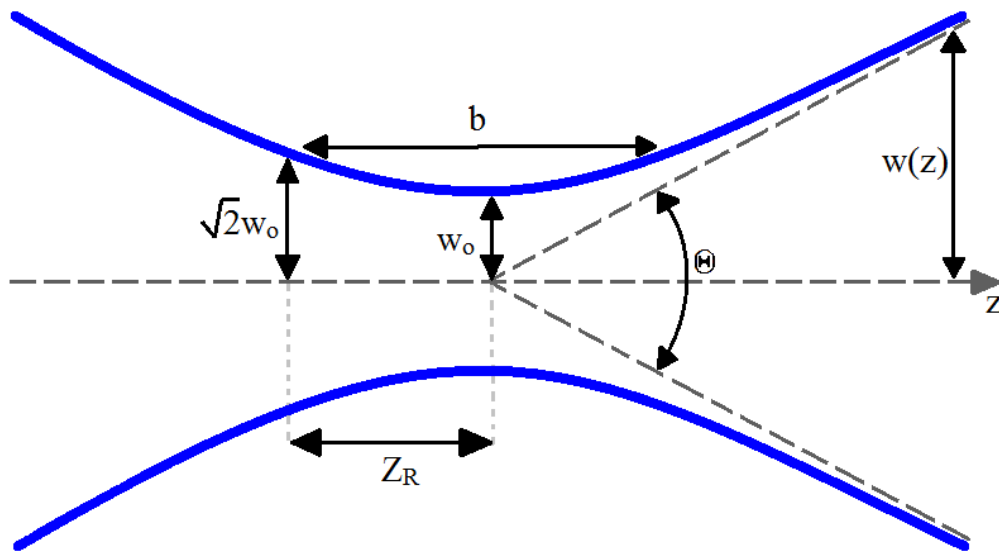


Figure 1.  $w(z)$  is the beam width as a function of the axial distance  $z$ ;  $w_0$  is the beam waist;  $b$  is the confocal parameter;  $Z_R$  is the Rayleigh range;  $\Theta$  is the total angular spread.

The beam waist,  $w_o$ , is maximized when the radius of curvature of the mirrors is equal to the distance of separation of the mirrors, creating the confocal arrangement of distance  $b$ . At the confocal arrangement  $w_o$  is determined by Equation 1

$$w_o = \sqrt{2} \left( \frac{R\lambda}{2\pi} \right)^{1/2}$$

Equation 1

where  $R$  is the radius of curvature and  $\lambda$  is the wavelength being emitted.

### *Electromagnetic Field Regions*

The electromagnetic field emitted from an antenna can be broken up into three regions, evanescent, Fresnel, and Fraunhofer.

The evanescent region exists a limited distance from the antenna which is  $r$  in Equation 2

$$r_0 \leq r \leq r_0 + \frac{5\lambda}{\pi}$$

Equation 2

where  $r_0$  is the radius of the antenna's wire,  $r$  is the distance away from the center of the antenna, and  $\lambda$  is the wavelength. Equation 2 can only be used for a qualitative approximation of the evanescent region because the electromagnetic field in this region is very complex with many variations for each system. Typically, the evanescent region must be mapped out to get the true nature of its field because it requires a receiver to take in the field that is emitted, otherwise the field will remain in the region.

The next region is the Fresnel or optical-Fresnel region of the field. This region is an intermediate distance away from the antenna which is defined as  $r$  in Equation 3.

$$r_0 + \frac{5\lambda}{\pi} \leq r \leq \frac{8r_0^2}{\lambda} + \frac{40r_0}{\pi} + \frac{200\lambda}{\pi^2}$$

Equation 3

The Fresnel region is less defined and is normally distinguished from the Fraunhofer region by the appearance of shadow regions or dark bands of the field. The wave front in the Fresnel region should be curved which in a resonator would give a Gaussian beam as in Figure 1.

The Fraunhofer region is considered to be the far-field region. It is thought to be a distance of  $r$  in Equation 4.

$$\frac{8r_0^2}{\lambda} + \frac{40r_0}{\pi} + \frac{200\lambda}{\pi^2} \leq r \leq \infty$$

Equation 4

In this region, shadow regions should be present and the wave front is a planar wave with an even field distribution. Also, the Fraunhofer region has the generalized form of waves undergoing linear diffraction in the region beyond the Raleigh range on Figure 1. Due to the standard diffraction the Fraunhofer region experiences an intensity drop off  $\propto \frac{1}{r^2}$  since energy must be conserved and the wave amplitude decreases  $\propto \frac{1}{r}$ .<sup>4, 9-11</sup>

### *Q Factor*

The ability of a resonator to contain the electromagnetic field is numerically measured by the Q factor, or quality factor. The Q factor is defined as the amount of energy stored in a cavity compared to the amount of energy dissipated per cycle. This ultimately denotes the path length of the electromagnetic field for a resonator. The Q factor can be approximated by Equation 5.

$$Q \approx \frac{\text{Resonant Frequency}}{\text{Frequency Bandwidth}}$$

Equation 5



Modes of the cavity can be manipulated for a specific resonant frequency by adjusting the distance between the mirrors. Through constructive and destructive interference, certain modes can have much greater amplitude for a particular frequency range than the frequencies surrounding that region. In Equation 5, the center of the mode is considered the resonant frequency and the full width half height of the mode is considered the frequency bandwidth.<sup>12</sup>

## Classic Balle-Flygare FTMW Spectrometer



Figure 2. Representation of the Classic Balle-Flygare FTMW Spectrometer of UNT.

A Balle-Flygare type Fourier transform microwave spectrometer has been constructed at the University of North Texas to operate in the region of 6-26 GHz. It is modeled very closely to the coaxially oriented beam resonator arrangement (COBRA) constructed by Grabow et al. It is unique in that it can operate the entire 6-26 GHz region without changing components and the low noise amplifiers are as close as possible to the receiving antennas to allow optimal sensitivity. It should be noted that a water line is used to cool these amps since they are under vacuum.<sup>13</sup>

## Resonator

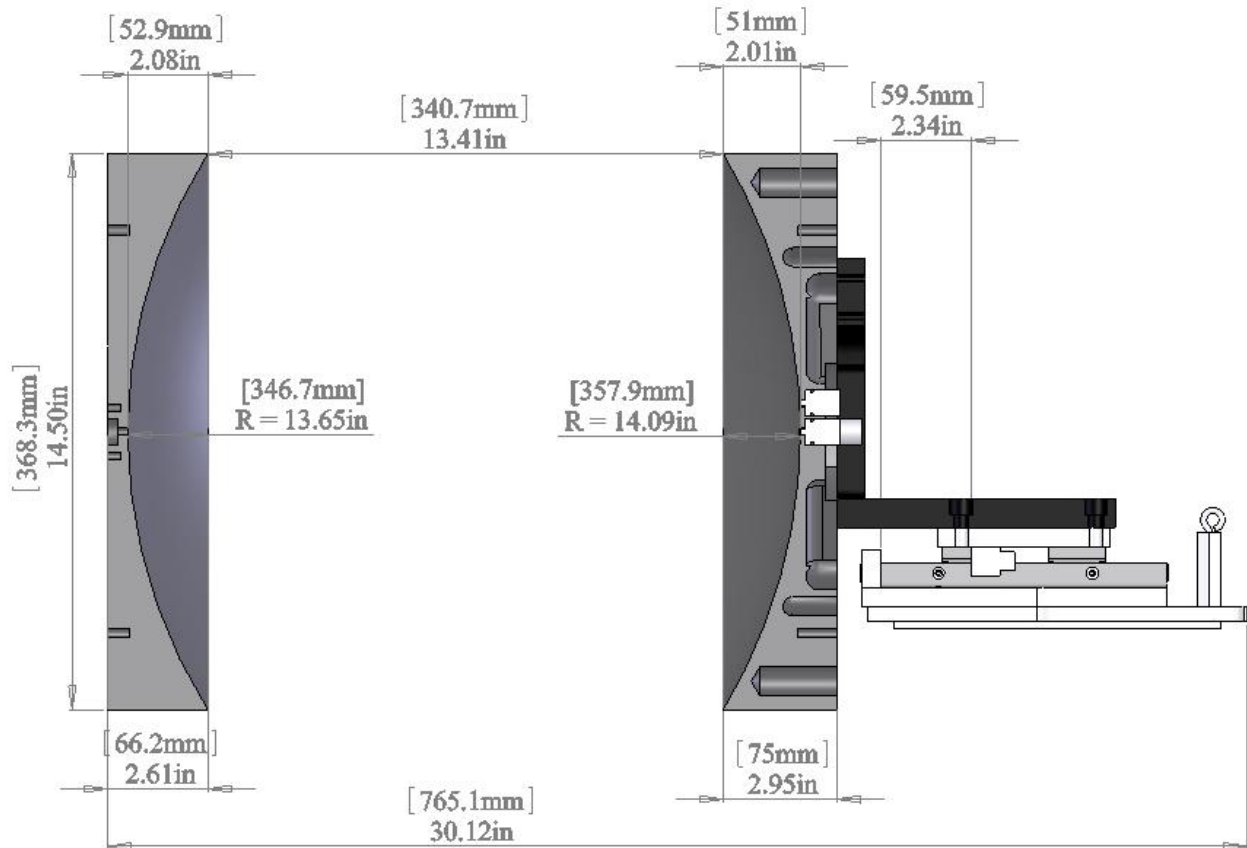


Figure 3. Side view of the classic Balle-Flygare spectrometer's mirrors.

### *Mirrors*

The two spherical mirrors purchased from NIST were constructed from 6061 grade aluminum and diamond polished to remove surface defects. The radius of curvature on the moving mirror is 357.9 mm while the stationary mirror is 346.7 mm. The stationary mirror houses the nozzle and 4 antennas, while the other mirror is mounted on a rail system connected to a stepping motor that allows the mirror to move approximately 59.5 mm.

### *Antenna*

Classic L-shaped copper antennas were used throughout the majority of this instrument's use. One set of 6.3 mm antennas were used for the 6-18 GHz region, while a different set of 3.4 mm antennas were used for the 18-26 GHz region. Each set consists of an emitting antenna and

a receiving antenna. The two sets of antenna make this instrument unique in that no components or antennas need to be replaced while observing transitions that occur in the frequency region of 6-26 GHz.

#### *Nozzle*

A Series 9, Parker Hannifin solenoid valve was used. It was placed in the center of the stationary mirror to maximize the sample's exposure to microwaves and capitalize on the increased resolution that comes from coaxial alignment. This type of nozzle orientation results in a doubling of the received peaks due to the Doppler doubling effect. To obtain the "true" peak an average of the two components is taken. This average allows for a reduced uncertainty of  $\sim 7$  kHz for the full width half maximum because the Doppler doublets have decreased peak widths compared to a non-split transition from a perpendicular nozzle orientation having  $\sim 20$  kHz of uncertainty at the full height half maximum.

#### *Vacuum System*

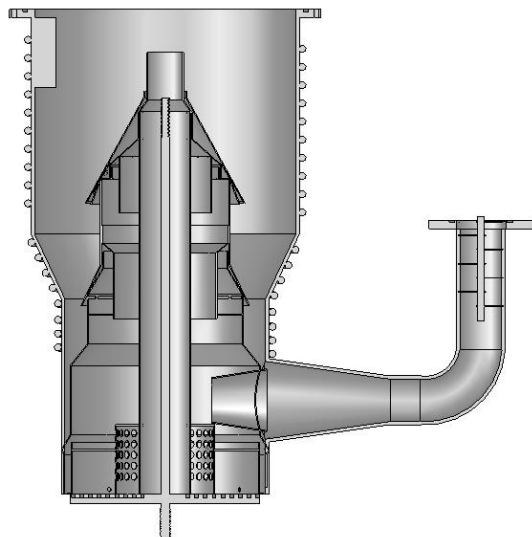


Figure 4. Depiction of the diffusion pump used.

#### *Diffusion Pump*

A Varian (0812) A023 diffusion pump is on the chamber to achieve an expedient high vacuum through molecular pumping. The pump has an inner diameter of 383.4 mm and is

located approximately 279.4 mm down the chamber's under belly from the nozzle. It has a pump speed of  $10000 \text{ ls}^{-1}$  allowing experiments to run 3 – 8 cycles per second. Ultimately, the diffusion pump maintains a pressure of ~ 5 millitorr inside the chamber when gas is not being pulsed and ~7 millitorr while gas is being pulsed.

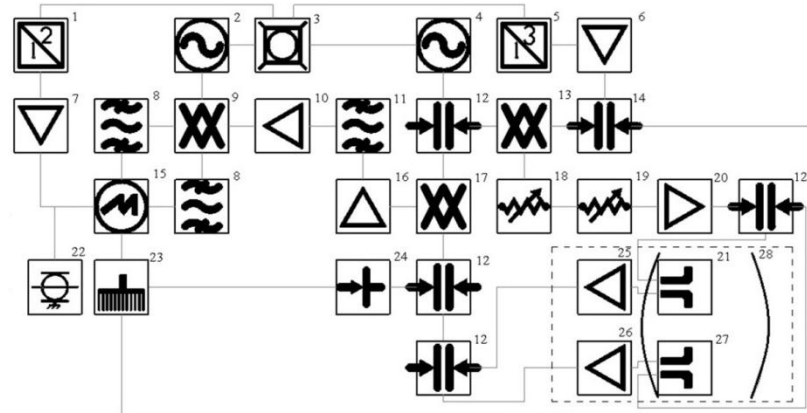
#### *Rotary Pump*

The rotary pump is used for viscous flow evacuation to back the diffusion pump. This chamber uses an Edwards E2M40 High Vacuum Pump. Starting at atmospheric pressure, the rotary pump takes about five minutes to get below 200 millitorr and about five hours to achieve its lowest pressure of 10 – 30 millitorr.

#### *Circuit*

The circuit for this instrument is unique in that it can operate the full range of 6-26 GHz without having to switch components or break vacuum to change out antenna. Figure 5 depicts the circuit used for this instrument.

6-26 GHz



1	10 MHz Doubler		Wenzel Associates, LNHD-10-13	16	RF low Noise Amplifier		Miteq AU-2A-0150
2	RF Synthesizer		HP 8656B	17	Image Rejection Mixer		2 - 26 GHz Miteq IRM0226LC1A
3	10 MHz Source		SRS FS725 Rubidium Frequency Standard	18	Attenuator Assembly		HP 84907K, 70dB
4	MW Synthesizer		HP 8340B	19	Attenuator Assembly		HP 84904K, 11 dB
5	10 MHz Tripler		Wenzel Associates, LNOM-10-3-13-13-BM-BM	20	MW Power Amplifier		Agilent 83017A (.5 - 26.5 GHz)
6	RF Voltage Gain Control Amplifier		Minicircuits ZFL-1000GH	21	Antenna Set		Classic L copper antennas
7	Wideband Linear Amplifier		Motorola, Inc. TRW/CA - 2820	22	Termination BNC		Minicircuits BTRM - 50
8	RF Low Pass Filters		Minicircuits SLP-5	23	Computer Control Connection Interface		Configurable Connector Accessory Enclosure, National Instruments CA-100
9	I/Q Demodulator		Minicircuits MIQC-60WD	24	Diode Detector		Agilent Technologies 8474C
10	RF Voltage Gain Amplifier		Minicircuits ZFL-1000G	25	Low noise Amplifier		AML AML818P4502 (gain 45 dB, noise figure 2.5 dB)
11	30 MHz Bandpass Filter		Reactel INC. 3B4-30-5-1 S11				Miteq AFS42-08001200-10-10P-42 (gain 40 dB, noise figure 1 dB)
12	SPDT Switch		Sierra MicrowaveTechnology SFD0526-001				Miteq JS4-06001800-145-10A (gain 34 dB, noise figure 1.45 dB)
13	Single-Sideband Modulator		2 - 26 GHz Miteq SM0226LC1MDA	26	Low noise Amplifier		Miteq AMF-5S-180260-45 (gain 45 dB, noise figure 1.5 dB)
14	RF SPDT Switch		Minicircuits ZYSW-2-50DR	27	Antenna Set		Classic L copper antennas
15	Personal Computer		Option Industrial Computers I0771130A77	28	Mirrors		Diamond Polished Mirrors

Figure 5. Circuit diagram of the classic Balle-Flygare spectrometer. The dashed square encompasses the components under vacuum. The components highlighted in blue have been found to work the best.

*MW Synthesizer*

The synthesizer used in this instrument is an HP 8340B, which is rated to work from 10 MHz to 26.5 GHz. The microwave synthesizer is set to a frequency with an accuracy of 1-4 Hz where the frequency is set 30 MHz below the frequency of interest. A 10 MHz signal from the

rubidium standard is tripled to 30 MHz. The 30 MHz signal is mixed with the microwave synthesizer to obtain the actual frequency of interest.

### *RF Synthesizer*

This instrument uses an HP 8656B radio frequency synthesizer to output 27.5 MHz. The signal received by the receiving antenna is the base signal from the MW synthesizer + 30 MHz +/- interaction difference from the sample. This signal is mixed with the base signal of the MW synthesizer to yield only the 30 MHz +/- interaction difference from the sample. Then, the 27.5 MHz signal of the RF synthesizer is mixed with the resulting signal to yield 57.5 MHz +/- interaction difference from the sample and 2.5 +/- interaction difference from the sample. Band pass filters are used to isolate the 2.5 +/- interaction difference from the sample. As a result, one scan can be done to observe the transitional frequency versus running two scans at slightly different frequencies to determine if the transition is above or below the original frequency emitted into the chamber.

## Efficient Low Frequency FTMW Spectrometer



Figure 6. Depiction of ELF-FTMW at UNT.

The efficient low frequency (ELF) FTMW spectrometer was developed and constructed at the University of North Texas to improve the range of the classic Balle Flygare FTMW. There are several interests in the low frequency region, which is arbitrarily defined as below 4 GHz. The main difference in this FTMW spectrometer is the use of highly curved mirrors to allow the instrument to operate at this desired frequency region at a relatively low cost.

### *Interest*

Being a gas phase technique, FTMW spectroscopy has traditionally studied small volatile liquids or gases. Recently, microwave spectroscopists have successfully transferred larger volatile liquids into the gas phase along with several solids. As microwave spectroscopists begin to study large organic molecules and heavy transition metal-compounds with FTMW



experiments, the demands for venturing into the lower frequency region becomes apparent as large or heavy molecules have large moments of inertia giving small rotational constants. These small rotational constants cause lower J molecular transitions to occur in the radio frequency region. Lower J rotational transitions are very useful in obtaining vital information about a molecule. The transitions caused by hyperfine structure are spread further out at lower J levels making the hyperfine structure more resolvable. Also, lower J transitions have simpler spectra, easing spectral assignment when compared to the often dense spectra of higher J transitions. Centrifugal distortion effects can cause different J level transitions to overlap at higher J levels and make spectral assignment considerably more difficult.<sup>6, 12</sup>

#### *Past Work*

There are two cases in which researchers have been able to tune and record spectra below 2 GHz. The first was Arunan et al., who used a Balle Flygare spectrometer and added “collars” to the edge of the mirrors to reduce the effects of a large microwave beam waist and diffraction losses. This used 1/4 wavelength antenna of the desired frequency (1888.7 MHz). It was noted that most of the components of the circuit were operating beyond their specification. The 1888.7580 MHz transition of the benzene water trimer was the lowest of the works. Storm et al. followed with the use of a cylindrical resonator for the TE<sub>01</sub> mode instead of the TEM<sub>00q</sub> mode used in Balle Flygare FTMW spectrometers which allowed the electromagnetic field to travel as a circular wall current versus a Gaussian beam. The cylindrical resonator allowed Storm to avoid using large mirrors, but several sets of antennas had to be used to cover the whole 1-4 GHz region. Their lowest observed transition was at 1325.17 MHz for 1-azabicyclo [2.2.2] octane-H<sub>2</sub>S.<sup>12, 14, 15</sup>

### *Premise*

The reason so few efforts have been made to look at low frequencies is the difficulty associated with constructing a suitable Fabry-Perot cavity. This difficulty is better understood by considering the Fresnel number given in Equation 6 that is based on Balle and Flygare's work.

$$\frac{a^2}{R\lambda} = N$$

Equation 6

In the equation,  $a$  is the radius of the mirrors,  $R$  is the radius of curvature and  $\lambda$  is the resonant wavelength. Also,  $N$  must be equal to 1 for the lowest frequency of interest to insure a good resonator with a high  $Q$  factor. This suggests the way of obtaining lower frequency spectra is through either increasing the mirror's radius and/or decreasing its radius of curvature. This principle of Equation 6 was the foundation for the "extreme geometry" of this low frequency cavity.<sup>4</sup>

Ideally, the construction of mirrors with a larger diameter would be necessary to achieve a lower frequency tunable cavity. This would be extremely costly and also experimentally impractical. With larger mirrors would come a larger chamber to accommodate them, which would cause vacuum issues. To account for this, a chamber would have to be equipped with more and bigger diffusion pumps and a stronger rotary pump. Also, this instrument would take a lot of physical space in a lab. In order to achieve a resonator operable at 2 GHz, the mirrors would have diameters of over 2.818 meters if constructed with the traditional radius of curvature of 840 mm. It should be stated, this last year the Kukolich group in Arizona presented an instrument with very large mirrors as described above, which was costly and took two floors of a building to hold. At the time of the ELF-FTMW's construction there was no FTMW instrument that was truly designed to operate below 4 GHz.<sup>4,16</sup>

## Resonator

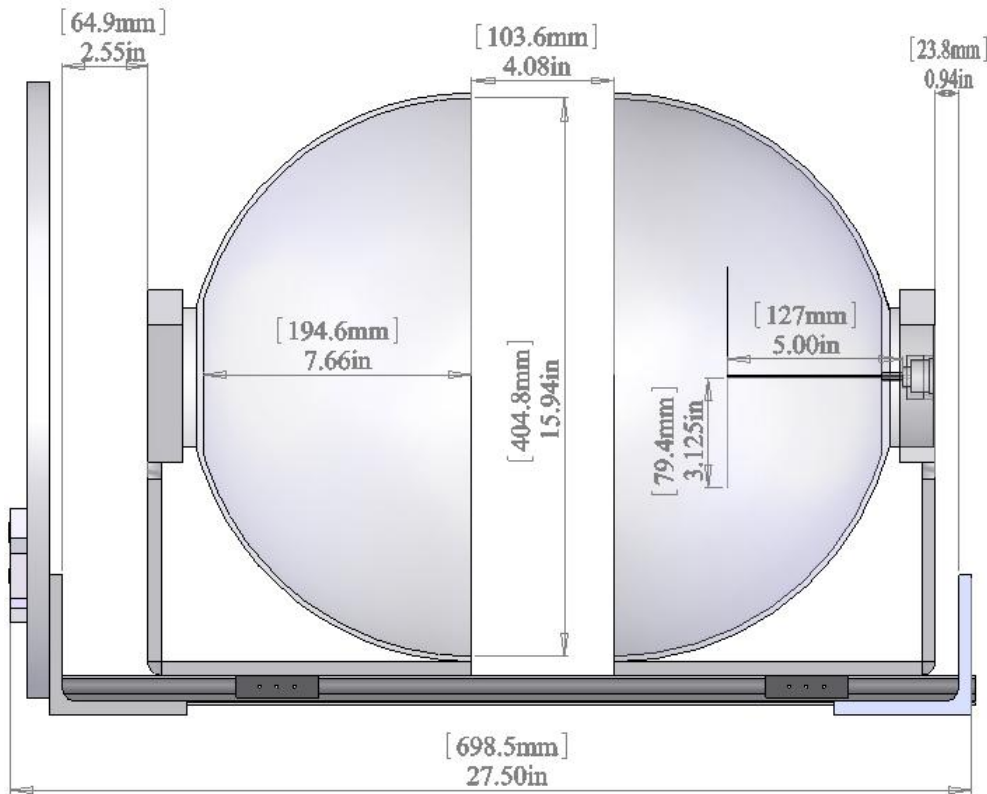


Figure 7. Depiction of ELF-FTMW's mirrors on the rail system.

### Mirrors

As stated, in order to have a stable resonator at lower frequencies, i.e., less than 2 GHz, the radius of the mirrors must be increased or the radius of curvature must be decreased.

$$\frac{a^2}{R\lambda} = N$$

Equation 6

The radius of the mirrors that could be used was limited by the size of the vacuum chamber available, so the only variable that could be manipulated was the radius of curvature. The smallest radius of curvature possible would be hemispherical mirrors. Taking Arunan's success with "collars" into consideration, it was conceivable that hemispherical mirrors could work.<sup>12</sup>

Given the uncertainty of the success of this project, an inexpensive method for acquiring hemispherical mirrors was desirable. AMS industries, Ltd. sells commercially available aluminum hemispheres for the general use as "pigs" to clean out oil lines. The hemispheres are constructed out of 6061 grade aluminum using a spinning process, resulting in several large, undesirable surface defects, along with a 25.4 mm diameter hole in the center from being attached to the spinning apparatus. The University of North Texas's physics machine shop was able to polish the mirrors and weld aluminum plugs into the holes. This produced two hemispherical aluminum mirrors with radii of 206.375 mm and reducing the surface defects to approximately 2-3 mm or less. The mirrors are mounted on a rail, having one stationary mirror with holes for antennas and a nozzle, and one mirror that can move approximately 150 mm.

Figure 8 shows a photograph of the mirrors.<sup>12</sup>



Figure 8. A photograph of preliminary testing before placing under vacuum that proved that the mirrors could be tuned to form standing waves at lower frequencies.

## *Antenna*

The shape of the antennas can have a great effect on the spectrometer's performance.

Classic L-shaped copper antennas were used throughout the beginning of this instrument's use as shown on Figure 9.

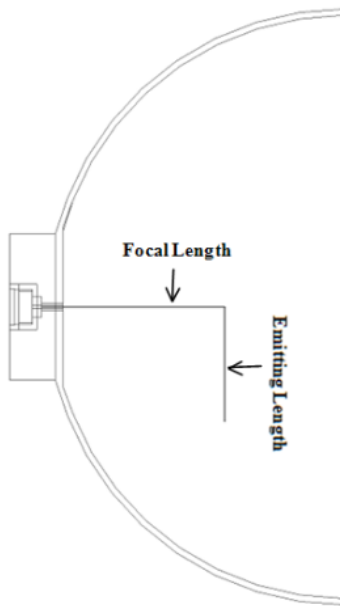


Figure 9. A sketch of the antenna in the mirror designating the focal and emitting lengths of the antenna. The antenna depicted has a 12.7 cm focal length and 7.94 cm emitting length.

Through testing the mirrors, it was determined that the best focal lengths for the antennas are 50.8, 101.6, and 127.0 mm from the flat surface of the stationary mirror with the longest focal length working the best. Besides the focal length, the emitting length of the antenna can be lengthened to improve the signal for lower frequency measurements. Also, it has been observed that longer antennas are better for a larger range of frequencies than its counterpart short antennas. However, the short antennas are still the best for higher frequencies. Several antennas were made with the emitting lengths set to be a quarter of the desired wavelength; unfortunately, this required breaking the vacuum to change them out for a given frequency region to achieve the best results.

Through several tests with different antenna designs, a new variable antenna has been created and has recently been used in the ELF-FTMW spectrometer. It has a 127.0 mm focal length, which had previously been found to work the best out of the three focal lengths. The rest of the dimensions are shown in Figure 10.

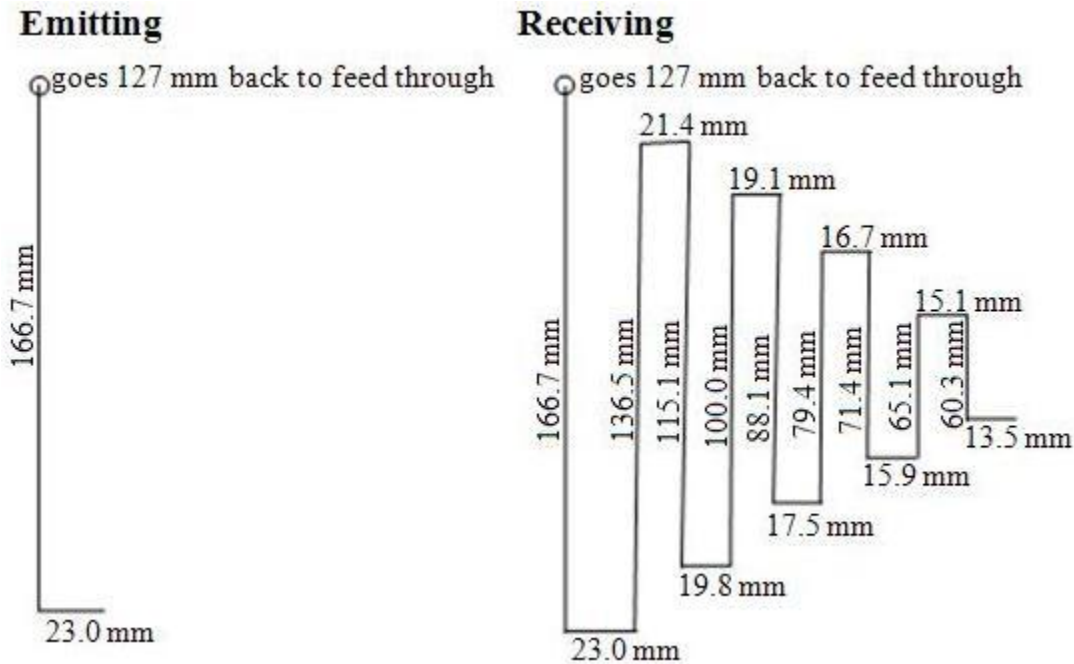


Figure 10. Drawing of the emitting and receiving variable antennas. The circle on both the emitting and receiving antennas represent the antenna going 12.7 cm into the paper. The length of the longer sides of the receiving antenna are to the left of the antenna length.

Please note that when placed into the resonator the longer end of the emitting antenna is parallel with the longer lengths of the receiving antenna.

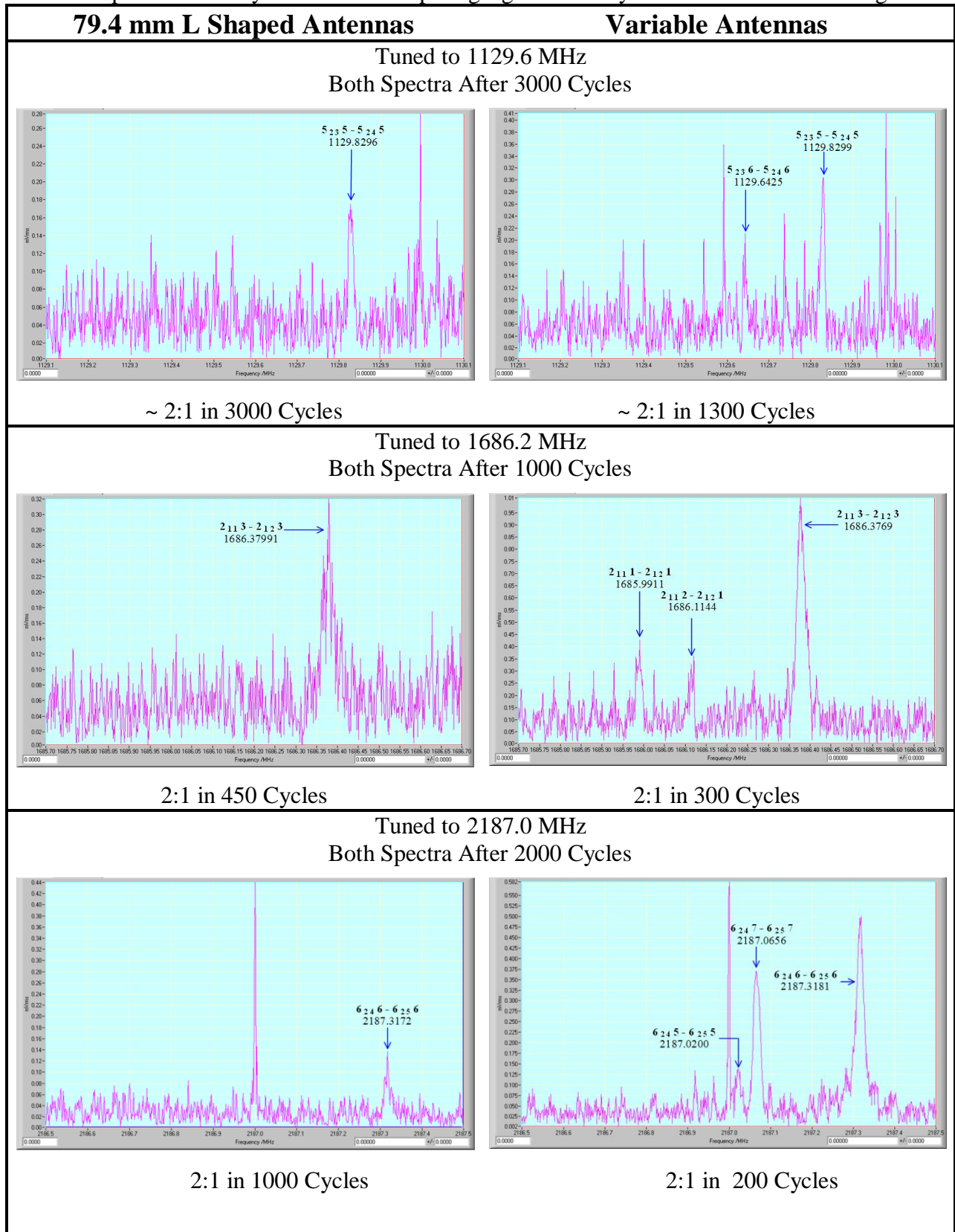
The emitting antenna was designed to allow for the longer side to be optimal for low frequency (longer wavelengths) and the shorter side to be optimal for high frequency (shorter wavelengths). Theoretically, the two emitting sides should not interfere with each other since the fields they produce are perpendicular to each other. A prototype double L antenna, with the same emitting lengths, was tested and showed an increase in peak intensity, which suggests that the double L shape doesn't hinder the wave field of the other antenna enough to prohibit an

overall improvement over a normal L shape antenna. Also, the short emitting side was purposely oriented the farthest from the feed through, since higher frequencies have more energy. Both lengths of the emitting antenna are the same length as the longest side of their respective components of the receiving antenna. This was done because previous work had shown that the longer emitting lengths for the antenna could cover a larger range of frequencies than a shorter emitting length for the antenna.

The receiving antenna was made to be optimal for a large range of frequencies between 450 MHz and 22200 MHz, in a similar design to a meander line antenna. Since this antenna is not emitting there was no worry of the sides interfering with one another and multiple lengths could be placed in the same direction. The smaller lengths were positioned farthest from the feed through since the higher energy short wavelengths would offset the loss from travelling through more wire. Teflon was melted onto the edges of the receiving antenna to prevent the copper from touching the sides of the mirrors and to add rigidity to the copper system preventing shape distortions. Teflon does not absorb or reflect in the microwave region, making it a well suited material for this purpose.<sup>17</sup>

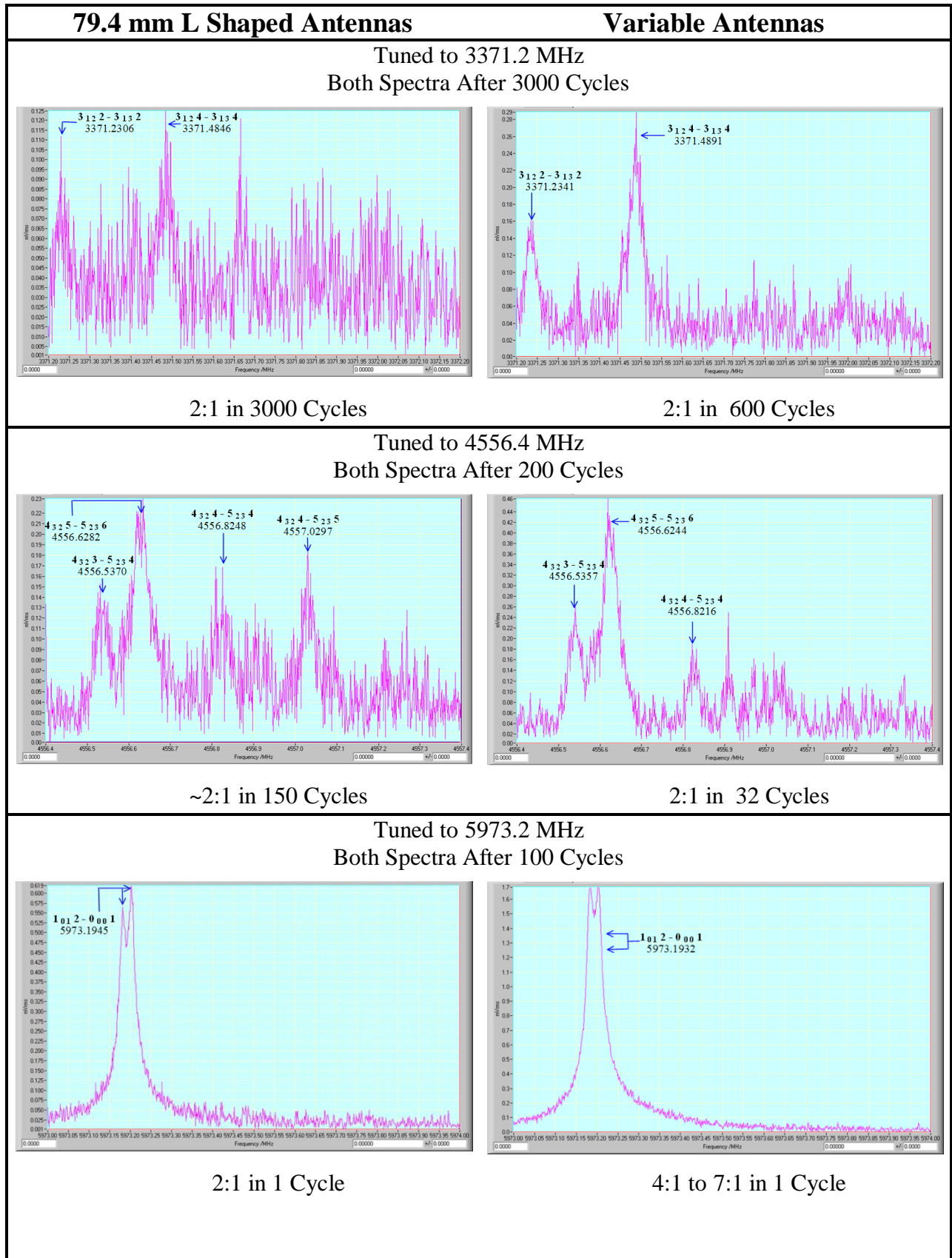
A performance test of the variable antennas was conducted by comparing observed spectra of n-butyronitrile with standard L shaped antennas with a 127.0 mm focal length and a 79.4 mm emitting length. Both sets of antennas were tested over a range of approximately 1 to 22 GHz within a four day period to limit random error. The results are shown in Table 2.

Table 2. Spectra of n-butyronitrile for comparing signal intensity for different antenna designs.





(Table 2 continued)



(Table 2 continued)

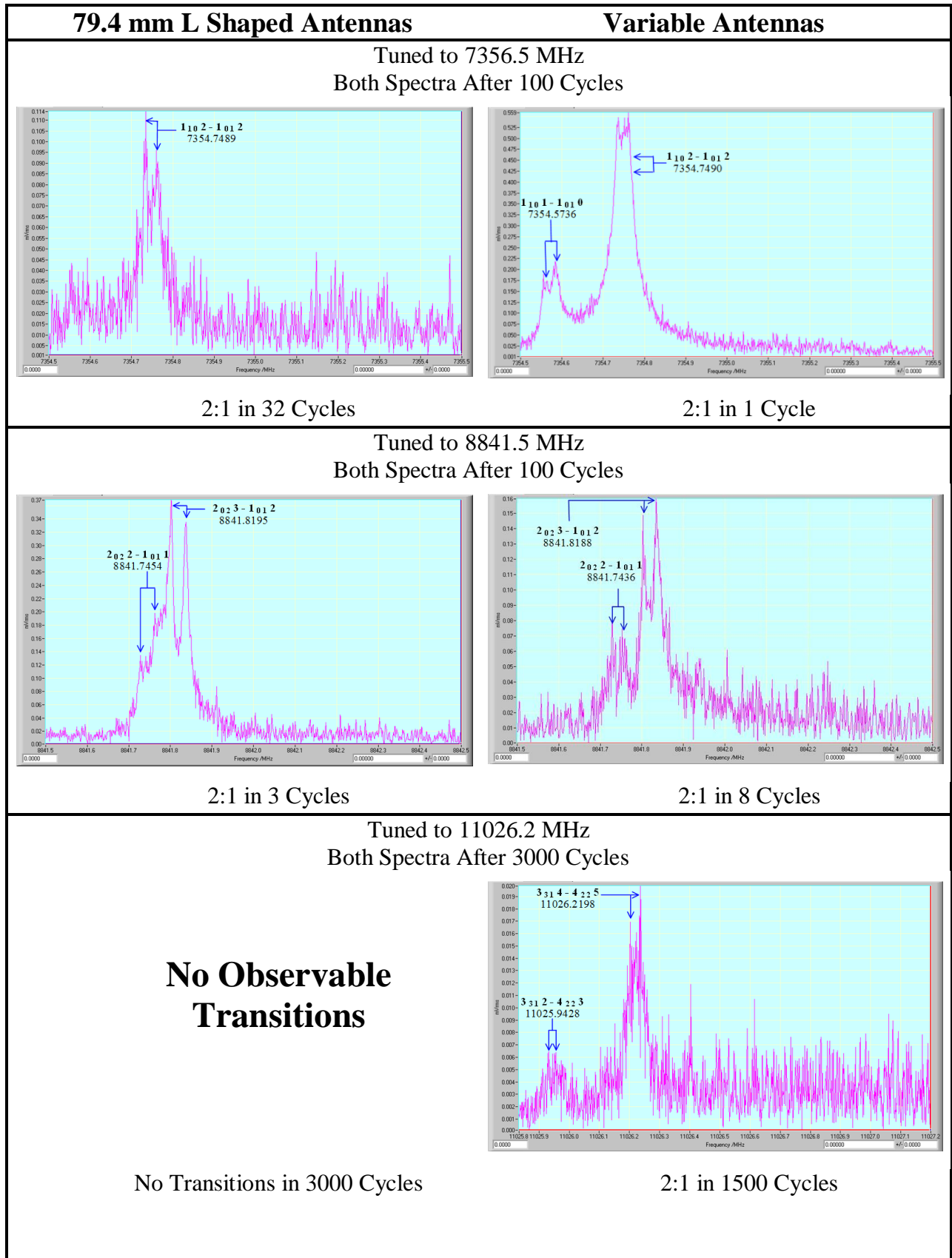
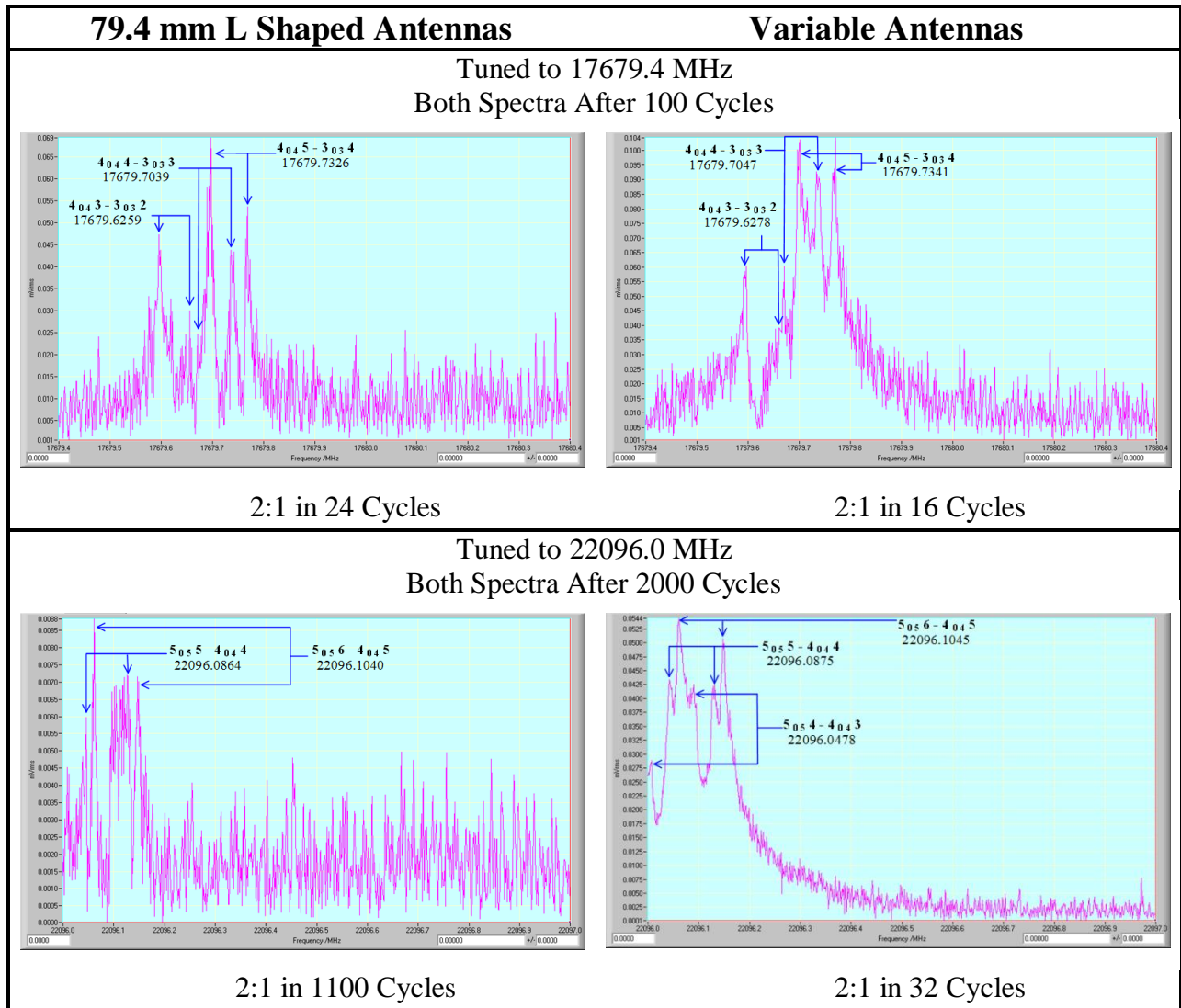


(Table 2 continued)



Each set of spectra for the different antenna designs were acquired after the same number of cycle.

Table 2 shows that the variable antennas allowed the signal to noise ratio to be 2:1 in fewer shots for the majority of the transitions. The only instance where the 79.4 mm antennas did better was for the 8841.5 frequency, but the spectra show that the variable antennas resolved the second transition better and the most intense transition is still comparable. The variable antennas work reasonably well for a large range of frequencies and are good for searching purposes, but a

custom antenna optimized for a specific frequency still works better at that specific frequency. For this reason, the ELF-FTMW typically uses the variable antennas to expedite research.

### *Nozzle*

Just as for the traditional Balle-Flygare FTMW spectrometer discussed above, a Series 9, Parker Hannifin solenoid valve was used. It was placed in the center of the stationary mirror to maximize the sample's exposure to microwaves and capitalize on the increased resolution that comes from coaxial alignment. Normally, this type of nozzle orientation results in a doubling of peaks due to the Doppler doubling effect, but it was found that the two peaks are no longer resolvable with an argon backing gas around 3.5 GHz. The Doppler effect on an observed frequency follows Equation 7

$$\nu = \nu_0 \pm \nu \left( \frac{V}{V_p} \right)$$

Equation 7

where  $\nu$  is the observed frequency,  $\nu_0$  is the resonant frequency without Doppler shift,  $V$  is the molecular velocity and  $V_p$  is the velocity of phase propagation of the radiation (normally the speed of light). A perpendicular orientation of the nozzle was tested in hopes of narrowing the peak widths in the lower frequency region. The test showed that the peak widths were about the same for both orientations but the coaxial orientation came in considerably stronger in intensity as shown in Figure 11.<sup>6, 18</sup>

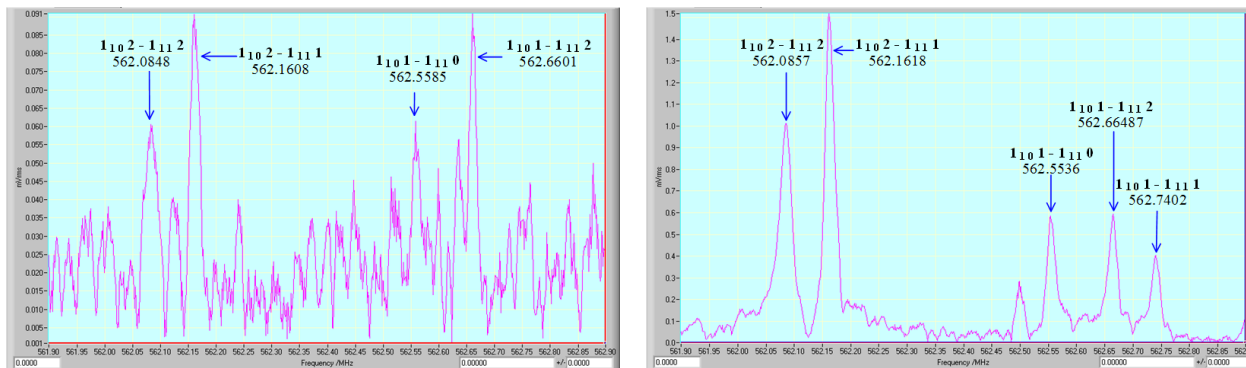


Figure 11. Both spectra were taken while tuned to 562.4 MHz as n-butyronitrile was bubbled through the line. Each spectrum is an average of 12000 cycles. The spectrum on the left was obtained with the nozzle in a perpendicular orientation. The spectrum on the right displays a stronger signal from the nozzle being in a coaxial orientation.

### *Vacuum System*

#### *Diffusion Pump*

A Balzers Temperaturemelder B5-540-677-D diffusion pump is on the chamber to achieve an expedient high vacuum through molecular pumping. The pump has an inner diameter of 317.5 mm and is located in the middle of the chamber's under belly. It has a pump speed of  $10000 \text{ ls}^{-1}$  allowing experiments to run 3 – 8 cycles per second with a pressure of ~7 millitorr.

#### *Rotary Pump*

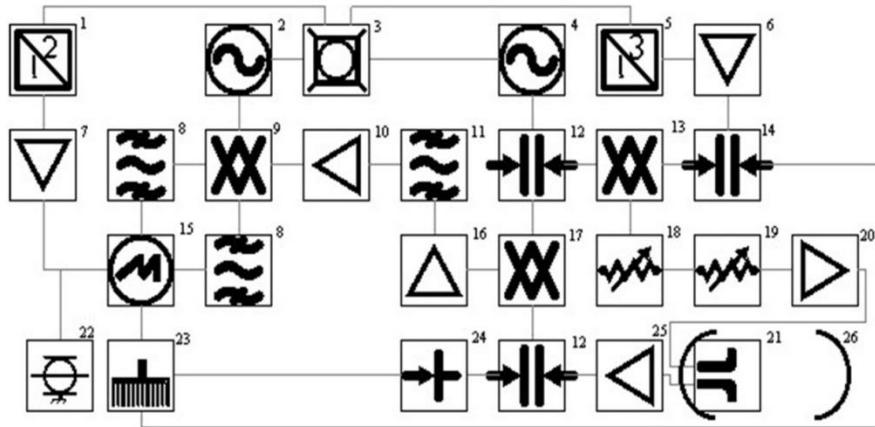
The rotary pump is used for viscous flow evacuation to back the diffusion pump. This chamber used an Edwards High Vacuum Pump (Model: E2M40, Serial: 12981). Starting at atmosphere, the rotary pump would take about five minutes to get below 200 millitorr and about five hours to achieve its lowest pressure of 10 – 30 millitorr.

### *Circuit*

The ELF-FTMW utilizes two different circuits depending on the frequency range of interest, 2-26 GHz and 0.5-2.2 GHz. The circuit components are outside of the vacuum chamber which allows for the operational frequency range to be changed without opening the system to air. The 2-26 GHz circuit is nearly identical to the circuit used for the Balle Flygare FTMW.

The 0.5 – 2.2 GHz circuit is interesting not only for its low range, but also for its relatively low cost. Low noise amplifiers are approximately \$700 compared to the \$3000 higher frequency counterpart. The switches are on an order of magnitude cheaper than the higher frequency circuit, \$80 and \$800, respectively. The circuits are depicted in Figure 12 and Figure 13.

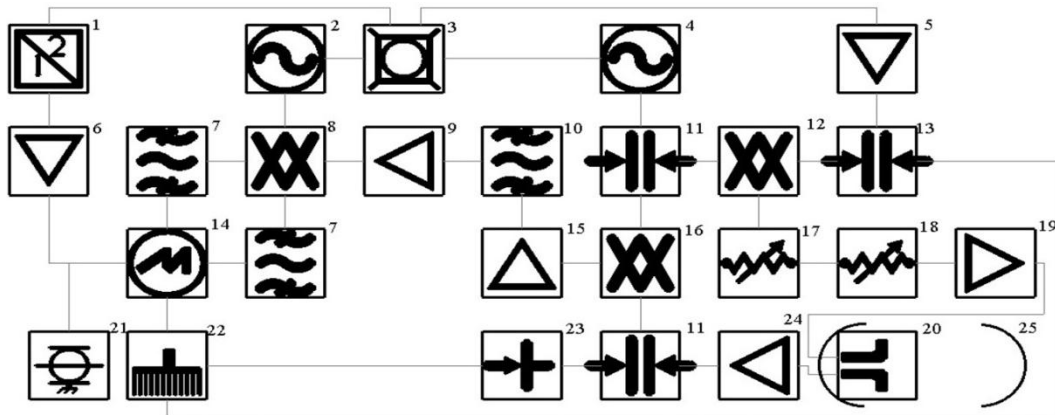
2-26 GHz



1	10 MHz Doubler		Wenzel Associates, LNHD-10-13	16	RF low Noise Amplifier		Miteq AU-2A-0150
2	RF Synthesizer		HP 8656B	17	Image Rejection Mixer		2 - 26 GHz Miteq IRM0226LC1A
3	10 MHz Source		SRS FS725 Rubidium Frequency Standard	18	Attenuator Assembly		HP 84907K, 70dB
4	MW Synthesizer		HP 8340B	19	Attenuator Assembly		HP 84904K, 11 dB
5	10 MHz Tripler		Wenzel Associates, LNOM-10-3-13-13-BM-BM	20	MW Power Amplifier		Agilent 83017A (.5 - 26.5 GHz)
6	RF Voltage Gain Control Amplifier		Mmicircuits ZFL-1000GH	21	Antenna Set		Typically, classic L copper antennas
7	Wideband Linear Amplifier		Motorola, Inc. TRW/CA - 2820	22	Termination BNC		Mmicircuits BTRM - 50
8	RF Low Pass Filters		Mmicircuits SLP-5	23	Computer Control Connection Interface		Configurable Connector Accessory Enclosure, National Instruments CA-100
9	I/Q Demodulator		Mmicircuits MIQC-60WD	24	Diode Detector		Agilent Technologies 8474C
10	RF Voltage Gain Amplifier		Mmicircuits ZFL-1000G	25	Low noise Amplifier		AML AML 818P4502 (gain 45 dB, noise figure 2.5 dB)
11	30 MHz Bandpass Filter		Reactel INC. 3B4-30.5-1 S11				Miteq AFS42-08001200-10-10P-42 (gain 40 dB, noise figure 1 dB)
12	SPDT Switch		Sierra MicrowaveTechnology SFD0526-001				Miteq JS4-06001800-145-10A (gain 34 dB, noise figure 1.45 dB)
13	Single-Sideband Modulator		2 - 26 GHz Miteq SM0226LC1MDA				Lucix S001040L4501 (gain 45 dB, noise figure 1.5 dB)
14	RF SPDT Switch		Mmicircuits ZYSW-2-50DR				Miteq AMF-6F-00100400 (gain 65 dB, noise figure 1.0 dB)
15	Personal Computer		Option Industrial Computers I0771130A77	26	Mirrors		Hemispherical Mirrors

Figure 12. Circuit diagram of 2-26 GHz circuit for the ELF-FTMW. The components highlighted in blue work best.

0.5-2.2 GHz



1	10 MHz Doubler	 Wenzel Associates, LNHD-10-13	14	Personal Computer	 Option Industrial Computers I0771130A77
2	RF Synthesizer	 HP 8656B	15	RF low Noise Amplifier	 Miteq AU-2A-0150
3	10 MHz Source	 SRS FS725 Rubidium Frequency Standard	16	Image Rejection Mixer	 300 - 1000 MHz 10 MHz $\pm$ 1MHz IF, Polyphase Microwave IRM0310X
4	MW Synthesizer	 HP 8340B			 700 - 2200 MHz, 10 MHz $\pm$ 1 MHz IF, Polyphase Microwave IRM0722A
5	RF Voltage Gain Control Amplifier	 Minicircuits ZFL-1000GH	17	Attenuator Assembly	 HP 84907K, 70dB
6	Wideband Linear Amplifier	 Motorola, Inc. TRW/CA - 2820	18	Attenuator Assembly	 HP 84904K, 11 dB
7	RF Low Pass Filters	 Minicircuits SLP-5	19	MW Power Amplifier	 Agilent 83017A (.5 - 26.5 GHz)
8	I/Q Demodulator	 Minicircuits MIQC-60WD	20	Antenna Set	 Typically, classic L copper antennas
9	RF Voltage Gain Amplifier	 Minicircuits ZFL-1000G	21	Termination BNC	 Minicircuits BTRM - 50
10	10 MHz Bandpass Filter	 KR Electronics, Inc. 2588	22	Computer Control Connection Interface	 Configurable Connector Accessory Enclosure National Instruments CA-100
11	SPDT Switch	 Sierra Microwave Technology SFD0526-001	23	Diode Detector	 Agilent Technologies 8474C
12	Single-Sideband Modulator	 300 - 100 MHz, 10 MHz $\pm$ 1 MHz IF, Polyphase Microwave SSB0310X	24	Low noise Amplifier	 Lucix S001040L4501 (gain 45 dB, noise figure 1.5 dB)
		 750 - 2200 MHz, 10 MHz $\pm$ 1 MHz IF, Polyphase Microwave SSB0722A			 Miteq AMF-6F-00100400 (gain 65 dB, noise figure 1.0 dB)
13	RF SPDT Switch	 Minicircuits ZYSW-2-50DR	25	Mirrors	 Hemispherical Mirrors

Figure 13. Circuit diagram of 0.5 - 2.2 GHz circuit for the ELF-FTMW. The components highlighted in blue work the best.

*MW Synthesizer*

The microwave synthesizer is set to a frequency with an accuracy of 1-4 Hz where the frequency is set 30 MHz below the frequency of interest. A 10 MHz signal from the rubidium

standard is tripled to 30 MHz. The 30 MHz signal is mixed with the microwave synthesizer to obtain the actual frequency of interest. The synthesizer used in this instrument is an HP 8340B, which is rated to work from 10 MHz to 26.5 GHz.

#### *RF Synthesizer*

This instrument uses an HP 8656B radio frequency synthesizer to output 27.5 MHz. The signal received by the receiving antenna is the base signal from the MW synthesizer + 30 MHz +/- interaction difference from the sample. This signal is mixed with the base signal of the MW synthesizer to yield only the 30 MHz +/- interaction difference from the sample. Then, the 27.5 MHz signal of the RF synthesizer is mixed with the resulting signal to yield 57.5 MHz +/- interaction difference from the sample and 2.5 +/- interaction difference from the sample. Band pass filters are used to isolate the 2.5 +/- interaction difference from the sample. As a result, one scan can be done to observe the transitional frequency versus running two scans at slightly different frequencies to determine if the transition is above or below the original frequency emitted into the chamber.



## Broadband Instrument

Broadband, as the name suggests, covers a large frequency region at one time. Recent advances in electronics have provided the computing speed necessary to perform fast linear sweeps. The process begins with an arbitrary waveform generator producing a fast linear sweep or chirped pulse that is then mixed with a center frequency to put the sweep in the desired frequency range. This sweep interacts with the sample that is pulsed into vacuum chamber and the free induction decay is recorded on an oscilloscope.

There are two fundamental developments that have recently been overcome to allow this type of spectrometer to be developed. One main key is the advancement of arbitrary wave generators that execute a sweep of the entire frequency region relatively quickly, i.e.,  $\sim 1 \mu\text{s}$ , before the polarized molecules undergo decoherence. Another essential part is an oscilloscope that can process the large amount of data acquired that covers the full range of the sweep with enough data points to prevent aliasing.<sup>19</sup>

In order to have a chirped pulse that is quick enough to work, the multiple reflections desired in cavity techniques must be avoided to prevent the sweep from taking too long. Horn antennas are normally used to avoid the reflections caused by the mirrors of a cavity, but this also makes the Q factor equal to 1 for this type of instrument. The low Q factor means the instrument is less sensitive. However, the speed at which the instrument can collect data allows for several tens of thousands of cycles to be averaged in a short time to have a relative improvement in sensitivity.

## Chirped Pulse FTMW Spectrometer



Figure 14. Depiction of chirped pulse FTMW spectrometer at UNT.

The chirped pulse FTMW spectrometer constructed at University of North Texas was the first broadband instrument in the microwave region to implement laser ablation. It was strongly influenced by the broadband spectrometer developed by Brooks Pate. The spectrometer is able to record 2 GHz scans in the region of 8-18 GHz.<sup>19</sup>

### *Chirped Pulse Region*



Figure 15. Depiction of the horn antennas of the chirped pulse FTMW spectrometer.

### *Horns*

Two horns are set facing each other in the same vacuum chamber as the classic Balle-Flygare spectrometer. The horns are used to help directionalize and amplify the electromagnetic field. Microwave absorbing foam is placed on the moving mirror of the cavity experiment to prevent ringing while the chirped pulse experiment is running. The horns used in this spectrometer are Amplifier Research AT 4004's rated to operate in the 7.5 – 18 GHz region.

### *Waveguide To Coaxial Converter*

The waveguide to coaxial converters used in the chirped pulse spectrometer are AT 4004 horn antennas from Amplifier Research. These are used to work in conjunction with the horns to allow a broad frequency range and the ability to broadcast a distance of approximately 75 cm to allow the sample a large enough mean free path to adiabatically expand between the waveguide to coaxial converters in a collision free environment.

### *Nozzle*

The same Series 9, Parker Hannifin solenoid valve as the classic Balle-Flygare spectrometer was used which was placed in the center of the stationary mirror of the cavity instrument. This causes the sample to be pulsed in a perpendicular orientation to the propagation of the microwave field. This results in single peaks, free from Doppler doubling, and keeping the assignment of the vast number of lines as simple as possible since the instrument is designed for acquiring mass quantities of data rather than extreme precision measurements.

### *Vacuum System*

#### *Diffusion Pump*

A Varian (0812) A023 diffusion pump is on the chamber to achieve an expedient high vacuum through molecular pumping. The pump has an inner diameter of 383.4 mm and is

located approximately 28.0 mm down the chamber's under belly from the nozzle. It has a pump speed of  $10000 \text{ ls}^{-1}$  allowing experiments to run 3 – 8 cycles per second.

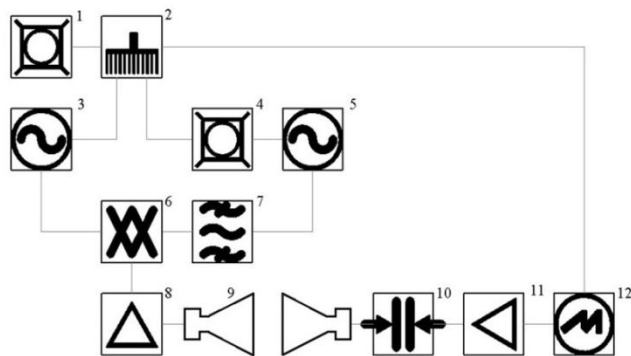
### Rotary Pump

The rotary pump is used for viscous flow evacuation to back the diffusion pump. This chamber used an Edwards High Vacuum Pump (Model: E2M40, Serial: 12981). Starting from atmosphere, the rotary pump would take about five minutes to get below 200 millitorr and about five hours to achieve its lowest pressure of 10 – 30 millitorr.

### Circuit

The circuit for the chirped pulse spectrometer consists of only a small number of components due to the oscilloscope being able to directly digitize up to an 18 GHz frequency. This simplifies the process by not requiring the signal to be mixed down to a lower frequency.

### 8-18 GHz














1	10 MHz Source		SRS FS725 Rubidium Frequency Standard	7	Low Pass Filter		Mircircuits 15542
2	Distribution Amplifier		Wenzel Associates	8	MW Power Amplifier		Microwave Power L0818-37-T351
3	MW Synthesizer		HP 8341A	9	Horn Antennas		Amplifier Research AT 4004
4	Phase Lock Oscillators		NXPLOS-0064-02381	10	SPST Switch		ATM S1517D
5	Waveform Generator		Tektronix AWG 710B	11	Low Noise Amplifier		Miteq AMF-6F-08001800-14-10P
6	Mixer		Miteq DM0520LW1	12	Oscilloscope		Tektronix TDS 6124C

Figure 16. Circuit Diagram for the chirped pulse spectrometer.

### *MW Synthesizer*

The microwave synthesizer is set to a frequency with an accuracy of 1-4 Hz. This device determines the center frequency for the sweeps or chirps of the instrument. The synthesizer used in this instrument is an HP 8341A, which is rated to work from 10 MHz to 20 GHz.

### *Waveform Generator*

The waveform generator is used to create the linear frequency sweep of microwave radiation, or chirps. This is done by sweeping from 0 GHz to 1 GHz, in typically 4  $\mu$ s, while mixing with the center frequency from the microwave synthesizer. Ultimately, this creates a chirp that sweeps from the center frequency  $\pm$  1 GHz. The waveform generator used in this instrument is a Tektronix AWG 710B.

### *Phase Lock Oscillators*

The phase lock oscillators help stabilize the arbitrary wave form generator. Nexyn Corporation NXPLOS-0064-02381 are used in this spectrometer.

### *Oscilloscope*

In order to acquire a large amount of data in a short time a broadband oscilloscope is required. For this instrument a Tektronix TDS 6124C is used and is able to directly digitize 8-18 GHz. Some caution is used regarding the oscilloscopes full range since it suffers a considerable loss in signal above 12 GHz. It has the ability to acquire 40 gigasamples/s, or 1 data point every  $25 \times 10^{-12}$  s.

## Laser Ablation

Laser ablation works by pulsing a laser onto the surface of material to create a plasma. The plasma formed is able to react with different gasses, allowing gas phase spectroscopy techniques the ability to look at heavy atom containing compounds, such as transition metal.

### Nd:YAG Laser

A solid state laser uses a crystalline rod such as yttrium aluminum garnet,  $Y_3Al_5O_{12}$ , to house the doped material like neodymium to serve as the gain medium of the laser. The doped material on the crystalline denotes the fundamental wavelength of the laser. In the case of Nd:YAG, the frequency is 1064nm, caused by the emission of the excited  $Nd^{3+}$  ions undergoing a  ${}^4F_{3/2} \rightarrow {}^4I_{11/2}$  transition. Typically, this transition would be considered forbidden, but the YAG crystal interacts with the  $Nd^{3+}$  in such a way as to help mix the J levels to allow the  $\Delta J = 4$  transition to occur.<sup>20</sup>

A pulsed laser can be used to increase the peak pulse power of the laser versus a weaker continuous beam. This allows the laser to be intense enough to create a plasma when lasing a metal. This is achieved through the use of a Q-switch, which disrupts the Q-factor of the open resonator encompassing the gain medium. This disturbance allows the gain medium to store the maximum pump energy from the flash lamp as the passive Q-switch absorbs a portion of the fluence until it becomes fully saturated. The saturated Q-switch allows a high transmittance of the laser oscillation resulting in a laser pulse and the Q-switch returns back to an unsaturated state with the energy being discharged from the gain medium. This allows a laser to have short intense pulses.<sup>21</sup>

Two lasers were used in this research, the Minilase II and Polaris II Pulsed Nd:YAG Laser Systems from New-Wave. Both emit up to a 50 mJ pulse at 1064 nm for 4-5 ns.

Typically, the laser power is attenuated to 80%, making most pulses approximately 40 mJ of energy. Limited by the chamber's pumping speed, each laser is set to run at only 1-4 Hz. A depiction of the Minilase II is shown in Figure 17.

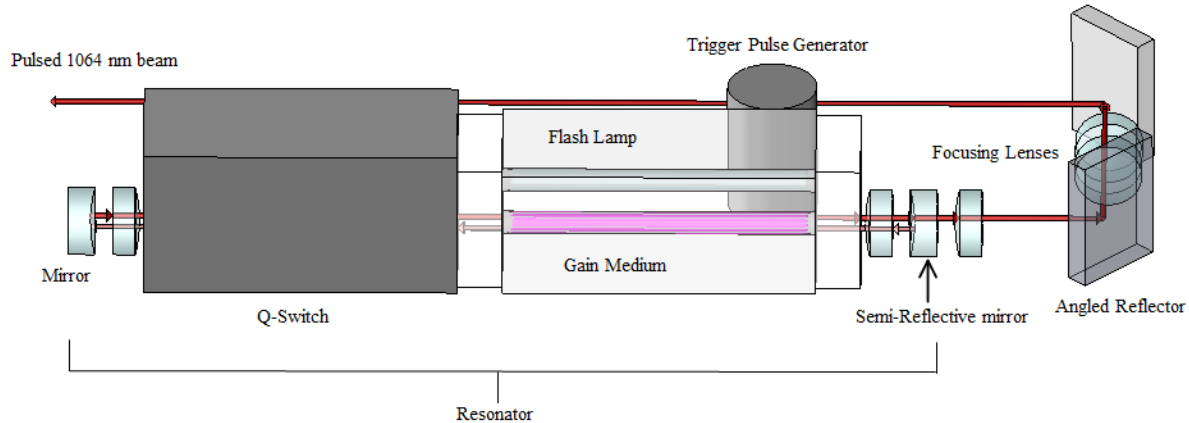


Figure 17. Diagram of New Wave Minilase II Nd:YAG laser.

#### Walker-Gerry Nozzle

In order to properly allow the carrier gas to react with the plasma of the ablated metal a special nozzle head must be used to get the newly made species into the path of the microwave field. A Walker-Gerry nozzle, based on the Smalley nozzle, meets the needs of this requirement. The nozzle has a small hole in the side to allow a laser to ablate a rod that fits through a hole in the top of the nozzle. This rod is normally rotated so that it continuously has a fresh surface. The backing gas is pulsed through a hole perpendicular to both the laser and rod holes. This backing gas is mainly Ar with about 1% of a gas that will react with the metal as it is blown over the plasma. The backing gas is at a high pressure so that it will carry the newly made species far enough into the vacuum chamber to be in the region of the microwave field. Like the other nozzle systems, the gas is going from high pressure to low pressure causing the molecules to rotationally cool as they adiabatically expand. A depiction of the Walker-Gerry nozzle is shown in Figure 18.

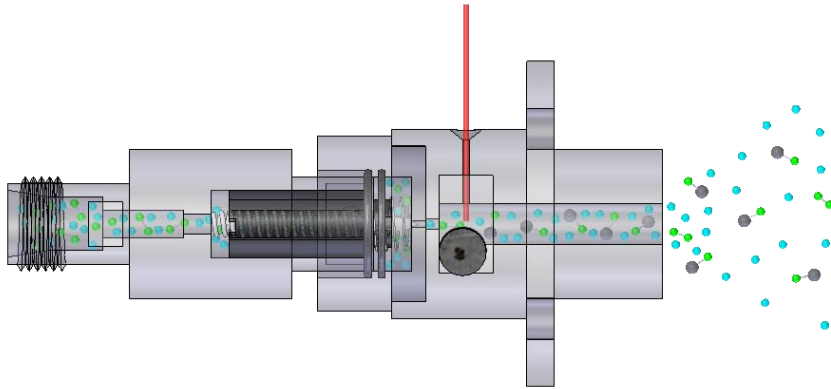


Figure 18. Walker-Gerry ablation nozzle is shown from a top view orientation. The red line represents a laser pulse at 1064 nm, the greyish black circle is a top view of a metal rod, and the blue and green spheres represent the backing gas.

### Rod Building

Making metal rods can be done through an assortment of ways. Typically, foils can be rolled on wire or on themselves to be cylindrical in nature. Chunks of metal can be shaped into rods and put on a mount. Some metals are expensive and are purchased as powders. In this case, an epoxy can be mixed with the powder and put into a mold. During my work, I have found that usually rolled foils give the strongest signals compared to a solid rod, but have a tendency to clog up the holes in the nozzle, requiring them to be cleaned every few days. The faster setting epoxies tend to work better than the slower setting ones, but all powder/epoxy rods tend to stop working well after about a week of use.

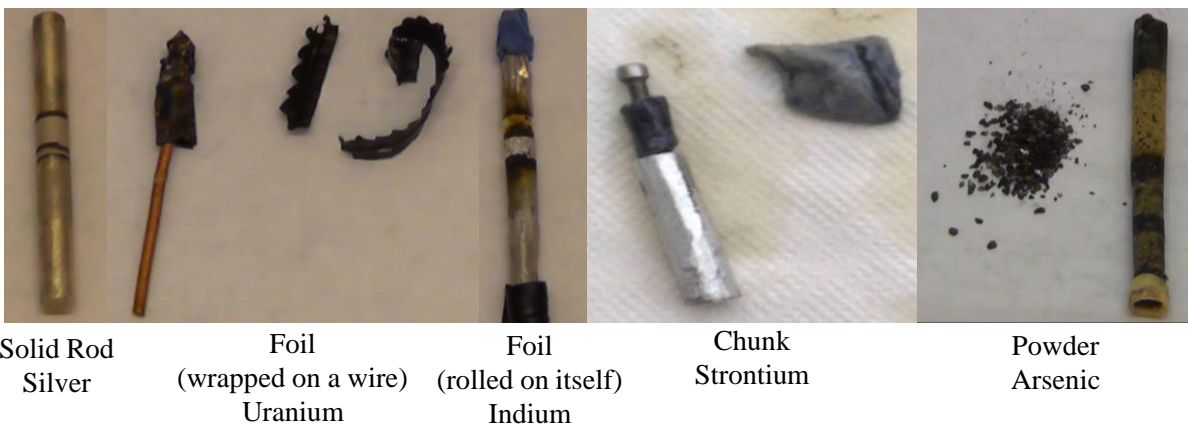


Figure 19. Various metal rods and their starting materials.



## CASE STUDIES

I have studied several molecules during my research some of which were only able to be performed because of the instruments that I have constructed. Each of the following molecules exemplifies the uses of the four instruments mentioned: the classic Balle-Flygare FTMW; the ELF-FTMW; the chirped pulse FTMW; and the laser ablation apparatus.

### Theory

#### Rotational Constants

The center of mass of a molecule is a point in space where the mass of the molecule is equal in the x, y, and z coordinate directions. This point denotes the intersection of the three principal axes a, b, and c. Convention has the a principal axis containing the largest amount of mass, followed by b, and then c with the least. The moment of inertia of the molecule is expanded into three components  $I_a$ ,  $I_b$ , and  $I_c$ .  $I_a$  is the moment of inertia of the molecule rotating about the a principal axis with  $I_b$  and  $I_c$  rotating about their respective axes. The magnitude of the moment of inertia for a molecule is determined through diagonalizing the matrix of Equation 8 whose terms are determined by Equation 9 through Equation 14.

$$I = \begin{bmatrix} I_{xx} & I_{xy} & I_{xz} \\ I_{yx} & I_{yy} & I_{yz} \\ I_{zx} & I_{zy} & I_{zz} \end{bmatrix}$$

Equation 8

$$I_{xx} = \sum_{i=1}^N m_i (y_i^2 + z_i^2)$$

Equation 9

$$I_{yy} = \sum_{i=1}^N m_i (x_i^2 + z_i^2)$$

Equation 10

$$I_{zz} = \sum_{i=1}^N m_i (x_i^2 + y_i^2)$$

Equation 11

$$I_{xy} = - \sum_{i=1}^N m_i x_i y_i$$

Equation 12

$$I_{xz} = - \sum_{i=1}^N m_i x_i z_i$$

Equation 13

$$I_{yz} = - \sum_{i=1}^N m_i y_i z_i$$

Equation 14

After diagonalizing the matrix of Equation 8,  $I_{xx}$  is one of the components of the moment of inertia,  $I_a$ ,  $I_b$ , or  $I_c$ .  $m_i$  is each of the single components of the mass along the respective axis of component of the moment of inertia of interest.  $x_i$ ,  $y_i$ , and  $z_i$  are the distance from the center of mass along each respective axis for each single mass component. Due to the a axis having the most mass along the axis and therefore least off axis mass,  $I_a$  is the smallest moment of inertia quantity. Each component of the moment of inertia denotes a rotational constant by Equation 15.

$$A = \frac{h}{8\pi^2 I_a}$$

Equation 15

A is the rotational constant that corresponds with the component of the moment of inertia,  $I_a$ .  $h$  is Planck's constant. Also, this equation works for B and C rotational constant corresponding to  $I_b$  and  $I_c$  components of the moment of inertia.

## Geometry

Molecules have one of four different classifications: linear, spherical, symmetric top, or asymmetric top. The molecules chosen for the case studies are either linear or asymmetric tops. For linear molecules, the A rotational constant is determined by  $I_a$  where the a principal axis lies along the molecular bonds. Due to the nearly nonexistent off axis mass along the a principal axis, A is generally approximated to be undefined and is not required in the energy expression. All the principal axes, a, b, and c, are orthogonal to each other making both b and c principal axes perpendicular to the molecular bonds. The rotational constants along the b and c principal axes are of the same value, so typically only B is reported.

Asymmetric tops have different values for each of the rotational constants due to the asymmetry of the molecule where  $A > B > C$ . Some asymmetric molecules are nearly symmetric tops with only slight asymmetry properties. These molecules are classified as nearly prolate,  $A > B \approx C$ , or nearly oblate,  $A \approx B > C$ . The degree of symmetry is quantified by Ray's asymmetry parameter given in Equation 16

$$\kappa = \frac{2B - A - C}{A - C}$$

Equation 16

where  $\kappa$  is Ray's asymmetry parameter and A, B, and C are rotational constants.

If  $\kappa$  is nearing -1, then the molecule is approaching an ideal prolate symmetric top. If  $\kappa$  is nearing 1, then the molecule is approaching an ideal oblate symmetric top.

## Observed Rotational Transitions

Molecular rotational energy levels are determined by Equation 17

$$W = \frac{P_x^2}{2I_x} + \frac{P_y^2}{2I_y} + \frac{P_z^2}{2I_z}$$

Equation 17

where  $W$  is the energy of rotation,  $P$  is the angular momentum, and  $I$  is the moment of inertia.

These energy levels are normally converted into terms of the rotational constants by  $I_x$ ,  $I_y$ , and  $I_z$  being designated as  $I_b$ ,  $I_c$ , and  $I_a$ . Equation 18 and Equation 19 show the relationship between the angular momentum operators and the quantum numbers  $J$  and  $K$ .

$$P^2 = P_x^2 + P_y^2 + P_z^2 = \frac{J(J+1)h^2}{4\pi^2}$$

Equation 18

$J$  is an integer that represents the rotational quantum number associated with the total angular momentum of the molecule.

$$P_z^2 = \frac{K^2 h^2}{4\pi^2}$$

Equation 19

$K$  is an integer that represents the rotational quantum number associated with a component of the angular momentum about a molecular axis. These equations make a diatomic's energy levels equal to Equation 20.

$$W = 2BhJ(J+1)$$

Equation 20

The  $B$  rotational constant is the only one shown due to  $I_a \approx 0$  and  $I_c = I_b$ . The actual observed frequency is the transition from one energy level to another shown in Equation 21.

$$\nu = \frac{W_{\text{higher}} - W_{\text{lower}}}{h}$$

Equation 21

Under the normal selection rule of  $\Delta J = 1$ , the frequency of a rotational transition for a diatomic molecule is shown in Equation 22.

$$\nu = 2B(J+1)$$

Equation 22

As shown in Equation 23, the energy level of an asymmetric molecule is a bit more complicated than a diatomic molecule.

$$\frac{W}{h} = \frac{1}{2}(A+C)J(J+1) + \frac{1}{2}(A - C)E_{mn(\kappa)}$$

Equation 23

$E_{mn(\kappa)}$  is a term whose value corresponds to Ray's asymmetry parameter and changes as  $J$ ,  $k_{-1}$ , and  $k_{+1}$  differ. Due to the tedious math involved in determining the asymmetric molecule's rotational energy levels, fitting programs are normally used to diagonalize a matrix form of the Hamiltonian.

### Centrifugal Distortion

As the molecule rotates, the centrifugal force pulls the atoms further away from each other. This causes the moment of inertia to increase and ultimately lowers the rotational energy levels. The effect of this distortion increases as the molecule rotates faster, at higher  $J$  levels, as shown in Equation 24

$$\Delta W = - \frac{J^2(J+1)^2 h^4}{128 \kappa_B \pi^4} \left[ \frac{\partial \frac{1}{I}}{\partial r} \right]^2$$

Equation 24

where  $\Delta W$  is the change in rotational energy due to the centrifugal distortion,  $\kappa_B$  is the Boltzmann constant, and  $r$  is the distance between masses. For diatomics, the centrifugal distortion causes the observed frequency to be Equation 25

$$\nu = 2B(J+1) - 4D(J+1)^3$$

Equation 25

where  $D$  is the centrifugal distortion constant specific to a molecule.

## Nuclear Quadrupole Coupling

Nuclei with a spin of 1 or greater have energy splittings when the surrounding electric field gradients interact with the spin of the nuclei. This effect is greatly dependent on molecular shape and is weaker in symmetric molecules. The energy due to this effect can be calculated by Equation 26

$$W_Q = \frac{1}{2} eQq_J \frac{\frac{3}{4}(F^4 + I^4 + J^4 + F - I - J) + \frac{3}{2}(F^3 + I^3 + J^3 + F^2 - F^2I^2 - F^2J^2 - F^2I - F^2J - FI^2 - FJ^2 - FI - FJ) + \frac{1}{2}(I^2J^2 + I^2J + IJ^2 + IJ)}{4I^2J^2 - 2I^2J - 2IJ^2 + IJ}$$

Equation 26

where  $W_Q$  is the energy of the quadrupole coupling,  $eQq_J$  is the quadrupole coupling constant.  $F$  is the quantum number for the total angular momentum including nuclear spin,  $I$  is the nuclear spin, and  $J$  is the angular momentum excluding nuclear spin quantum number. For the quadrupole coupling constant,  $e$  is the charge of one proton,  $q_J$  is the negative electric field gradient in the direction of  $J$ , and  $Q$  is the nuclear quadrupole moment.  $F$  is defined as shown in Equation 27.

$$F = I + J, I + J - 1, I + J - 2, \dots, |I - J|$$

Equation 27

## Spectral Analysis

### Simple Patterns

Identifying spectral patterns is very important when attempting to create a good parameter fit for a molecule. In the simplified model of a linear molecule, all the transitions are evenly spaced and the intensities are determined by the Boltzmann distribution of the populated energy levels as depicted in Figure 20.



Figure 20. Depiction of a simple spectral pattern for a linear molecule.

A symmetric top is very similar to the linear molecular pattern except the moment of inertia along the molecular axis causes additional transitions to occur at slightly different frequencies. These additional lines are distinguished through the  $K$  quantum number. There are two types of symmetric tops, prolate and oblate. In the prolate case, the molecular axis lies on the  $A$  axis causing the additional lines to be lower in frequency than  $K = 0$ . For an oblate symmetric top, the molecular axis lies upon the  $C$  axis causing the additional lines to be higher in frequency than  $K = 0$ . Figure 21 represents the spectral pattern for a prolate symmetric top while Figure 22 shows the pattern for an oblate symmetric top.

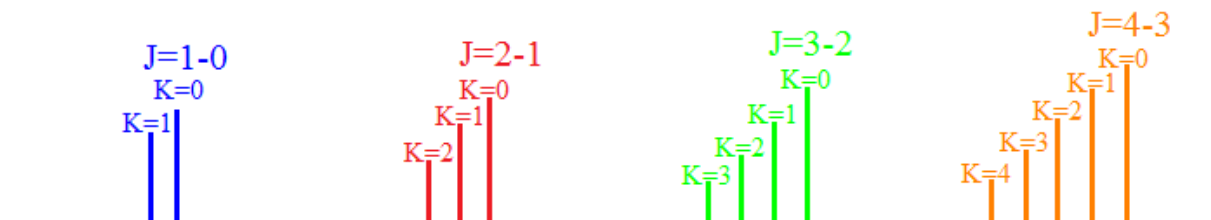


Figure 21. Depiction of a simple spectral pattern for a prolate symmetric top.

$K$  represents a change in  $K$ , for  $J = 2 \leftarrow 1$ :  $K = 0$  is  $K = 0 \leftarrow 0$ ;  $K = 1$  is  $K = 1 \leftarrow 0$ ; and  $K = 2$  is  $K = 2 \leftarrow 1$ .

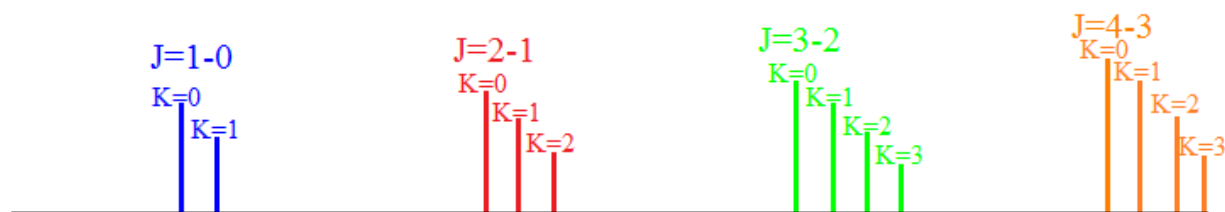


Figure 22. Depiction of a simple spectral pattern for an oblate symmetric top.

$K$  represents a change in  $K$ , for  $J = 2 \leftarrow 1$ :  $K = 0$  is  $K = 0 \leftarrow 0$ ;  $K = 1$  is  $K = 1 \leftarrow 0$ ; and  $K = 2$  is  $K = 2 \leftarrow 1$ .

For an asymmetric molecule, a single K quantum number is no longer sufficient to describe the spectral pattern, so K is described by both  $k_{-1}$  and  $k_{+1}$ . The spectral pattern for an asymmetric molecule is intermediate between that of a prolate and oblate symmetric top; some transitions are like a prolate top occurring below the main  $J'' \leftarrow J'$  transition denoted by  $k_{-1} = 0$  and some transitions are like an oblate occurring top above the main  $J'' \leftarrow J'$  transition denoted by  $k_{+1} = 0$ . If the molecule is a near prolate symmetric top then it will more closely resemble the prolate symmetric top spectral pattern, and a near oblate symmetric top will more closely resemble the oblate symmetric top pattern. Figure 23 represents the spectral pattern of an asymmetric top with a Ray's asymmetry parameter equal to zero.

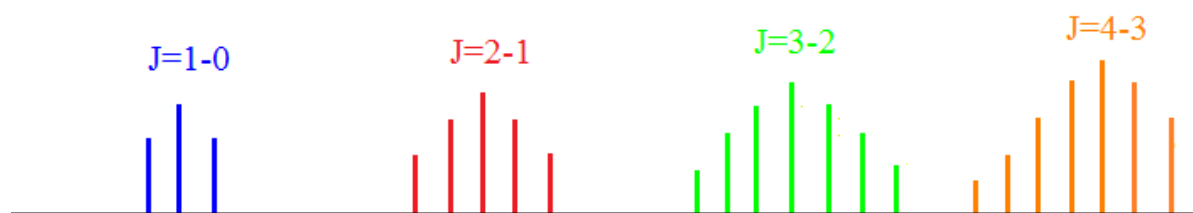


Figure 23. Depiction of a simple spectral pattern for an asymmetric top, where  $\kappa = 0$ .

#### Changes To The Simple Pattern

There are several factors that can change these simplified spectral patterns such as centrifugal distortion and nuclear quadrupole coupling. Closer examination of Equation 24 for centrifugal distortion shows that the  $\Delta W \propto -J^4$ , making the energy levels less separated at high J states. This can cause overlapping of different  $J'' \leftarrow J'$  transitions as shown in Figure 24.

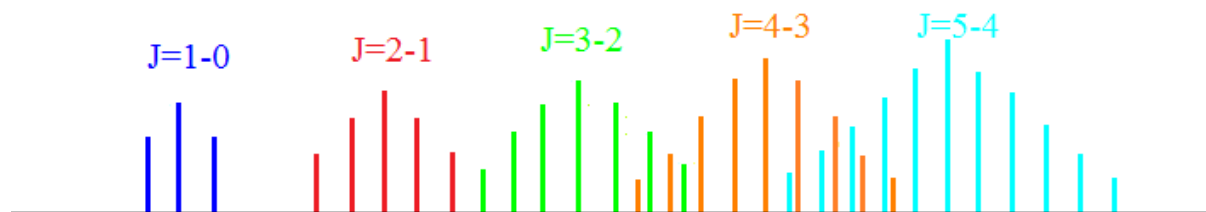


Figure 24. Depiction of the effects of centrifugal distortion on a simple spectral pattern for an asymmetric top.



Nuclear quadrupole coupling has the effect of splitting a single transition into multiple transitions. Equation 26 shows that the  $W_Q \propto \frac{F^4 - I^4 - J^4}{I^2 J^2}$ , which means that the largest splitting occurs at lower J states as shown on Figure 25.



Figure 25. Depiction of the effects of nuclear quadrupole coupling (Split) on a simple spectral pattern for a linear molecule (Unsplit).

#### Parameters

When fitting a molecule, several different parameters are used to describe the assumed Hamiltonian. Table 3 lists the parameters discussed in the following sections.

Table 3. List of Parameters

Parameter	Description
A	Largest rotational constant
B	Intermediate rotational constant
C	Smallest rotational constant
$C_A$	Formal charge (on atom A)
$c_1$	Nuclear Spin-Rotation Term
D	Dipole moment
$\Delta_{01}^A$	Born-Oppenheimer breakdown term for atom A
$\Delta_J$	Quartic centrifugal distortion terms for a Watson A Hamiltonian
$\Delta_{JK}$	Quartic centrifugal distortion terms for a Watson A Hamiltonian
$\Delta_K$	Quartic centrifugal distortion terms for a Watson A Hamiltonian
$\delta_J$	Quartic centrifugal distortion terms for a Watson A Hamiltonian
$\delta_K$	Quartic centrifugal distortion terms for a Watson A Hamiltonian
$D_J$	Quartic centrifugal distortion terms for a Watson S Hamiltonian
$D_{JK}$	Quartic centrifugal distortion terms for a Watson S Hamiltonian
$D_K$	Quartic centrifugal distortion terms for a Watson S Hamiltonian
$\delta_1$	Quartic centrifugal distortion terms for a Watson S Hamiltonian
$\delta_2$	Quartic centrifugal distortion terms for a Watson S Hamiltonian
$E_{\text{diss}}$	Dissociation Energy
F	Quantum number for the total angular momentum including nuclear spin
$H_{KJ}$	Sextet Centrifugal Distortion Constant
I	Quantum number for the spin of nucleus
J	Quantum number for the total angular momentum
K	Quantum number for a component of angular momentum along a molecular axis
$k_{-1}$	Label for the K quantum number in an asymmetric top for the prolate limit

Parameter	Description
$k_{+1}$	Label for the K quantum number in an asymmetric top for the oblate limit
$M_{aa}$	Nucleus spin-rotation tensor elements
$M_{bb}$	Nucleus spin-rotation tensor elements
$M_{cc}$	Nucleus spin-rotation tensor elements
$m_p$	Mass of a proton
$\eta_x$	Asymmetry of NQC tensor
P	Angular momentum
$P_{mix}$	Parameter indicating the purity of a state
$r_e$	Equilibrium distance between nuclei
$r_e^{BO}$	Equilibrium distance between nuclei at the bottom of the Born-Oppenheimer potential
$\theta_{za}$	Angles between the z axis and the molecular a axis
$\theta_{zb}$	Angles between the z axis and the molecular b axis
$(\mu g_J)_B$	Rotational g-factor
$U_{01}$	Mass-independent Dunham Parameter related to B
$U_{02}$	Mass-independent Dunham Parameter related to D
$U_{03}$	Mass-independent Dunham Parameter related to H
$U_{11}$	Mass-independent Dunham Parameter related to $\alpha$
$U_{12}$	Mass-independent Dunham Parameter related to $\alpha_D$
$U_{21}$	Mass-independent Dunham Parameter related to $\gamma$
$U_{22}$	Mass-independent Dunham Parameter related to $\gamma_D$
$U_{31}$	Mass-independent Dunham Parameter related to $\epsilon$
$\Phi_J$	Sextet Centrifugal Distortion Terms
$\Phi_{JK}$	Sextet Centrifugal Distortion Terms
$\Phi_{KJ}$	Sextet Centrifugal Distortion Terms
$\Phi_K$	Sextet Centrifugal Distortion Terms

Parameter	Description
$\Phi_J$	Sextet Centrifugal Distortion Terms
$\omega_e$	Vibrational frequency
$\omega_e \chi_e$	Anharmonicity constant
$\chi_{aa}$	Nuclear quadrupole coupling tensor element
$\chi_{bb}$	Nuclear quadrupole coupling tensor element
$\chi_{cc}$	Nuclear quadrupole coupling tensor element
$\chi_{ab}$	Nuclear quadrupole coupling tensor element
$\chi_{ac}$	Nuclear quadrupole coupling tensor element
$\chi_{xx}$	Nuclear quadrupole coupling in nuclei's x principal axis
$\chi_{yy}$	Nuclear quadrupole coupling in nuclei's y principal axis
$\chi_{zz}$	Nuclear quadrupole coupling in nuclei's z principal axis
$Y_{01}$	Mass-dependent Dunham Parameter related to B
$Y_{02}$	Mass-dependent Dunham Parameter related to D
$Y_{03}$	Mass-dependent Dunham Parameter related to H
$Y_{11}$	Mass-dependent Dunham Parameter related to $\alpha$
$Y_{12}$	Mass-dependent Dunham Parameter related to $\alpha_D$
$Y_{21}$	Mass-dependent Dunham Parameter related to $\gamma$
$Y_{22}$	Mass-dependent Dunham Parameter related to $\gamma_D$
$Y_{31}$	Mass-dependent Dunham Parameter related to $\epsilon$

### Experimental Practice

#### Basic Outline of Experiment

##### *Preparation of Gas*

Microwave spectroscopy is a gas phase technique that requires correct conditions in order to observe rotational transitions of a particular molecule. The correct amount of sample must first be introduced into the vacuum chamber as a gas. If the desired sample is readily available

as a gas, the sample simply needs to be mixed with a rotationally inert gas such as argon. For liquid samples, it is important that the sample has a large vapor pressure. Typically, an inert carrier gas is bubbled through the sample before being pulsed into the vacuum chamber. The temperature around the gas line containing the liquid sample can be adjusted to control the amount of sample that becomes mixed with the carrier gas. For heavy metal containing samples, a pulsed laser ablates a solid metal to create a plasma that can react with a precursor gas. The precursor gas is normally created with a very small percentage of gas that can react with the plasma and contains a majority of an inert gas. The resulting gas mixture is normally referred to as the backing gas.

The inert gas allows the backing gas to be at a high pressure which rotationally cools the sample through adiabatic expansion upon being pulsed into the low pressure vacuum chamber. There is an ideal amount of sample for a given system because the more sample that interacts with the microwaves the more intense the receiving signal, but too much sample will cause the molecules of the sample to collide in the vacuum system and decrease signal intensity. Also, getting the correct overall backing pressure is a delicate balance. Increasing the backing gas pressure allows the sample to better populate the lower rotational energy levels, but this also increases the pressure in the vacuum chamber which can lead to pressure broadening.

#### *Observing Rotational Transitions*

After the sample is in the vacuum chamber, microwaves are introduced into the molecular matrix to induce a rotational transition. As this transition occurs, the molecules begin to coherently gyrate. A receiving antenna generates a current induced by the rotating dipole of the sample as it undergoes the molecular transition. This limits FTMW spectroscopy to only observing molecules with a dipole moment. The signal is amplified and recorded in the time

domain. Then the spectra recorded in the time domain is Fourier transformed into the frequency domain giving the frequency of the rotational transition.

### Fitting

A very rough prediction of the molecules rotational parameters is created through the use of computational chemistry. The spectra produced by the computations give a general approximation of the rotational transitions. After several transitions are observed, they are analyzed for suspected spectral patterns and given tentative quantum number assignments. These assignments are inputted into a fitting program like Pickett's SPFIT program where the originally predicted rotational parameters are adjusted to best fit the newly assigned transitions through a least squares analysis. The new rotational parameters are used to predict more transitions. If the prediction is approximately correct, more lines are added to the fit. If the prediction is incorrect, the transitions are reassigned and another fit is attempted. This last process is repeated until the fit can predict transitions within the uncertainty of the instrument.

## Trans-1-Iodoperfluoropropane<sup>22</sup>

The classic Balle-Flygare spectrometer that was constructed at the University of North Texas is able to highly resolve spectra and maintain high sensitivity. This instrument was vital in the study of trans-1-iodoperfluoropropane in its ability to resolve the <sup>13</sup>C rotational transitions from the nearby parent isotopologue transitions and the sensitivity to observe forbidden transitions.

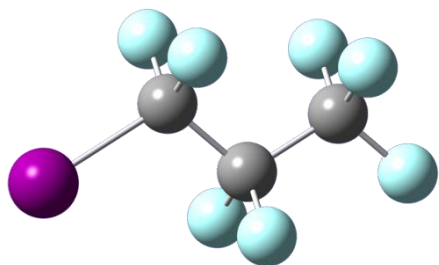


Figure 26. Depiction of trans-1-iodoperfluoropropane.

### Introduction

Forbidden transitions do not adhere to the normal selection rules for a given technique. In microwave spectroscopy, transitions of  $J \pm 1 \leftarrow J$  are observed. However, Javan proposed that using a molecule with large quadrupole coupling could saturate  $\Delta J = \pm 2$  or  $\Delta J = \pm 3$  forbidden rotational transitions. In 1966, Oka observed the first  $\Delta J = 3$  transitions while looking at ethyl iodide,  $J_{k,-1,k+1} F: 3_{0,3} \frac{7}{2} \leftarrow 0_{0,0} \frac{5}{2}$  and  $3_{0,3} \frac{5}{2} \leftarrow 0_{0,0} \frac{5}{2}$ . Oka concluded that the off diagonal quadrupole coupling term,  $\chi_{ab}$ , caused the  $3_{03}$  state to mix with the  $1_{11}$  state. Then a b-type transition that linked the  $1_{11}$  to the  $0_{00}$  state facilitated the observed  $\Delta J = 3$  transition. It appears that in order to see forbidden transitions of this nature there needs to be near degeneracy between the rotational energy levels and large off diagonal component of the quadrupole coupling tensor. With these factors in mind, 1-Iodofluoropropane seems like a rational choice to observe this phenomenon. The rotational constants were predicted to be small,  $B + C \approx 800$  MHz, allowing a

large number of energy levels to be degenerate. Also, iodine has a large quadrupole moment which should correlate into a large off diagonal quadrupole coupling tensor.<sup>23,24</sup>

## Experimental Method

Several spectrometers were used during this study of 1-Iodoperfluoropropane. The chirped pulse spectrometer was used to quickly scan a large region of frequencies to obtain enough data for the assignment of the rotational constants. The ELF-FTMW was used to measure transitions below 4 GHz. The classic Balle-Flygare Spectrometer was used to get weak transitions that needed to be highly resolved, namely the <sup>13</sup>C data and forbidden transitions.

The molecule was prepared by placing the sample in the gas line 20-30 cm before the nozzle. Approximately, 1-2 mL of 1-iodoperfluoropropane was placed in the line and had Ar backing gas bubble through it at about 1200 Torr. The 1-iodoperfluoropropane sample was purchased through Sigma-Aldrich at 98% purity with no refining necessary.

## Results

The first data was obtained with the chirped pulse FTMW spectrometer observing 2 GHz regions at a time. The data from this instrument being of correct relative intensity greatly aided the original assignment of the parent species of 1-iodopropane. First, several a-type R branch transitions were assigned where the A, B, and C rotational constants were roughly determined. Then the b-type transitions were easily assigned to refine the A rotational constant. Now having a good prediction, several transitions were observed below 2 GHz with ELF-FTMW to reduce the uncertainty of the centrifugal distortion constants and the iodine nuclear quadrupole coupling components. Then several highly resolved measurements were made on the weaker transitions with the classic Balle-Flygare spectrometer to lower the uncertainty of the constants. For the main isotopologue, 776 transitions were assigned and are in Table 9. The 710 transitions



using the chirped pulse spectrometer were given a gracious uncertainty of 25 kHz to ere on the side of caution from the line widths of approximately 30 kHz. The uncertainties attributed to the 66 cavity based measurements are 2 kHz since the spectral line widths are about 7-10 kHz. The  $^{13}\text{C}$  isotopologues were measured with only the classic Balle-Flygare spectrometer with 32, 58, and 51 transitions being recorded for C(1), C(2), and C(3)  $^{13}\text{C}$  species with the C(1) carbon being nearest to the iodine. These transitions are assigned in Table 10 - Table 12. The  $^{13}\text{C}$  transitions were difficult to observe due to the intensity of the transitions of the parent isotopologue. By far the most cumbersome isotopologue was C(1) due to the carbon being close to the center of mass of the molecule. The measurement of the  $^{13}\text{C}$  species required the high resolution of the classic Balle-Flygare spectrometer.

Pickett's SPFIT program was used in conjunction with transitions observed to obtain a weighted least squares fit for the Hamiltonian. A Watson S reduced Hamiltonian was used in the fits for each isotopologue to account for them being nearly prolate asymmetric tops. The parameters from this fitting procedure are given in Table 4.

Table 4. Parameters For Isotopologues of Trans-1-iodoperfluoropropane

Parameter	CF <sub>3</sub> CF <sub>2</sub> CF <sub>2</sub> I	CF <sub>3</sub> CF <sub>2</sub> <sup>13</sup> CF <sub>2</sub> I	CF <sub>3</sub> <sup>13</sup> CF <sub>2</sub> CF <sub>2</sub> I	<sup>13</sup> CF <sub>3</sub> CF <sub>2</sub> CF <sub>2</sub> I
A/MHz	1572.127966(99)	1569.5686(12)	1571.08577(60)	1572.17498(60)
B/MHz	398.458568(34)	398.48367(16)	398.132786(87)	396.461622(70)
C/MHz	382.831125(34)	382.72872(14)	382.465835(61)	380.987202(47)
D <sub>J</sub> /kHz	0.008305(39)	0.00837(36)	0.0081(15)	0.00799(12)
D <sub>JK</sub> /kHz	0.00986(12)	[0.00986]	[0.00986]	[0.00986]
D <sub>K</sub> /kHz	0.05172(94)	[0.05172]	[0.05172]	[0.05172]
δ <sub>1</sub> /kHz	-0.000394(11)	[-0.000394]	[-0.000394]	[-0.000394]
δ <sub>2</sub> /kHz	0.0000377(25)	[0.0000377]	[0.0000377]	[0.0000377]
χ <sub>aa</sub> /MHz	-1798.4013(48)	-1798.69(38)	-1797.67(21)	-1798.65(18)
χ <sub>bb</sub> /MHz	716.0883(62)	716.12(63)	715.25(39)	716.2(33)
χ <sub>cc</sub> /MHz	1082.313(11)	1082.57(25)	1082.42(12)	1082.45(10)
χ <sub>ab</sub> /MHz	991.7058(35)	992.34(63)	991.80(27)	992.05(25)
N	776	32	58	51
σ <sub>rms</sub> /kHz	5.14	2.87	2.22	1.82

Numbers in parenthesis indicate one standard deviation in units of the least significant figure. Numbers in brackets are the distortion constants held fix to the values obtained for the parent isotopologue. N is the number of observed transitions used in the fit. σ<sub>rms</sub> is the root mean square deviation of the fit,  $\sqrt{\left(\sum \left[\left(\frac{\text{obs-calc}}{\text{error}}\right)^2\right] / N_{\text{lines}}\right)}$ .

Several forbidden transitions were observed that had ΔJ = 2 and one transition which had ΔJ = 3. These forbidden transitions were predicted to be relatively strong for forbidden transitions due to the large off diagonal quadrupole coupling tensor, but most of these transitions did require the extra sensitivity of the classic Balle-Flygare spectrometer to be accurately measured. Table 5 lists all the forbidden transitions observed during the study of trans-1-iodoperfluoropropane.

Table 5. Observed Forbidden Transitions For Trans-1-iodopropane

J'	K-1	K+1	F'	$P_{mix}$	J''	K-1	K+1	F''	$P_{mix}$	Frequency (MHz)	Obs-Calc (kHz)
14	0	14	27/2	0.6424	12	3	9	25/2	0.9959	10165.2841	-3.8
14	4	11	31/2	0.9959	12	5	8	29/2	0.9658	10361.2984	3.9
14	4	10	31/2	0.7418	12	5	7	29/2	0.9657	10361.4639	3.3
14	4	11	23/2	0.9489	12	5	8	21/2	0.8760	10648.5261	-3.1
14	4	10	23/2	0.9490	12	5	7	21/2	0.8759	10648.6937	-4.7
15	0	15	29/2	0.9991	13	3	10	27/2	0.6416	11642.9576	-5.2
15	4	12	33/2	0.9816	13	5	9	31/2	0.7416	11950.6428	6.0
15	4	11	33/2	0.9816	13	5	8	31/2	0.7419	11950.9650	6.4
16	9	7	31/2	0.9991	13	10	4	29/2	0.9689	12641.0894	0.0
17	5	13	37/2	0.9270	15	6	10	35/2	0.9676	12690.0811	-1.7
17	5	12	37/2	0.7157	15	6	9	35/2	0.9676	12690.0948	1.0
17	5	13	29/2	0.9454	15	6	10	27/2	0.8857	12976.9394	6.0
19	6	13	33/2	0.8951	17	7	10	31/2	0.9872	13688.4654	4.4
20	6	15	41/2	0.9120	18	7	12	39/2	0.9874	15047.9181	-0.5
20	6	15	37/2	0.9462	18	7	12	35/2	0.9586	15210.7676	-6.3
20	6	15	35/2	0.9416	18	7	12	33/2	0.8945	15305.6898	-5.2

$P_{mix}$  is the mixing coefficient for the rotational energy level obtained from the SPCAT software, where 1 indicates the state to be free of perturbation and 0.5 indicates complete two state mixing.

## Discussion

The iodine quadrupole coupling tensors,  $\chi_{aa}$ ,  $\chi_{bb}$ ,  $\chi_{cc}$ , and  $\chi_{ab}$ , were determined in this study. The quadrupole coupling tensors are rotated in the principal axis system to compare with trans-1-iodopropane in Table 6. The expected effect of increasing the electronegativity of the

alkyl group upon fluorination is demonstrated with the increase of magnitude of the  $\chi_{zz}$  term of the fluorinated specie.<sup>25</sup>

Table 6. The Iodine Nuclear Quadrupole Coupling Tensor Rotated Into The Principal Axis System For The Parent Isotopologue of Trans-1-iodoperfluoropropane With Comparison to Trans-1-iodopropane.

Parameter	CF <sub>3</sub> CF <sub>2</sub> CF <sub>2</sub> I	CH <sub>3</sub> CH <sub>2</sub> CH <sub>2</sub> I
$\chi_{zz}$ /MHz	-2142.4512(49)	-1814.55(55)
$\chi_{yy}$ /MHz	1082.3130(11)	914.12(12)
$\chi_{xx}$ /MHz	1060.1382(60)	900.44(47)
$\eta_x$	0.01035(7)	0.0075(5)
$\theta_{za}$	19.133°	19.23°
$\theta_{zb}$	70.867°	70.37°

The trans-1-iodopropane data comes from the work of Fujitake and Hayashi.<sup>25</sup>  $\eta_x$  is the asymmetry of the  $\chi$  tensor in the principal axis system,  $\eta_x = (\chi_{xx} - \chi_{yy})/\chi_{zz}$ .  $\theta_{za}$  and  $\theta_{zb}$  are the angles between the z and a axis and the z and b axis, respectively.

A comparison of the iodine  $\chi_{zz}$  values from a selection of alkyl and perfluoro alkyl iodides are compared in Table 7. In the selected alkyl iodides, the  $\chi_{zz}$  component increases by approximately 10% when compared to the perfluoro counterpart. This further indicates an increase in the electronegativity of the alkyl group upon fluorination. It should be noted that the alkyl group's electronegativity decreases significantly from the CH<sub>3</sub>- to CH<sub>3</sub>CH<sub>2</sub>-, where the change is very small from the CH<sub>3</sub>CH<sub>2</sub>- to CH<sub>3</sub>CH<sub>2</sub>CH<sub>2</sub>-. This effect was not observed for the fluorinated species where the change in  $\chi_{zz}$  was small from the CF<sub>3</sub>- to CF<sub>3</sub>CF<sub>2</sub>-. This suggest that the replacement of F- with CF<sub>3</sub>- makes little difference to the perfluoroalkyl group electronegativity.

Table 7. Comparison of Iodine Nuclear Quadrupole Coupling Constant  $\chi_{zz}$  in Select Alkyl and Perfluoro Alkyl Iodides

Molecule	$\chi_{zz}$ (MHz)	Reference
CH <sub>3</sub> I	-1934.080(10)	( 26)
CH <sub>3</sub> CH <sub>2</sub> I	-1815.693(210)	( 27)
Trans-CH <sub>3</sub> CH <sub>2</sub> CH <sub>2</sub> I	-1814.55(55)	( 25)
CF <sub>3</sub> I	-2144.7(6)	( 28)
CF <sub>3</sub> CF <sub>2</sub> I	-2135.79(27)	( 29)
Trans-CF <sub>3</sub> CF <sub>2</sub> CF <sub>2</sub> I	2142.4509(76)	This Work

Part of the structure of trans-1-iododperfluoropropane was able to be determined. Each of the carbons was able to be substituted with a <sup>13</sup>C isotopologue allowing the carbon backbone to be calculated through Kraichman substitution. The structural results are on Table 8.<sup>30</sup>

Table 8. Structural Parameters Calculated Through Kraitchman Substitution of The Carbon Atoms of Trans-1-iodoperfluoropropane.

Kraitchman's Substitution Structure	Value
r (C(1) – C(2))	1.5634(2) Å
r (C(2) – C(3))	1.5781(2) Å
∠ (C(1), C(2), C(3))	113.633(14)°

Several forbidden transitions were observed during the study of trans-1-iodoperfluoropropane. The observance of these transitions has been rationalized through nearly degenerate rotational energy levels which are linked through the off diagonal quadrupole coupling component,  $\chi_{ab}$ . SPCAT was used to analyze the energy matrix the molecule. Table 5 shows the calculated mixing coefficient,  $P_{mix}$ , for each of the rotational states. Looking at the two states of the  $14_{4,10} \frac{23}{2} \leftarrow 12_{5,7} \frac{21}{2}$  transition, it can be seen that the  $P_{mix}$  values are 0.948975

and 0.875938, respectively. This indicates that the  $12_{5,7} \frac{21}{2}$  rotational state is mixing the most with an intermediate state, which was determined to be 375.82 MHz lower in frequency for the  $13_{4,9} \frac{21}{2}$  state with a  $P_{mix}$  value of 0.876786. The  $14_{4,10} \frac{23}{2} \leftarrow 13_{4,9} \frac{21}{2}$  transition is an observed allowed transition. The large  $\chi_{ab}$  value allows the  $12_{5,7} \frac{21}{2}$  state to mix and contain  $13_{4,9} \frac{21}{2}$  state character, which allowed the forbidden transition to be observed. The mechanism for this forbidden transition is illustrated in Figure 27.

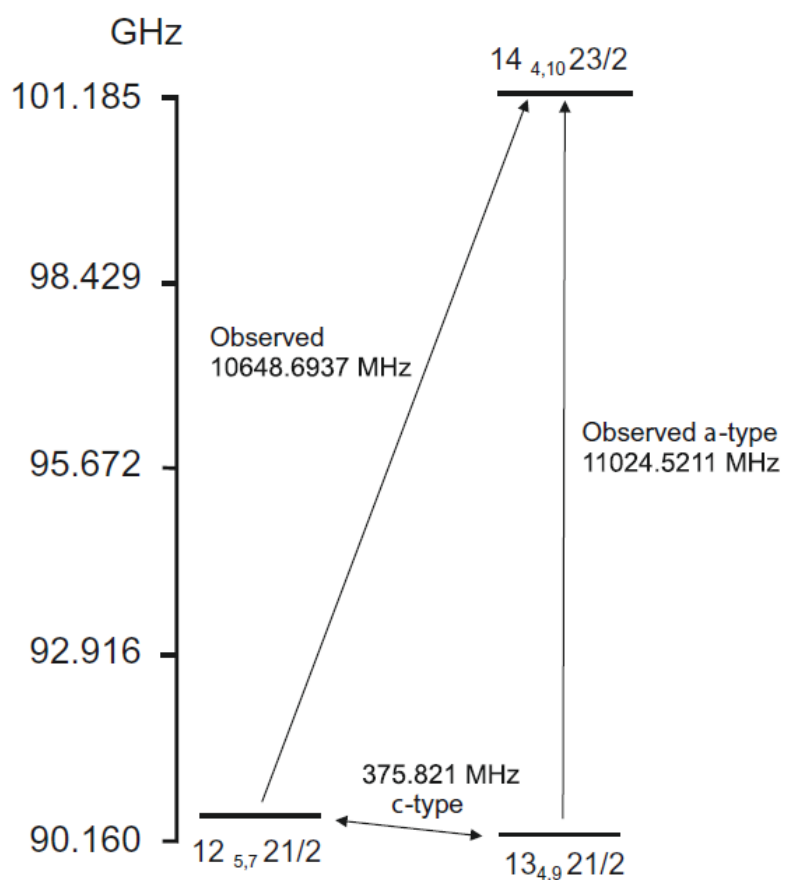


Figure 27. Schematic of the forbidden transition mechanism for the  $14_{4,10} \frac{23}{2} \leftarrow 12_{5,7} \frac{21}{2}$  transition of trans-1-iodoperfluoropropane.

The other forbidden transitions are rationalized in the same way.<sup>31</sup>

## Conclusion

This is the first time for the pure rotational spectrum of trans-1-iodoperfluoropropane to be observed. The quadrupole coupling tensors were determined including the off diagonal term  $\chi_{ab}$ . Through the high resolvability of the classic Balle-Flygare spectrometer the rotational constants of the  $^{13}\text{C}$  isotopologues were determined allowing the C-C-C bond angle and bond distances to be determined. Also, the increased sensitivity of the classic Balle-Flygare spectrometer allowed several forbidden transitions to be observed, including a  $\Delta J = 3$  transition.

Table 9. Observed Transitions For Parent Isotopologue of Trans-1-Iodoperfluoropropane, CF<sub>3</sub>CF<sub>2</sub>CF<sub>2</sub>I

Transition	Frequency (MHz)	Obs-Calc (kHz)	Uncertainty (MHz)	Transition	Frequency (MHz)	Obs-Calc (kHz)	Uncertainty (MHz)
2 <sub>0,2</sub> 5/2 ← 1 <sub>0,1</sub> 5/2	1857.9444	6.6	0.002	13 <sub>2,12</sub> 27/2 ← 12 <sub>2,11</sub> 25/2	10145.8555	1.4	0.025
2 <sub>0,2</sub> 9/2 ← 1 <sub>0,1</sub> 7/2	1613.6188	-1.4	0.002	13 <sub>2,12</sub> 29/2 ← 12 <sub>2,11</sub> 27/2	10148.7671	-1	0.025
2 <sub>1,1</sub> 3/2 ← 1 <sub>1,0</sub> 5/2	1584.9962	0	0.002	13 <sub>2,12</sub> 31/2 ← 12 <sub>2,11</sub> 29/2	10152.5907	2	0.025
2 <sub>1,1</sub> 9/2 ← 1 <sub>1,0</sub> 7/2	1742.3858	-1.5	0.002	13 <sub>3,10</sub> 21/2 ← 12 <sub>3,9</sub> 19/2	10164.8588	2.7	0.025
2 <sub>1,2</sub> 7/2 ← 1 <sub>1,1</sub> 5/2	1347.7836	7.1	0.002	13 <sub>3,10</sub> 23/2 ← 12 <sub>3,9</sub> 21/2	10158.3736	0.4	0.025
2 <sub>1,2</sub> 9/2 ← 1 <sub>1,1</sub> 7/2	1684.5452	-11.4	0.002	13 <sub>3,10</sub> 25/2 ← 12 <sub>3,9</sub> 23/2	10159.5495	-6.1	0.025
4 <sub>0,4</sub> 13/2 ← 3 <sub>0,3</sub> 11/2	3141.845	1.6	0.002	13 <sub>3,10</sub> 27/2 ← 12 <sub>3,9</sub> 25/2	10157.7182	1.9	0.002
5 <sub>0,5</sub> 15/2 ← 4 <sub>0,4</sub> 13/2	3916.1633	0	0.002	13 <sub>3,10</sub> 29/2 ← 12 <sub>3,9</sub> 27/2	10159.1559	-0.5	0.025
13 <sub>0,13</sub> 21/2 ← 12 <sub>0,12</sub> 19/2	10102.3651	-0.8	0.025	13 <sub>3,10</sub> 31/2 ← 12 <sub>3,9</sub> 29/2	10173.3986	3	0.025
13 <sub>0,13</sub> 23/2 ← 12 <sub>0,12</sub> 21/2	10098.7844	5.4	0.025	13 <sub>3,11</sub> 21/2 ← 12 <sub>3,10</sub> 19/2	10162.1803	-0.2	0.025
13 <sub>0,13</sub> 25/2 ← 12 <sub>0,12</sub> 23/2	10099.7446	-0.8	0.025	13 <sub>3,11</sub> 23/2 ← 12 <sub>3,10</sub> 21/2	10156.3918	0	0.025
13 <sub>0,13</sub> 27/2 ← 12 <sub>0,12</sub> 25/2	10103.0559	-0.3	0.025	13 <sub>3,11</sub> 25/2 ← 12 <sub>3,10</sub> 23/2	10156.8855	-1.2	0.025
13 <sub>0,13</sub> 29/2 ← 12 <sub>0,12</sub> 27/2	10106.2965	1.3	0.025	13 <sub>3,11</sub> 27/2 ← 12 <sub>3,10</sub> 25/2	10157.4723	-1.3	0.025
13 <sub>0,13</sub> 31/2 ← 12 <sub>0,12</sub> 29/2	10107.4222	-0.7	0.025	13 <sub>3,11</sub> 29/2 ← 12 <sub>3,10</sub> 27/2	10155.9248	0.4	0.025
13 <sub>1,12</sub> 21/2 ← 12 <sub>1,11</sub> 19/2	10241.5015	-4.4	0.025	13 <sub>3,11</sub> 31/2 ← 12 <sub>3,10</sub> 29/2	10170.2398	1.6	0.025
13 <sub>1,12</sub> 23/2 ← 12 <sub>1,11</sub> 21/2	10238.6856	3.6	0.025	13 <sub>4,9</sub> 21/2 ← 12 <sub>4,8</sub> 19/2	10136.9375	12.4	0.025
13 <sub>1,12</sub> 27/2 ← 12 <sub>1,11</sub> 25/2	10242.4482	1.4	0.025	13 <sub>4,9</sub> 23/2 ← 12 <sub>4,8</sub> 21/2	10145.0867	23.2	0.025
13 <sub>1,12</sub> 29/2 ← 12 <sub>1,11</sub> 27/2	10244.8375	0.4	0.025	13 <sub>4,9</sub> 25/2 ← 12 <sub>4,8</sub> 23/2	10153.0329	-1.7	0.025
13 <sub>1,12</sub> 31/2 ← 12 <sub>1,11</sub> 29/2	10246.1424	-0.3	0.025	13 <sub>4,10</sub> 25/2 ← 12 <sub>4,9</sub> 23/2	10152.9938	14.9	0.025
13 <sub>1,13</sub> 21/2 ← 12 <sub>1,12</sub> 19/2	10041.7044	0.6	0.025	13 <sub>4,10</sub> 29/2 ← 12 <sub>4,9</sub> 27/2	10146.7265	2.5	0.025
13 <sub>1,13</sub> 25/2 ← 12 <sub>1,12</sub> 23/2	10038.8129	-5.8	0.025	13 <sub>4,10</sub> 31/2 ← 12 <sub>4,9</sub> 29/2	10174.2558	-17.9	0.025
13 <sub>1,13</sub> 27/2 ← 12 <sub>1,12</sub> 25/2	10042.388	-5.1	0.025	13 <sub>5,8</sub> 25/2 ← 12 <sub>5,7</sub> 23/2	10103.2699	5.6	0.025
13 <sub>1,13</sub> 29/2 ← 12 <sub>1,12</sub> 27/2	10045.5035	-2.1	0.025	13 <sub>5,9</sub> 21/2 ← 12 <sub>5,8</sub> 19/2	10172.9935	-0.3	0.025
13 <sub>1,13</sub> 31/2 ← 12 <sub>1,12</sub> 29/2	10045.8322	4.2	0.025	13 <sub>5,9</sub> 27/2 ← 12 <sub>5,8</sub> 25/2	10142.254	7.9	0.025
13 <sub>2,11</sub> 21/2 ← 12 <sub>2,10</sub> 19/2	10198.9302	1.7	0.025	13 <sub>5,9</sub> 29/2 ← 12 <sub>5,8</sub> 27/2	10132.7872	1	0.025
13 <sub>2,11</sub> 23/2 ← 12 <sub>2,10</sub> 21/2	10196.2424	0.2	0.025	13 <sub>6,7</sub> 21/2 ← 12 <sub>6,6</sub> 19/2	10181.0423	-3.5	0.025
13 <sub>2,11</sub> 25/2 ← 12 <sub>2,10</sub> 23/2	10197.3987	1.1	0.025	13 <sub>6,7</sub> 23/2 ← 12 <sub>6,6</sub> 21/2	10159.9421	-3.7	0.025
13 <sub>2,11</sub> 27/2 ← 12 <sub>2,10</sub> 25/2	10200.0565	0	0.025	13 <sub>6,7</sub> 25/2 ← 12 <sub>6,6</sub> 23/2	10144.4078	-0.9	0.025
13 <sub>2,11</sub> 29/2 ← 12 <sub>2,10</sub> 27/2	10202.1662	0.2	0.025	13 <sub>6,7</sub> 27/2 ← 12 <sub>6,6</sub> 25/2	10139.4759	0.6	0.025
13 <sub>2,11</sub> 31/2 ← 12 <sub>2,10</sub> 29/2	10203.9206	7.1	0.025	13 <sub>6,7</sub> 31/2 ← 12 <sub>6,6</sub> 29/2	10182.0049	1.2	0.025
13 <sub>2,12</sub> 21/2 ← 12 <sub>2,11</sub> 19/2	10147.6372	-3	0.025	13 <sub>6,8</sub> 29/2 ← 12 <sub>6,7</sub> 27/2	10150.064	1.1	0.025
13 <sub>2,12</sub> 23/2 ← 12 <sub>2,11</sub> 21/2	10143.2371	0	0.025	13 <sub>7,6</sub> 21/2 ← 12 <sub>7,5</sub> 19/2	10188.5304	-1.1	0.025
13 <sub>2,12</sub> 25/2 ← 12 <sub>2,11</sub> 23/2	10143.3782	-0.3	0.025	13 <sub>7,6</sub> 23/2 ← 12 <sub>7,5</sub> 21/2	10153.4352	3.6	0.025



(Table 9 continued)

Transition	Frequency (MHz)	Obs-Calc (kHz)	Uncertainty (MHz)	Transition	Frequency (MHz)	Obs-Calc (kHz)	Uncertainty (MHz)
13 <sub>7,6</sub> 25/2 ← 12 <sub>7,5</sub> 23/2	10134.4042	-0.4	0.025	13 <sub>5,9</sub> 31/2 ← 13 <sub>4,10</sub> 29/2	10755.7316	-22.4	0.025
13 <sub>7,6</sub> 27/2 ← 12 <sub>7,5</sub> 25/2	10131.1762	2.1	0.025	14 <sub>0,14</sub> 23/2 ← 13 <sub>0,13</sub> 21/2	10873.7577	-0.5	0.025
13 <sub>7,6</sub> 29/2 ← 12 <sub>7,5</sub> 27/2	10145.4532	-0.2	0.025	14 <sub>0,14</sub> 25/2 ← 13 <sub>0,13</sub> 23/2	10870.3121	0.4	0.025
13 <sub>7,6</sub> 31/2 ← 12 <sub>7,5</sub> 29/2	10187.1048	0	0.025	14 <sub>0,14</sub> 27/2 ← 13 <sub>0,13</sub> 25/2	10872.2722	0.8	0.002
13 <sub>8,5</sub> 21/2 ← 12 <sub>8,4</sub> 19/2	10200.9837	-0.8	0.025	14 <sub>0,14</sub> 27/2 ← 13 <sub>0,13</sub> 27/2	10917.8187	-9.6	0.002
13 <sub>8,5</sub> 25/2 ← 12 <sub>8,4</sub> 23/2	10131.611	2.1	0.025	14 <sub>0,14</sub> 29/2 ← 13 <sub>0,13</sub> 27/2	10871.9865	-0.8	0.025
13 <sub>8,5</sub> 27/2 ← 12 <sub>8,4</sub> 25/2	10122.6382	3.2	0.025	14 <sub>0,14</sub> 31/2 ← 13 <sub>0,13</sub> 29/2	10874.4854	0.8	0.025
13 <sub>8,5</sub> 29/2 ← 12 <sub>8,4</sub> 27/2	10140.8231	1.9	0.025	14 <sub>0,14</sub> 33/2 ← 13 <sub>0,13</sub> 31/2	10876.5326	2.8	0.025
13 <sub>8,5</sub> 31/2 ← 12 <sub>8,4</sub> 29/2	10194.3106	1.7	0.025	14 <sub>1,13</sub> 23/2 ← 13 <sub>1,12</sub> 21/2	11026.7998	-1.8	0.025
13 <sub>9,4</sub> 21/2 ← 12 <sub>9,3</sub> 19/2	10214.1495	-5.5	0.025	14 <sub>1,13</sub> 25/2 ← 13 <sub>1,12</sub> 23/2	11024.256	0.7	0.025
13 <sub>9,4</sub> 23/2 ← 12 <sub>9,3</sub> 21/2	10161.5931	-3.1	0.025	14 <sub>1,13</sub> 27/2 ← 13 <sub>1,12</sub> 25/2	11025.0386	-0.1	0.025
13 <sub>9,4</sub> 25/2 ← 12 <sub>9,3</sub> 23/2	10125.8822	2.3	0.025	14 <sub>1,13</sub> 29/2 ← 13 <sub>1,12</sub> 27/2	11027.4412	4.4	0.025
13 <sub>9,4</sub> 27/2 ← 12 <sub>9,3</sub> 25/2	10114.4619	0	0.025	14 <sub>1,13</sub> 31/2 ← 13 <sub>1,12</sub> 29/2	11029.6987	0.1	0.025
13 <sub>9,4</sub> 29/2 ← 12 <sub>9,3</sub> 27/2	10136.3924	2.8	0.025	14 <sub>1,13</sub> 33/2 ← 13 <sub>1,12</sub> 31/2	11030.7238	1.6	0.025
13 <sub>9,4</sub> 31/2 ← 12 <sub>9,3</sub> 29/2	10202.7571	-5.3	0.025	14 <sub>1,14</sub> 23/2 ← 13 <sub>1,13</sub> 21/2	10811.1569	0.1	0.025
13 <sub>10,3</sub> 23/2 ← 12 <sub>10,2</sub> 21/2	10163.3668	-0.5	0.025	14 <sub>1,14</sub> 25/2 ← 13 <sub>1,13</sub> 23/2	10807.7632	1.8	0.025
13 <sub>10,3</sub> 25/2 ← 12 <sub>10,2</sub> 23/2	10114.9596	1.3	0.025	14 <sub>1,14</sub> 27/2 ← 13 <sub>1,13</sub> 25/2	10810.0355	2.6	0.025
13 <sub>10,3</sub> 27/2 ← 12 <sub>10,2</sub> 25/2	10095.6118	-11.2	0.025	14 <sub>1,14</sub> 29/2 ← 13 <sub>1,13</sub> 27/2	10813.2352	2.8	0.025
13 <sub>10,3</sub> 29/2 ← 12 <sub>10,2</sub> 27/2	10125.7227	4.8	0.025	14 <sub>1,14</sub> 31/2 ← 13 <sub>1,13</sub> 29/2	10816.2782	0	0.025
13 <sub>10,3</sub> 31/2 ← 12 <sub>10,2</sub> 29/2	10210.2098	2.7	0.025	14 <sub>1,14</sub> 33/2 ← 13 <sub>1,13</sub> 31/2	10816.0102	2.3	0.025
13 <sub>11,2</sub> 25/2 ← 12 <sub>11,1</sub> 23/2	10109.6966	-10.6	0.025	14 <sub>2,12</sub> 23/2 ← 13 <sub>2,11</sub> 21/2	10989.7676	1.4	0.025
13 <sub>11,2</sub> 27/2 ← 12 <sub>11,1</sub> 25/2	10092.2537	-7.5	0.025	14 <sub>2,12</sub> 25/2 ← 13 <sub>2,11</sub> 23/2	10987.7751	-0.6	0.025
14 <sub>0,14</sub> 27/2 ← 12 <sub>3,9</sub> 25/2	10165.2841	-3.8	0.002	14 <sub>2,12</sub> 27/2 ← 13 <sub>2,11</sub> 25/2	10988.9526	1.9	0.025
14 <sub>4,10</sub> 23/2 ← 12 <sub>5,7</sub> 21/2	10648.6937	-4.7	0.025	14 <sub>2,12</sub> 29/2 ← 13 <sub>2,11</sub> 27/2	10991.3385	-0.5	0.025
14 <sub>4,10</sub> 31/2 ← 12 <sub>5,7</sub> 29/2	10361.4639	3.3	0.002	14 <sub>2,12</sub> 31/2 ← 13 <sub>2,11</sub> 29/2	10993.1623	-0.6	0.025
14 <sub>4,11</sub> 23/2 ← 12 <sub>5,8</sub> 21/2	10648.5261	-3.1	0.025	14 <sub>2,12</sub> 33/2 ← 13 <sub>2,11</sub> 31/2	10994.0185	5.1	0.025
14 <sub>4,11</sub> 31/2 ← 12 <sub>5,8</sub> 29/2	10361.2984	3.9	0.002	14 <sub>2,13</sub> 23/2 ← 13 <sub>2,12</sub> 21/2	10926.6256	-0.7	0.025
13 <sub>3,10</sub> 27/2 ← 13 <sub>0,13</sub> 25/2	10864.7056	5.9	0.002	14 <sub>2,13</sub> 25/2 ← 13 <sub>2,12</sub> 23/2	10922.8694	-2.3	0.025
13 <sub>3,10</sub> 27/2 ← 13 <sub>0,13</sub> 27/2	10910.2596	2.9	0.002	14 <sub>2,13</sub> 27/2 ← 13 <sub>2,12</sub> 25/2	10923.0222	-1.1	0.025
13 <sub>5,8</sub> 21/2 ← 13 <sub>4,9</sub> 21/2	10632.6831	1.4	0.002	14 <sub>2,13</sub> 31/2 ← 13 <sub>2,12</sub> 29/2	10927.9149	-1.2	0.025
13 <sub>5,8</sub> 23/2 ← 13 <sub>4,9</sub> 21/2	10457.6902	11.5	0.025	14 <sub>2,13</sub> 33/2 ← 13 <sub>2,12</sub> 31/2	10930.8286	-2.5	0.025
13 <sub>5,9</sub> 21/2 ← 13 <sub>4,10</sub> 21/2	10632.7749	2	0.002	14 <sub>3,11</sub> 23/2 ← 13 <sub>3,10</sub> 21/2	10949.8029	-1.6	0.025
13 <sub>5,9</sub> 23/2 ← 13 <sub>4,10</sub> 21/2	10457.7498	-10.1	0.025	14 <sub>3,11</sub> 27/2 ← 13 <sub>3,10</sub> 25/2	10945.6711	20.1	0.025

(Table 9 continued)

Transition	Frequency (MHz)	Obs-Calc (kHz)	Uncertainty (MHz)	Transition	Frequency (MHz)	Obs-Calc (kHz)	Uncertainty (MHz)
14 <sub>3,11</sub> 27/2 ← 13 <sub>3,10</sub> 27/2	10980.3683	-6.2	0.002	14 <sub>7,7</sub> 33/2 ← 13 <sub>7,6</sub> 31/2	10963.6421	4.1	0.025
14 <sub>3,11</sub> 29/2 ← 13 <sub>3,10</sub> 27/2	10948.5467	0.5	0.002	14 <sub>8,6</sub> 23/2 ← 13 <sub>8,5</sub> 21/2	10974.2662	2.9	0.025
14 <sub>3,11</sub> 31/2 ← 13 <sub>3,10</sub> 29/2	10946.7448	-0.8	0.025	14 <sub>8,6</sub> 25/2 ← 13 <sub>8,5</sub> 23/2	10942.0198	-0.5	0.025
14 <sub>3,11</sub> 33/2 ← 13 <sub>3,10</sub> 31/2	10953.3211	-5.9	0.025	14 <sub>8,6</sub> 27/2 ← 13 <sub>8,5</sub> 25/2	10920.4196	2.1	0.025
14 <sub>3,12</sub> 25/2 ← 13 <sub>3,11</sub> 23/2	10940.9005	6.9	0.025	14 <sub>8,6</sub> 29/2 ← 13 <sub>8,5</sub> 27/2	10913.5245	1	0.025
14 <sub>3,12</sub> 27/2 ← 13 <sub>3,11</sub> 25/2	10940.408	-2.6	0.025	14 <sub>8,6</sub> 31/2 ← 13 <sub>8,5</sub> 29/2	10926.4085	-0.7	0.025
14 <sub>3,12</sub> 29/2 ← 13 <sub>3,11</sub> 27/2	10941.5176	1.8	0.025	14 <sub>8,6</sub> 33/2 ← 13 <sub>8,5</sub> 31/2	10969.2207	2.3	0.025
14 <sub>3,12</sub> 31/2 ← 13 <sub>3,11</sub> 29/2	10943.0757	-3.2	0.025	14 <sub>9,5</sub> 23/2 ← 13 <sub>9,4</sub> 21/2	10983.1376	4.5	0.025
14 <sub>3,12</sub> 33/2 ← 13 <sub>3,11</sub> 31/2	10951.2778	4.1	0.025	14 <sub>9,5</sub> 27/2 ← 13 <sub>9,4</sub> 25/2	10912.6992	-1	0.025
14 <sub>4,10</sub> 23/2 ← 13 <sub>4,9</sub> 21/2	11024.5211	-10.8	0.002	14 <sub>9,5</sub> 29/2 ← 13 <sub>9,4</sub> 27/2	10904.2831	0.3	0.025
14 <sub>4,10</sub> 25/2 ← 13 <sub>4,9</sub> 23/2	10986.0441	-14.7	0.025	14 <sub>9,5</sub> 31/2 ← 13 <sub>9,4</sub> 29/2	10922.5042	3.3	0.025
14 <sub>4,10</sub> 29/2 ← 13 <sub>4,9</sub> 27/2	10957.278	5.7	0.025	14 <sub>9,5</sub> 33/2 ← 13 <sub>9,4</sub> 31/2	10975.937	5.5	0.025
14 <sub>4,11</sub> 25/2 ← 13 <sub>4,10</sub> 23/2	10985.9648	-6.8	0.025	14 <sub>10,4</sub> 23/2 ← 13 <sub>10,3</sub> 21/2	10994.6039	-2.8	0.025
14 <sub>4,11</sub> 29/2 ← 13 <sub>4,10</sub> 27/2	10957.1913	9.2	0.025	14 <sub>10,4</sub> 27/2 ← 13 <sub>10,3</sub> 25/2	10909.4463	1.5	0.025
14 <sub>4,11</sub> 33/2 ← 13 <sub>4,10</sub> 31/2	10953.234	8.1	0.025	14 <sub>10,4</sub> 29/2 ← 13 <sub>10,3</sub> 27/2	10902.999	3.7	0.025
14 <sub>5,9</sub> 25/2 ← 13 <sub>5,8</sub> 23/2	10954.6962	4.4	0.025	14 <sub>10,4</sub> 33/2 ← 13 <sub>10,3</sub> 31/2	10984.2861	3.2	0.025
14 <sub>5,9</sub> 29/2 ← 13 <sub>5,8</sub> 27/2	10932.1583	8.3	0.025	14 <sub>10,5</sub> 29/2 ← 13 <sub>10,4</sub> 29/2	10966.0377	-3.8	0.002
14 <sub>5,10</sub> 23/2 ← 13 <sub>5,9</sub> 21/2	10950.5238	0.4	0.025	14 <sub>10,5</sub> 31/2 ← 13 <sub>10,4</sub> 29/2	10922.5037	0.4	0.002
14 <sub>5,10</sub> 27/2 ← 13 <sub>5,9</sub> 25/2	10945.8436	0.7	0.025	14 <sub>11,3</sub> 23/2 ← 13 <sub>11,2</sub> 21/2	11007.556	-7.4	0.025
14 <sub>5,10</sub> 29/2 ← 13 <sub>5,9</sub> 27/2	10932.1583	-5.6	0.025	14 <sub>11,3</sub> 25/2 ← 13 <sub>11,2</sub> 23/2	10943.2216	-11.9	0.025
14 <sub>5,10</sub> 31/2 ← 13 <sub>5,9</sub> 29/2	10946.9133	-1.8	0.025	14 <sub>11,3</sub> 27/2 ← 13 <sub>11,2</sub> 25/2	10900.1952	-5.1	0.025
14 <sub>5,10</sub> 33/2 ← 13 <sub>5,9</sub> 31/2	11009.9424	0	0.002	14 <sub>11,3</sub> 29/2 ← 13 <sub>11,2</sub> 27/2	10887.4238	3.1	0.025
14 <sub>6,8</sub> 23/2 ← 13 <sub>6,7</sub> 21/2	10957.624	-3.5	0.025	14 <sub>11,3</sub> 31/2 ← 13 <sub>11,2</sub> 29/2	10914.8325	-1.3	0.025
14 <sub>6,8</sub> 27/2 ← 13 <sub>6,7</sub> 25/2	10930.3534	-7.4	0.025	14 <sub>11,3</sub> 33/2 ← 13 <sub>11,2</sub> 31/2	10992.3146	-7.7	0.025
14 <sub>6,8</sub> 29/2 ← 13 <sub>6,7</sub> 27/2	10925.1922	7.8	0.025	14 <sub>12,2</sub> 27/2 ← 13 <sub>12,1</sub> 25/2	10892.2073	-1.8	0.025
14 <sub>6,8</sub> 31/2 ← 13 <sub>6,7</sub> 29/2	10934.4866	0.7	0.025	14 <sub>12,2</sub> 29/2 ← 13 <sub>12,1</sub> 27/2	10876.854	-10.8	0.025
14 <sub>6,8</sub> 33/2 ← 13 <sub>6,7</sub> 31/2	10961.5763	3.9	0.025	14 <sub>12,2</sub> 31/2 ← 13 <sub>12,1</sub> 29/2	10909.8189	5.8	0.025
14 <sub>6,9</sub> 25/2 ← 13 <sub>6,8</sub> 23/2	10944.4413	-1	0.025	14 <sub>12,2</sub> 33/2 ← 13 <sub>12,1</sub> 31/2	11000.413	7.8	0.025
14 <sub>7,7</sub> 23/2 ← 13 <sub>7,6</sub> 21/2	10964.7825	3.1	0.025	15 <sub>0,15</sub> 29/2 ← 13 <sub>3,10</sub> 27/2	11642.9576	-5.2	0.025
14 <sub>7,7</sub> 25/2 ← 13 <sub>7,6</sub> 23/2	10939.8559	-1.2	0.025	15 <sub>4,11</sub> 33/2 ← 13 <sub>5,8</sub> 31/2	11950.965	6.4	0.002
14 <sub>7,7</sub> 27/2 ← 13 <sub>7,6</sub> 25/2	10923.4038	-2.5	0.025	15 <sub>4,12</sub> 33/2 ← 13 <sub>5,9</sub> 31/2	11950.6428	6	0.002
14 <sub>7,7</sub> 29/2 ← 13 <sub>7,6</sub> 27/2	10918.8245	-0.6	0.025	16 <sub>9,7</sub> 31/2 ← 13 <sub>10,4</sub> 29/2	12641.0894	-0.1	0.002
14 <sub>7,7</sub> 31/2 ← 13 <sub>7,6</sub> 29/2	10930.2534	8.3	0.025	14 <sub>3,11</sub> 29/2 ← 14 <sub>0,14</sub> 27/2	10940.986	11.6	0.025

(Table 9 continued)

Transition	Frequency (MHz)	Obs-Calc (kHz)	Uncertainty (MHz)	Transition	Frequency (MHz)	Obs-Calc (kHz)	Uncertainty (MHz)
14 <sub>5,10</sub> 33/2 ← 14 <sub>4,11</sub> 31/2	10728.2474	-1.7	0.002	15 <sub>3,12</sub> 25/2 ← 14 <sub>3,11</sub> 23/2	11734.1386	0.8	0.025
14 <sub>5,10</sub> 33/2 ← 14 <sub>4,11</sub> 33/2	10587.7297	1.7	0.002	15 <sub>3,12</sub> 27/2 ← 14 <sub>3,11</sub> 25/2	11730.2411	-1.7	0.025
15 <sub>0,15</sub> 25/2 ← 14 <sub>0,14</sub> 23/2	11640.3102	1	0.025	15 <sub>3,12</sub> 29/2 ← 14 <sub>3,11</sub> 27/2	11729.8594	0.9	0.025
15 <sub>0,15</sub> 27/2 ← 14 <sub>0,14</sub> 25/2	11636.7684	5.2	0.025	15 <sub>3,12</sub> 31/2 ← 14 <sub>3,11</sub> 29/2	11731.0595	-1.4	0.025
15 <sub>0,15</sub> 29/2 ← 14 <sub>0,14</sub> 27/2	11635.3931	1.8	0.002	15 <sub>3,12</sub> 33/2 ← 14 <sub>3,11</sub> 31/2	11733.0726	0.5	0.025
15 <sub>0,15</sub> 29/2 ← 14 <sub>0,14</sub> 29/2	11681.2246	-7.7	0.002	15 <sub>3,12</sub> 35/2 ← 14 <sub>3,11</sub> 33/2	11738.7651	1.2	0.025
15 <sub>0,15</sub> 31/2 ← 14 <sub>0,14</sub> 29/2	11641.147	2.9	0.025	15 <sub>3,13</sub> 25/2 ← 14 <sub>3,12</sub> 23/2	11728.5877	-2.6	0.025
15 <sub>0,15</sub> 33/2 ← 14 <sub>0,14</sub> 31/2	11645.2729	3.9	0.025	15 <sub>3,13</sub> 27/2 ← 14 <sub>3,12</sub> 25/2	11724.2868	0.3	0.025
15 <sub>0,15</sub> 35/2 ← 14 <sub>0,14</sub> 33/2	11644.4861	-0.3	0.025	15 <sub>3,13</sub> 29/2 ← 14 <sub>3,12</sub> 27/2	11723.7326	0.4	0.025
15 <sub>1,14</sub> 25/2 ← 14 <sub>1,13</sub> 23/2	11811.2162	-5.7	0.025	15 <sub>3,13</sub> 31/2 ← 14 <sub>3,12</sub> 29/2	11724.9703	1	0.025
15 <sub>1,14</sub> 27/2 ← 14 <sub>1,13</sub> 25/2	11808.8821	-1.9	0.025	15 <sub>3,13</sub> 33/2 ← 14 <sub>3,12</sub> 31/2	11727.0616	1.4	0.025
15 <sub>1,14</sub> 29/2 ← 14 <sub>1,13</sub> 27/2	11809.4958	0.5	0.025	15 <sub>3,13</sub> 35/2 ← 14 <sub>3,12</sub> 33/2	11732.7432	2.5	0.025
15 <sub>1,14</sub> 31/2 ← 14 <sub>1,13</sub> 29/2	11811.58	-1.7	0.025	15 <sub>4,11</sub> 25/2 ← 14 <sub>4,10</sub> 23/2	11713.8239	-1.2	0.025
15 <sub>1,14</sub> 33/2 ← 14 <sub>1,13</sub> 31/2	11813.639	1.7	0.025	15 <sub>4,11</sub> 29/2 ← 14 <sub>4,10</sub> 27/2	11718.603	0.1	0.025
15 <sub>1,14</sub> 35/2 ← 14 <sub>1,13</sub> 33/2	11814.616	-1.7	0.025	15 <sub>4,11</sub> 31/2 ← 14 <sub>4,10</sub> 29/2	11709.549	-13.2	0.025
15 <sub>1,15</sub> 25/2 ← 14 <sub>1,14</sub> 23/2	11582.0549	1.6	0.025	15 <sub>4,11</sub> 33/2 ← 14 <sub>4,10</sub> 31/2	11669.1515	-4.1	0.025
15 <sub>1,15</sub> 27/2 ← 14 <sub>1,14</sub> 25/2	11579.5945	3.9	0.025	15 <sub>4,11</sub> 35/2 ← 14 <sub>4,10</sub> 33/2	11733.665	3.2	0.025
15 <sub>1,15</sub> 29/2 ← 14 <sub>1,14</sub> 27/2	11580.6348	3.4	0.025	15 <sub>4,12</sub> 25/2 ← 14 <sub>4,11</sub> 23/2	11713.6773	3.5	0.025
15 <sub>1,15</sub> 31/2 ← 14 <sub>1,14</sub> 29/2	11583.3436	5.5	0.025	15 <sub>4,12</sub> 31/2 ← 14 <sub>4,11</sub> 29/2	11709.3825	-1.3	0.025
15 <sub>1,15</sub> 33/2 ← 14 <sub>1,14</sub> 31/2	11585.6654	0.9	0.025	15 <sub>4,12</sub> 33/2 ← 14 <sub>4,11</sub> 31/2	11668.9415	-2	0.002
15 <sub>1,15</sub> 35/2 ← 14 <sub>1,14</sub> 33/2	11585.9155	0	0.025	15 <sub>4,12</sub> 33/2 ← 14 <sub>4,11</sub> 33/2	11528.423	0.7	0.002
15 <sub>2,13</sub> 25/2 ← 14 <sub>2,12</sub> 23/2	11781.421	1.1	0.025	15 <sub>4,12</sub> 35/2 ← 14 <sub>4,11</sub> 33/2	11733.5231	3.5	0.025
15 <sub>2,13</sub> 27/2 ← 14 <sub>2,12</sub> 25/2	11779.9559	3.9	0.025	15 <sub>5,10</sub> 29/2 ← 14 <sub>5,9</sub> 27/2	11718.1811	-1.4	0.025
15 <sub>2,13</sub> 29/2 ← 14 <sub>2,12</sub> 27/2	11781.1307	2.9	0.025	15 <sub>5,10</sub> 31/2 ← 14 <sub>5,9</sub> 29/2	11714.2203	-4.7	0.025
15 <sub>2,13</sub> 31/2 ← 14 <sub>2,12</sub> 29/2	11783.2731	1.5	0.025	15 <sub>5,10</sub> 35/2 ← 14 <sub>5,9</sub> 33/2	11741.2024	-7.5	0.025
15 <sub>2,13</sub> 33/2 ← 14 <sub>2,12</sub> 31/2	11784.8227	1.7	0.025	15 <sub>5,11</sub> 25/2 ← 14 <sub>5,10</sub> 23/2	11726.6788	1.7	0.025
15 <sub>2,13</sub> 35/2 ← 14 <sub>2,12</sub> 33/2	11785.1031	1.8	0.025	15 <sub>5,11</sub> 27/2 ← 14 <sub>5,10</sub> 25/2	11722.5813	-6	0.025
15 <sub>2,14</sub> 25/2 ← 14 <sub>2,13</sub> 23/2	11705.2467	-1.7	0.025	15 <sub>6,9</sub> 25/2 ← 14 <sub>6,8</sub> 23/2	11735.4785	-1.6	0.025
15 <sub>2,14</sub> 27/2 ← 14 <sub>2,13</sub> 25/2	11701.9969	-1.5	0.025	15 <sub>6,9</sub> 33/2 ← 14 <sub>6,8</sub> 31/2	11720.5133	0.1	0.025
15 <sub>2,14</sub> 29/2 ← 14 <sub>2,13</sub> 27/2	11702.1585	-0.1	0.025	15 <sub>6,10</sub> 27/2 ← 14 <sub>6,9</sub> 25/2	11750.618	-4.6	0.025
15 <sub>2,14</sub> 31/2 ← 14 <sub>2,13</sub> 29/2	11704.1617	-1.7	0.025	15 <sub>6,10</sub> 29/2 ← 14 <sub>6,9</sub> 27/2	11724.666	-4.3	0.025
15 <sub>2,14</sub> 33/2 ← 14 <sub>2,13</sub> 31/2	11706.5738	1.2	0.025	15 <sub>6,10</sub> 31/2 ← 14 <sub>6,9</sub> 29/2	11710.3137	-0.2	0.025
15 <sub>2,14</sub> 35/2 ← 14 <sub>2,13</sub> 33/2	11708.887	0.7	0.025	15 <sub>6,10</sub> 35/2 ← 14 <sub>6,9</sub> 33/2	11748.5851	2.9	0.025

(Table 9 continued)

Transition	Frequency (MHz)	Obs-Calc (kHz)	Uncertainty (MHz)	Transition	Frequency (MHz)	Obs-Calc (kHz)	Uncertainty (MHz)
15 <sub>7,8</sub> 27/2 ← 14 <sub>7,7</sub> 25/2	11721.4927	0.3	0.025	16 <sub>0,16</sub> 29/2 ← 15 <sub>0,15</sub> 27/2	12405.15	1	0.025
15 <sub>7,8</sub> 29/2 ← 14 <sub>7,7</sub> 27/2	11708.1335	1.5	0.025	16 <sub>0,16</sub> 31/2 ← 15 <sub>0,15</sub> 29/2	12405.4885	0.3	0.025
15 <sub>7,8</sub> 31/2 ← 14 <sub>7,7</sub> 29/2	11704.5282	-2.3	0.025	16 <sub>0,16</sub> 33/2 ← 15 <sub>0,15</sub> 31/2	12407.6061	-0.4	0.025
15 <sub>7,8</sub> 35/2 ← 14 <sub>7,7</sub> 33/2	11741.5869	1.3	0.025	16 <sub>0,16</sub> 35/2 ← 15 <sub>0,15</sub> 33/2	12409.7259	-0.5	0.025
15 <sub>8,7</sub> 25/2 ← 14 <sub>8,6</sub> 23/2	11747.7366	-2.4	0.025	16 <sub>0,16</sub> 37/2 ← 15 <sub>0,15</sub> 35/2	12411.4084	-0.2	0.025
15 <sub>8,7</sub> 29/2 ← 14 <sub>8,6</sub> 27/2	11703.0861	-3.4	0.025	16 <sub>1,15</sub> 27/2 ← 15 <sub>1,14</sub> 25/2	12594.7421	-5.6	0.025
15 <sub>8,7</sub> 31/2 ← 14 <sub>8,6</sub> 29/2	11698.6341	4.8	0.025	16 <sub>1,15</sub> 29/2 ← 15 <sub>1,14</sub> 27/2	12592.5583	0	0.025
15 <sub>8,7</sub> 33/2 ← 14 <sub>8,6</sub> 31/2	11710.9376	0.1	0.025	16 <sub>1,15</sub> 31/2 ← 15 <sub>1,14</sub> 29/2	12593.02	0	0.025
15 <sub>8,7</sub> 35/2 ← 14 <sub>8,6</sub> 33/2	11745.7175	2.7	0.025	16 <sub>1,15</sub> 35/2 ← 15 <sub>1,14</sub> 33/2	12596.7358	2	0.025
15 <sub>9,6</sub> 25/2 ← 14 <sub>9,5</sub> 23/2	11758.9413	-4	0.025	16 <sub>1,15</sub> 37/2 ← 15 <sub>1,14</sub> 35/2	12597.7234	0.5	0.025
15 <sub>9,6</sub> 27/2 ← 14 <sub>9,5</sub> 25/2	11729.2325	-3.2	0.025	16 <sub>1,16</sub> 27/2 ← 15 <sub>1,15</sub> 25/2	12352.1652	-2.9	0.025
15 <sub>9,6</sub> 29/2 ← 14 <sub>9,5</sub> 27/2	11704.0876	19.2	0.025	16 <sub>1,16</sub> 29/2 ← 15 <sub>1,15</sub> 27/2	12349.9603	-1.9	0.025
15 <sub>9,6</sub> 31/2 ← 14 <sub>9,5</sub> 29/2	11694.0657	-2.6	0.025	16 <sub>1,16</sub> 31/2 ← 15 <sub>1,15</sub> 29/2	12350.8521	3.2	0.025
15 <sub>9,6</sub> 33/2 ← 14 <sub>9,5</sub> 31/2	11707.632	4.3	0.025	16 <sub>1,16</sub> 33/2 ← 15 <sub>1,15</sub> 31/2	12353.2477	-2.2	0.025
15 <sub>9,6</sub> 35/2 ← 14 <sub>9,5</sub> 33/2	11751.1004	1.4	0.025	16 <sub>1,16</sub> 35/2 ← 15 <sub>1,15</sub> 33/2	12355.3963	1.6	0.025
15 <sub>10,5</sub> 25/2 ← 14 <sub>10,4</sub> 23/2	11764.6119	-3.8	0.025	16 <sub>1,16</sub> 37/2 ← 15 <sub>1,15</sub> 35/2	12355.5371	5.5	0.025
15 <sub>10,5</sub> 27/2 ← 14 <sub>10,4</sub> 25/2	11721.7162	-9.4	0.025	16 <sub>2,14</sub> 29/2 ← 15 <sub>2,13</sub> 27/2	12572.6388	1.8	0.025
15 <sub>10,5</sub> 29/2 ← 14 <sub>10,4</sub> 27/2	11693.6708	0.7	0.025	16 <sub>2,14</sub> 33/2 ← 15 <sub>2,13</sub> 31/2	12575.7342	-0.6	0.025
15 <sub>10,5</sub> 31/2 ← 14 <sub>10,4</sub> 29/2	11685.7238	-4.9	0.025	16 <sub>2,15</sub> 27/2 ← 15 <sub>2,14</sub> 25/2	12483.4865	-2.6	0.025
15 <sub>10,5</sub> 33/2 ← 14 <sub>10,4</sub> 31/2	11704.3464	6.6	0.025	16 <sub>2,15</sub> 29/2 ← 15 <sub>2,14</sub> 27/2	12480.6368	-1.6	0.025
15 <sub>10,5</sub> 35/2 ← 14 <sub>10,4</sub> 33/2	11757.3167	-0.3	0.025	16 <sub>2,15</sub> 31/2 ← 15 <sub>2,14</sub> 29/2	12480.7992	-3	0.025
15 <sub>11,4</sub> 25/2 ← 14 <sub>11,3</sub> 23/2	11774.8012	10	0.025	16 <sub>2,15</sub> 33/2 ← 15 <sub>2,14</sub> 31/2	12482.6099	-1.4	0.025
15 <sub>11,4</sub> 29/2 ← 14 <sub>11,3</sub> 27/2	11687.0578	-5.4	0.025	16 <sub>2,15</sub> 35/2 ← 15 <sub>2,14</sub> 33/2	12484.7846	0	0.025
15 <sub>11,4</sub> 31/2 ← 14 <sub>11,3</sub> 29/2	11676.3031	-3.3	0.025	16 <sub>2,15</sub> 37/2 ← 15 <sub>2,14</sub> 35/2	12486.6851	-0.1	0.025
15 <sub>11,4</sub> 35/2 ← 14 <sub>11,3</sub> 33/2	11762.6317	4.1	0.025	16 <sub>3,13</sub> 27/2 ← 15 <sub>3,12</sub> 25/2	12518.7611	1.2	0.025
15 <sub>12,3</sub> 25/2 ← 14 <sub>12,2</sub> 23/2	11786.1951	2.6	0.025	16 <sub>3,13</sub> 29/2 ← 15 <sub>3,12</sub> 27/2	12515.4832	1.4	0.025
15 <sub>12,3</sub> 27/2 ← 14 <sub>12,2</sub> 25/2	11723.3172	-2.4	0.025	16 <sub>3,13</sub> 31/2 ← 15 <sub>3,12</sub> 29/2	12515.2257	-0.7	0.025
15 <sub>12,3</sub> 29/2 ← 14 <sub>12,2</sub> 27/2	11681.8386	-0.3	0.025	16 <sub>3,13</sub> 33/2 ← 15 <sub>3,12</sub> 31/2	12516.4966	0.7	0.025
15 <sub>12,3</sub> 31/2 ← 14 <sub>12,2</sub> 29/2	11670.1666	-7.7	0.025	16 <sub>3,13</sub> 35/2 ← 15 <sub>3,12</sub> 33/2	12518.4475	-2	0.025
15 <sub>12,3</sub> 33/2 ← 14 <sub>12,2</sub> 31/2	11697.2172	1.2	0.025	16 <sub>3,13</sub> 37/2 ← 15 <sub>3,12</sub> 35/2	12522.3341	2.7	0.025
15 <sub>12,3</sub> 35/2 ← 14 <sub>12,2</sub> 33/2	11771.5431	-1.1	0.025	16 <sub>3,14</sub> 27/2 ← 15 <sub>3,13</sub> 25/2	12511.0686	-2.6	0.025
15 <sub>13,2</sub> 33/2 ← 14 <sub>13,1</sub> 31/2	11693.327	3.2	0.025	16 <sub>3,14</sub> 29/2 ← 15 <sub>3,13</sub> 27/2	12507.3825	-0.9	0.025
16 <sub>0,16</sub> 27/2 ← 15 <sub>0,15</sub> 25/2	12408.1739	-0.5	0.025	16 <sub>3,14</sub> 31/2 ← 15 <sub>3,13</sub> 29/2	12506.9122	0	0.025

(Table 9 continued)

Transition	Frequency (MHz)	Obs-Calc (kHz)	Uncertainty (MHz)	Transition	Frequency (MHz)	Obs-Calc (kHz)	Uncertainty (MHz)
16 <sub>3,14</sub> 33/2 ← 15 <sub>3,13</sub> 31/2	12508.1643	1.9	0.025	16 <sub>8,8</sub> 37/2 ← 15 <sub>8,7</sub> 35/2	12523.4078	0.2	0.025
16 <sub>3,14</sub> 35/2 ← 15 <sub>3,13</sub> 33/2	12510.2728	2	0.025	16 <sub>9,7</sub> 27/2 ← 15 <sub>9,6</sub> 25/2	12527.8089	-8	0.025
16 <sub>4,12</sub> 27/2 ← 15 <sub>4,11</sub> 25/2	12507.8214	-0.3	0.025	16 <sub>9,7</sub> 31/2 ← 15 <sub>9,6</sub> 29/2	12479.6451	-1.2	0.002
16 <sub>4,12</sub> 33/2 ← 15 <sub>4,11</sub> 31/2	12502.6884	-20.7	0.025	16 <sub>9,7</sub> 33/2 ← 15 <sub>9,6</sub> 31/2	12478.2219	0	0.025
16 <sub>4,12</sub> 35/2 ← 15 <sub>4,11</sub> 33/2	12500.5218	1.2	0.025	16 <sub>9,7</sub> 37/2 ← 15 <sub>9,6</sub> 35/2	12527.6978	3.7	0.025
16 <sub>4,12</sub> 37/2 ← 15 <sub>4,11</sub> 35/2	12514.7914	3.2	0.025	16 <sub>10,6</sub> 27/2 ← 15 <sub>10,5</sub> 25/2	12537.333	-0.1	0.025
16 <sub>4,13</sub> 27/2 ← 15 <sub>4,12</sub> 25/2	12507.5931	3.2	0.025	16 <sub>10,6</sub> 29/2 ← 15 <sub>10,5</sub> 27/2	12501.6277	-1.2	0.025
16 <sub>4,13</sub> 33/2 ← 15 <sub>4,12</sub> 31/2	12502.4513	1.4	0.025	16 <sub>10,6</sub> 31/2 ← 15 <sub>10,5</sub> 29/2	12478.7159	-3.7	0.025
16 <sub>4,13</sub> 35/2 ← 15 <sub>4,12</sub> 33/2	12500.2785	0.3	0.025	16 <sub>10,6</sub> 33/2 ← 15 <sub>10,5</sub> 31/2	12472.6563	1.1	0.025
16 <sub>5,11</sub> 33/2 ← 15 <sub>5,10</sub> 31/2	12494.9464	7.8	0.025	16 <sub>10,6</sub> 35/2 ← 15 <sub>10,5</sub> 33/2	12489.0361	2.1	0.025
16 <sub>5,12</sub> 27/2 ← 15 <sub>5,11</sub> 25/2	12482.1244	6	0.025	16 <sub>10,6</sub> 37/2 ← 15 <sub>10,5</sub> 35/2	12532.7666	0.3	0.025
16 <sub>5,12</sub> 29/2 ← 15 <sub>5,11</sub> 27/2	12491.9567	15.7	0.025	16 <sub>11,5</sub> 27/2 ← 15 <sub>11,4</sub> 25/2	12545.7251	-3.9	0.025
16 <sub>5,12</sub> 31/2 ← 15 <sub>5,11</sub> 29/2	12499.2921	2.5	0.025	16 <sub>11,5</sub> 29/2 ← 15 <sub>11,4</sub> 27/2	12502.579	-1.4	0.025
16 <sub>5,12</sub> 35/2 ← 15 <sub>5,11</sub> 33/2	12492.1839	-0.3	0.025	16 <sub>11,5</sub> 31/2 ← 15 <sub>11,4</sub> 29/2	12474.8849	-5.1	0.025
16 <sub>5,12</sub> 37/2 ← 15 <sub>5,11</sub> 35/2	12516.9428	4.3	0.025	16 <sub>11,5</sub> 33/2 ← 15 <sub>11,4</sub> 31/2	12467.5806	6.3	0.025
16 <sub>6,10</sub> 27/2 ← 15 <sub>6,9</sub> 25/2	12514.1146	0.9	0.025	16 <sub>11,5</sub> 35/2 ← 15 <sub>11,4</sub> 33/2	12486.4511	3.3	0.025
16 <sub>6,10</sub> 37/2 ← 15 <sub>6,9</sub> 35/2	12415.9212	-9.9	0.002	16 <sub>11,5</sub> 37/2 ← 15 <sub>11,4</sub> 35/2	12538.5892	-0.5	0.025
16 <sub>6,11</sub> 31/2 ← 15 <sub>6,10</sub> 29/2	12452.798	12.8	0.025	16 <sub>12,4</sub> 27/2 ← 15 <sub>12,3</sub> 25/2	12554.8152	-2.9	0.025
16 <sub>6,11</sub> 33/2 ← 15 <sub>6,10</sub> 31/2	12491.0655	2.6	0.025	16 <sub>12,4</sub> 29/2 ← 15 <sub>12,3</sub> 27/2	12503.0765	-1.8	0.025
16 <sub>6,11</sub> 35/2 ← 15 <sub>6,10</sub> 33/2	12475.4087	-5.6	0.025	16 <sub>12,4</sub> 31/2 ← 15 <sub>12,3</sub> 29/2	12464.5271	-0.1	0.025
16 <sub>6,11</sub> 37/2 ← 15 <sub>6,10</sub> 35/2	12415.9214	-5.5	0.025	16 <sub>12,4</sub> 33/2 ← 15 <sub>12,3</sub> 31/2	12449.976	1.6	0.025
16 <sub>7,9</sub> 27/2 ← 15 <sub>7,8</sub> 25/2	12519.0104	-1.6	0.025	16 <sub>12,4</sub> 35/2 ← 15 <sub>12,3</sub> 33/2	12477.0568	0.1	0.025
16 <sub>7,9</sub> 27/2 ← 15 <sub>7,8</sub> 27/2	12614.5399	5.1	0.002	16 <sub>12,4</sub> 37/2 ← 15 <sub>12,3</sub> 35/2	12542.893	1.5	0.025
16 <sub>7,9</sub> 29/2 ← 15 <sub>7,8</sub> 27/2	12503.9155	0.5	0.025	16 <sub>13,3</sub> 27/2 ← 15 <sub>13,2</sub> 25/2	12564.9211	3.3	0.025
16 <sub>7,9</sub> 31/2 ← 15 <sub>7,8</sub> 29/2	12492.5392	-0.4	0.025	16 <sub>13,3</sub> 29/2 ← 15 <sub>13,2</sub> 27/2	12503.5981	3.4	0.025
16 <sub>7,9</sub> 33/2 ← 15 <sub>7,8</sub> 31/2	12489.2928	0.7	0.025	16 <sub>13,3</sub> 31/2 ← 15 <sub>13,2</sub> 29/2	12463.7687	-2.3	0.025
16 <sub>7,9</sub> 35/2 ← 15 <sub>7,8</sub> 33/2	12497.7239	0	0.025	16 <sub>13,3</sub> 33/2 ← 15 <sub>13,2</sub> 31/2	12453.1937	-2.5	0.025
16 <sub>7,9</sub> 37/2 ← 15 <sub>7,8</sub> 35/2	12520.8412	3.8	0.025	16 <sub>13,3</sub> 35/2 ← 15 <sub>13,2</sub> 33/2	12479.847	2.8	0.025
16 <sub>8,8</sub> 27/2 ← 15 <sub>8,7</sub> 25/2	12524.3067	-2.9	0.025	16 <sub>13,3</sub> 37/2 ← 15 <sub>13,2</sub> 35/2	12551.2623	5	0.025
16 <sub>8,8</sub> 29/2 ← 15 <sub>8,7</sub> 27/2	12502.0837	-4.1	0.025	17 <sub>5,12</sub> 37/2 ← 15 <sub>6,9</sub> 35/2	12690.0948	1	0.002
16 <sub>8,8</sub> 31/2 ← 15 <sub>8,7</sub> 29/2	12487.8887	-1.7	0.025	17 <sub>5,13</sub> 29/2 ← 15 <sub>6,10</sub> 27/2	12976.9394	5.7	0.002
16 <sub>8,8</sub> 33/2 ← 15 <sub>8,7</sub> 31/2	12484.366	-0.4	0.025	17 <sub>5,13</sub> 37/2 ← 15 <sub>6,10</sub> 35/2	12690.0811	-1.7	0.002
16 <sub>8,8</sub> 35/2 ← 15 <sub>8,7</sub> 33/2	12494.7383	1.1	0.025	16 <sub>5,11</sub> 31/2 ← 16 <sub>4,12</sub> 31/2	10632.923	3	0.002

(Table 9 continued)

Transition	Frequency (MHz)	Obs-Calc (kHz)	Uncertainty (MHz)	Transition	Frequency (MHz)	Obs-Calc (kHz)	Uncertainty (MHz)
16 <sub>6,10</sub> 29/2 ← 16 <sub>5,11</sub> 27/2	12818.0848	4.4	0.025	17 <sub>3,14</sub> 33/2 ← 16 <sub>3,13</sub> 31/2	13301.1441	6.1	0.025
16 <sub>6,10</sub> 37/2 ← 16 <sub>5,11</sub> 35/2	13112.5414	4.9	0.002	17 <sub>3,14</sub> 35/2 ← 16 <sub>3,13</sub> 33/2	13302.3971	4.1	0.025
17 <sub>0,17</sub> 29/2 ← 16 <sub>0,16</sub> 27/2	13174.6141	-3.7	0.025	17 <sub>3,14</sub> 37/2 ← 16 <sub>3,13</sub> 35/2	13304.1773	1.5	0.025
17 <sub>0,17</sub> 31/2 ← 16 <sub>0,16</sub> 29/2	13171.7816	1.3	0.025	17 <sub>3,14</sub> 39/2 ← 16 <sub>3,13</sub> 37/2	13306.9808	4.3	0.025
17 <sub>0,17</sub> 33/2 ← 16 <sub>0,16</sub> 31/2	13171.9767	1.6	0.025	17 <sub>3,15</sub> 29/2 ← 16 <sub>3,14</sub> 27/2	13293.5273	-4.9	0.025
17 <sub>0,17</sub> 35/2 ← 16 <sub>0,16</sub> 33/2	13173.8866	-1	0.025	17 <sub>3,15</sub> 31/2 ← 16 <sub>3,14</sub> 29/2	13290.3589	0.1	0.025
17 <sub>0,17</sub> 37/2 ← 16 <sub>0,16</sub> 35/2	13176.0859	-0.3	0.025	17 <sub>3,15</sub> 33/2 ← 16 <sub>3,14</sub> 31/2	13289.9966	1.1	0.025
17 <sub>0,17</sub> 39/2 ← 16 <sub>0,16</sub> 37/2	13177.4401	-0.9	0.025	17 <sub>3,15</sub> 37/2 ← 16 <sub>3,14</sub> 35/2	13293.1935	0.2	0.025
17 <sub>1,16</sub> 29/2 ← 16 <sub>1,15</sub> 27/2	13377.3023	0	0.025	17 <sub>4,13</sub> 29/2 ← 16 <sub>4,12</sub> 27/2	13292.0804	-0.2	0.025
17 <sub>1,16</sub> 31/2 ← 16 <sub>1,15</sub> 29/2	13375.2135	-1.6	0.025	17 <sub>4,13</sub> 33/2 ← 16 <sub>4,12</sub> 31/2	13287.1876	-17.8	0.025
17 <sub>1,16</sub> 33/2 ← 16 <sub>1,15</sub> 31/2	13375.5432	0.4	0.025	17 <sub>4,13</sub> 35/2 ← 16 <sub>4,12</sub> 33/2	13287.0756	3.8	0.025
17 <sub>1,16</sub> 35/2 ← 16 <sub>1,15</sub> 33/2	13377.154	0.8	0.025	17 <sub>4,13</sub> 37/2 ← 16 <sub>4,12</sub> 35/2	13288.1784	-0.2	0.025
17 <sub>1,16</sub> 37/2 ← 16 <sub>1,15</sub> 35/2	13378.9055	1.1	0.025	17 <sub>4,14</sub> 29/2 ← 16 <sub>4,13</sub> 27/2	13291.7233	0.4	0.025
17 <sub>1,16</sub> 39/2 ← 16 <sub>1,15</sub> 37/2	13379.936	3	0.025	17 <sub>4,14</sub> 33/2 ← 16 <sub>4,13</sub> 31/2	13286.1623	-0.3	0.025
17 <sub>1,17</sub> 29/2 ← 16 <sub>1,16</sub> 27/2	13121.8792	3.3	0.025	17 <sub>4,14</sub> 35/2 ← 16 <sub>4,13</sub> 33/2	13286.6626	7.2	0.025
17 <sub>1,17</sub> 31/2 ← 16 <sub>1,16</sub> 29/2	13119.8832	1.6	0.025	17 <sub>4,14</sub> 37/2 ← 16 <sub>4,13</sub> 35/2	13287.6136	0.7	0.025
17 <sub>1,17</sub> 33/2 ← 16 <sub>1,16</sub> 31/2	13120.6537	2.5	0.025	17 <sub>4,14</sub> 39/2 ← 16 <sub>4,13</sub> 37/2	13295.447	4.5	0.025
17 <sub>1,17</sub> 35/2 ← 16 <sub>1,16</sub> 33/2	13122.7908	4.7	0.025	17 <sub>5,12</sub> 31/2 ← 16 <sub>5,11</sub> 29/2	13328.7002	-13.8	0.025
17 <sub>1,17</sub> 37/2 ← 16 <sub>1,16</sub> 35/2	13124.7185	1.7	0.025	17 <sub>5,12</sub> 33/2 ← 16 <sub>5,11</sub> 31/2	13285.0857	-9.3	0.025
17 <sub>2,15</sub> 29/2 ← 16 <sub>2,14</sub> 27/2	13366.2223	0.6	0.025	17 <sub>5,12</sub> 35/2 ← 16 <sub>5,11</sub> 33/2	13306.0204	7.7	0.025
17 <sub>2,15</sub> 31/2 ← 16 <sub>2,14</sub> 29/2	13365.6597	0.4	0.025	17 <sub>5,12</sub> 37/2 ← 16 <sub>5,11</sub> 35/2	13386.711	11.9	0.002
17 <sub>2,15</sub> 33/2 ← 16 <sub>2,14</sub> 31/2	13366.8683	1	0.025	17 <sub>5,13</sub> 29/2 ← 16 <sub>5,12</sub> 27/2	13367.5832	-8.8	0.025
17 <sub>2,15</sub> 35/2 ← 16 <sub>2,14</sub> 33/2	13368.5681	-0.1	0.025	17 <sub>6,11</sub> 31/2 ← 16 <sub>6,10</sub> 29/2	13300.5953	-2.9	0.025
17 <sub>2,15</sub> 37/2 ← 16 <sub>2,14</sub> 35/2	13369.659	0	0.025	17 <sub>6,11</sub> 33/2 ← 16 <sub>6,10</sub> 31/2	13292.2037	-1.7	0.025
17 <sub>2,15</sub> 39/2 ← 16 <sub>2,14</sub> 37/2	13369.4144	2.4	0.025	17 <sub>6,11</sub> 35/2 ← 16 <sub>6,10</sub> 33/2	13278.3101	-3.3	0.025
17 <sub>2,16</sub> 29/2 ← 16 <sub>2,15</sub> 27/2	13261.2967	-3.5	0.025	17 <sub>6,11</sub> 37/2 ← 16 <sub>6,10</sub> 35/2	13294.8227	4.8	0.025
17 <sub>2,16</sub> 31/2 ← 16 <sub>2,15</sub> 29/2	13258.7998	-1.9	0.025	17 <sub>6,12</sub> 29/2 ← 16 <sub>6,11</sub> 27/2	13292.8404	0.4	0.025
17 <sub>2,16</sub> 33/2 ← 16 <sub>2,15</sub> 31/2	13258.9763	-2.2	0.025	17 <sub>6,12</sub> 39/2 ← 16 <sub>6,11</sub> 37/2	13356.7778	6	0.025
17 <sub>2,16</sub> 35/2 ← 16 <sub>2,15</sub> 33/2	13260.6024	-0.7	0.025	17 <sub>7,10</sub> 29/2 ← 16 <sub>7,9</sub> 27/2	13297.6534	-0.4	0.025
17 <sub>2,16</sub> 37/2 ← 16 <sub>2,15</sub> 35/2	13262.559	0.5	0.025	17 <sub>7,10</sub> 31/2 ← 16 <sub>7,9</sub> 29/2	13288.7073	-2.6	0.025
17 <sub>2,16</sub> 39/2 ← 16 <sub>2,15</sub> 37/2	13264.1765	1.1	0.025	17 <sub>7,10</sub> 33/2 ← 16 <sub>7,9</sub> 31/2	13277.4564	-2.2	0.025
17 <sub>3,14</sub> 29/2 ← 16 <sub>3,13</sub> 27/2	13303.9556	2.3	0.025	17 <sub>7,10</sub> 35/2 ← 16 <sub>7,9</sub> 33/2	13273.4118	-1.6	0.025
17 <sub>3,14</sub> 31/2 ← 16 <sub>3,13</sub> 29/2	13301.2358	-4.6	0.025	17 <sub>7,10</sub> 37/2 ← 16 <sub>7,9</sub> 35/2	13281.1281	0.9	0.025

(Table 9 continued)

Transition	Frequency (MHz)	Obs-Calc (kHz)	Uncertainty (MHz)	Transition	Frequency (MHz)	Obs-Calc (kHz)	Uncertainty (MHz)
17 <sub>7,10</sub> 39/2 ← 16 <sub>7,9</sub> 37/2	13301.8769	-1.1	0.025	18 <sub>0,18</sub> 31/2 ← 17 <sub>0,17</sub> 29/2	13940.2342	1.2	0.025
17 <sub>8,9</sub> 31/2 ← 16 <sub>8,8</sub> 29/2	13283.6881	-8.3	0.025	18 <sub>0,18</sub> 33/2 ← 17 <sub>0,17</sub> 31/2	13937.5844	5.1	0.025
17 <sub>8,9</sub> 33/2 ← 16 <sub>8,8</sub> 31/2	13271.9155	-0.6	0.025	18 <sub>0,18</sub> 35/2 ← 17 <sub>0,17</sub> 33/2	13937.6894	-2.9	0.025
17 <sub>8,9</sub> 35/2 ← 16 <sub>8,8</sub> 33/2	13269.1201	-0.8	0.025	18 <sub>0,18</sub> 37/2 ← 17 <sub>0,17</sub> 35/2	13939.4125	1.1	0.025
17 <sub>8,9</sub> 37/2 ← 16 <sub>8,8</sub> 35/2	13278.0405	2.3	0.025	18 <sub>0,18</sub> 39/2 ← 17 <sub>0,17</sub> 37/2	13941.4754	2.1	0.025
17 <sub>9,8</sub> 29/2 ← 16 <sub>9,7</sub> 27/2	13306.9029	0.4	0.025	18 <sub>0,18</sub> 41/2 ← 17 <sub>0,17</sub> 39/2	13942.7456	1.8	0.025
17 <sub>9,8</sub> 33/2 ← 16 <sub>9,7</sub> 31/2	13268.0469	-1.5	0.025	18 <sub>1,17</sub> 31/2 ← 17 <sub>1,16</sub> 29/2	14158.7968	-2.1	0.025
17 <sub>9,8</sub> 35/2 ← 16 <sub>9,7</sub> 33/2	13264.5227	-2.7	0.025	18 <sub>1,17</sub> 33/2 ← 17 <sub>1,16</sub> 31/2	14156.7782	-0.4	0.025
17 <sub>9,8</sub> 37/2 ← 16 <sub>9,7</sub> 35/2	13275.5481	2.1	0.025	18 <sub>1,17</sub> 35/2 ← 17 <sub>1,16</sub> 33/2	14156.9862	-0.9	0.025
17 <sub>9,8</sub> 39/2 ← 16 <sub>9,7</sub> 37/2	13305.3596	2.5	0.025	18 <sub>1,17</sub> 37/2 ← 17 <sub>1,16</sub> 35/2	14158.4086	-1.6	0.025
17 <sub>10,7</sub> 29/2 ← 16 <sub>10,6</sub> 27/2	13313.6764	-2.3	0.025	18 <sub>1,17</sub> 41/2 ← 17 <sub>1,16</sub> 39/2	14161.1441	-0.5	0.025
17 <sub>10,7</sub> 31/2 ← 16 <sub>10,6</sub> 29/2	13284.9245	-5.2	0.025	18 <sub>1,18</sub> 31/2 ← 17 <sub>1,17</sub> 29/2	13891.2133	2.4	0.025
17 <sub>10,7</sub> 33/2 ← 16 <sub>10,6</sub> 31/2	13266.3831	-2.8	0.025	18 <sub>1,18</sub> 33/2 ← 17 <sub>1,17</sub> 31/2	13889.3944	1.7	0.025
17 <sub>10,7</sub> 35/2 ← 16 <sub>10,6</sub> 33/2	13261.1281	1	0.025	18 <sub>1,18</sub> 35/2 ← 17 <sub>1,17</sub> 33/2	13890.0633	-1.5	0.025
17 <sub>10,7</sub> 37/2 ← 16 <sub>10,6</sub> 35/2	13273.0472	-1.4	0.025	18 <sub>1,18</sub> 37/2 ← 17 <sub>1,17</sub> 35/2	13891.978	3.6	0.025
17 <sub>10,7</sub> 39/2 ← 16 <sub>10,6</sub> 37/2	13309.5053	1.4	0.025	18 <sub>1,18</sub> 39/2 ← 17 <sub>1,17</sub> 37/2	13893.7223	2.5	0.025
17 <sub>11,6</sub> 29/2 ← 16 <sub>11,5</sub> 27/2	13319.1676	-4.3	0.025	18 <sub>1,18</sub> 41/2 ← 17 <sub>1,17</sub> 39/2	13893.8607	4	0.025
17 <sub>11,6</sub> 33/2 ← 16 <sub>11,5</sub> 31/2	13260.1241	-2.7	0.025	18 <sub>2,16</sub> 31/2 ← 17 <sub>2,15</sub> 29/2	14160.361	0.2	0.025
17 <sub>11,6</sub> 35/2 ← 16 <sub>11,5</sub> 33/2	13254.3675	1.3	0.025	18 <sub>2,16</sub> 33/2 ← 17 <sub>2,15</sub> 31/2	14159.3465	0.1	0.025
17 <sub>11,6</sub> 37/2 ← 16 <sub>11,5</sub> 35/2	13270.5523	0.1	0.025	18 <sub>2,16</sub> 37/2 ← 17 <sub>2,15</sub> 35/2	14161.7699	1.4	0.025
17 <sub>11,6</sub> 39/2 ← 16 <sub>11,5</sub> 37/2	13314.2579	7.6	0.025	18 <sub>2,16</sub> 39/2 ← 17 <sub>2,15</sub> 37/2	14163.2288	-0.6	0.025
17 <sub>12,5</sub> 29/2 ← 16 <sub>12,4</sub> 27/2	13326.5783	-19	0.025	18 <sub>2,16</sub> 41/2 ← 17 <sub>2,15</sub> 39/2	14162.1989	3.8	0.025
17 <sub>12,5</sub> 31/2 ← 16 <sub>12,4</sub> 29/2	13283.4361	-1.3	0.025	18 <sub>2,17</sub> 31/2 ← 17 <sub>2,16</sub> 29/2	14035.4161	2.6	0.025
17 <sub>12,5</sub> 33/2 ← 16 <sub>12,4</sub> 31/2	13260.2832	-4	0.025	18 <sub>2,17</sub> 35/2 ← 17 <sub>2,16</sub> 33/2	14036.6393	-3.4	0.025
17 <sub>12,5</sub> 35/2 ← 16 <sub>12,4</sub> 33/2	13258.1968	-6.9	0.025	18 <sub>2,17</sub> 37/2 ← 17 <sub>2,16</sub> 35/2	14038.0921	-1.7	0.025
17 <sub>12,5</sub> 37/2 ← 16 <sub>12,4</sub> 35/2	13272.625	-26	0.025	18 <sub>2,17</sub> 39/2 ← 17 <sub>2,16</sub> 37/2	14039.8435	-0.3	0.025
17 <sub>12,5</sub> 39/2 ← 16 <sub>12,4</sub> 37/2	13320.4511	4.8	0.025	18 <sub>2,17</sub> 41/2 ← 17 <sub>2,16</sub> 39/2	14041.311	-3.3	0.025
17 <sub>13,4</sub> 29/2 ← 16 <sub>13,3</sub> 27/2	13334.7562	-3.5	0.025	18 <sub>3,15</sub> 31/2 ← 17 <sub>3,14</sub> 29/2	14089.8433	-3.3	0.025
17 <sub>13,4</sub> 33/2 ← 16 <sub>13,3</sub> 31/2	13251.3628	-1.4	0.025	18 <sub>3,15</sub> 37/2 ← 17 <sub>3,14</sub> 35/2	14088.8758	-3.2	0.025
17 <sub>13,4</sub> 35/2 ← 16 <sub>13,3</sub> 33/2	13243.2955	5.2	0.025	18 <sub>3,15</sub> 39/2 ← 17 <sub>3,14</sub> 37/2	14090.4563	-1.1	0.025
17 <sub>13,4</sub> 37/2 ← 16 <sub>13,3</sub> 35/2	13265.8531	-5	0.025	18 <sub>3,15</sub> 41/2 ← 17 <sub>3,14</sub> 39/2	14092.4861	1.7	0.025
17 <sub>13,4</sub> 39/2 ← 16 <sub>13,3</sub> 37/2	13325.687	1.1	0.025	18 <sub>3,16</sub> 33/2 ← 17 <sub>3,15</sub> 31/2	14073.2472	-4.7	0.025
17 <sub>5,13</sub> 33/2 ← 17 <sub>4,14</sub> 33/2	10632.4042	-1.8	0.002	18 <sub>3,16</sub> 35/2 ← 17 <sub>3,15</sub> 33/2	14072.9833	-3.2	0.025

(Table 9 continued)

Transition	Frequency (MHz)	Obs-Calc (kHz)	Uncertainty (MHz)	Transition	Frequency (MHz)	Obs-Calc (kHz)	Uncertainty (MHz)
18 <sub>3,16</sub> 37/2 ← 17 <sub>3,15</sub> 35/2	14074.1418	-6.4	0.025	18 <sub>9,9</sub> 35/2 ← 17 <sub>9,8</sub> 33/2	14052.0503	-0.4	0.025
18 <sub>3,16</sub> 39/2 ← 17 <sub>3,15</sub> 37/2	14075.9638	-2.7	0.025	18 <sub>9,9</sub> 37/2 ← 17 <sub>9,8</sub> 35/2	14049.2612	0.3	0.025
18 <sub>3,16</sub> 41/2 ← 17 <sub>3,15</sub> 39/2	14078.5737	-1.9	0.025	18 <sub>9,9</sub> 39/2 ← 17 <sub>9,8</sub> 37/2	14058.7373	3.2	0.025
18 <sub>4,14</sub> 31/2 ← 17 <sub>4,13</sub> 29/2	14075.2828	-1.7	0.025	18 <sub>9,9</sub> 41/2 ← 17 <sub>9,8</sub> 39/2	14083.8503	-0.6	0.025
18 <sub>4,14</sub> 33/2 ← 17 <sub>4,13</sub> 31/2	14067.6809	1.9	0.025	18 <sub>10,8</sub> 31/2 ← 17 <sub>10,7</sub> 29/2	14089.0376	-7.4	0.025
18 <sub>4,14</sub> 37/2 ← 17 <sub>4,13</sub> 35/2	14070.9199	2	0.025	18 <sub>10,8</sub> 35/2 ← 17 <sub>10,7</sub> 33/2	14048.2434	-1.3	0.025
18 <sub>4,14</sub> 39/2 ← 17 <sub>4,13</sub> 37/2	14072.4781	-2.6	0.025	18 <sub>10,8</sub> 37/2 ← 17 <sub>10,7</sub> 35/2	14044.8797	2.2	0.025
18 <sub>4,14</sub> 41/2 ← 17 <sub>4,13</sub> 39/2	14078.0226	0.1	0.025	18 <sub>10,8</sub> 39/2 ← 17 <sub>10,7</sub> 37/2	14056.5372	0.8	0.025
18 <sub>4,15</sub> 31/2 ← 17 <sub>4,14</sub> 29/2	14074.7428	-2.9	0.025	18 <sub>10,8</sub> 41/2 ← 17 <sub>10,7</sub> 39/2	14087.215	-1.9	0.025
18 <sub>4,15</sub> 37/2 ← 17 <sub>4,14</sub> 35/2	14070.3379	-4.1	0.025	18 <sub>11,7</sub> 31/2 ← 17 <sub>11,6</sub> 29/2	14099.5526	-8.7	0.025
18 <sub>4,15</sub> 39/2 ← 17 <sub>4,14</sub> 37/2	14072.0997	-4	0.025	18 <sub>11,7</sub> 33/2 ← 17 <sub>11,6</sub> 31/2	14074.5877	-6.4	0.025
18 <sub>4,15</sub> 41/2 ← 17 <sub>4,14</sub> 39/2	14078.4079	-1.3	0.025	18 <sub>11,7</sub> 35/2 ← 17 <sub>11,6</sub> 33/2	14050.9915	-2.4	0.025
18 <sub>5,13</sub> 31/2 ← 17 <sub>5,12</sub> 29/2	14056.9639	-2.7	0.025	18 <sub>11,7</sub> 37/2 ← 17 <sub>11,6</sub> 35/2	14042.2546	2.2	0.025
18 <sub>5,14</sub> 33/2 ← 17 <sub>5,13</sub> 31/2	14054.4825	8	0.025	18 <sub>11,7</sub> 39/2 ← 17 <sub>11,6</sub> 37/2	14054.326	0	0.025
18 <sub>5,14</sub> 37/2 ← 17 <sub>5,13</sub> 35/2	14051.8405	4.9	0.025	18 <sub>11,7</sub> 41/2 ← 17 <sub>11,6</sub> 39/2	14091.1565	-0.6	0.025
18 <sub>5,14</sub> 39/2 ← 17 <sub>5,13</sub> 37/2	14008.4043	1.7	0.025	18 <sub>12,6</sub> 31/2 ← 17 <sub>12,5</sub> 29/2	14100.5768	-8.4	0.025
18 <sub>6,12</sub> 37/2 ← 17 <sub>6,11</sub> 35/2	14060.0474	-1.7	0.025	18 <sub>12,6</sub> 37/2 ← 17 <sub>12,5</sub> 35/2	14035.8314	-3.3	0.025
18 <sub>6,12</sub> 39/2 ← 17 <sub>6,11</sub> 37/2	14063.8688	-7.6	0.025	18 <sub>12,6</sub> 39/2 ← 17 <sub>12,5</sub> 37/2	14052.1889	1	0.025
18 <sub>6,12</sub> 41/2 ← 17 <sub>6,11</sub> 39/2	14084.1598	-0.1	0.025	18 <sub>12,6</sub> 41/2 ← 17 <sub>12,5</sub> 39/2	14095.6002	-7.2	0.025
18 <sub>6,13</sub> 33/2 ← 17 <sub>6,12</sub> 31/2	14067.8648	-3.6	0.025	18 <sub>13,5</sub> 31/2 ← 17 <sub>13,4</sub> 29/2	14107.2885	-10.3	0.025
18 <sub>7,11</sub> 33/2 ← 17 <sub>7,10</sub> 31/2	14093.5576	-6.8	0.002	18 <sub>13,5</sub> 33/2 ← 17 <sub>13,4</sub> 31/2	14064.3059	-11.5	0.025
18 <sub>7,11</sub> 35/2 ← 17 <sub>7,10</sub> 33/2	14070.0978	-9.8	0.025	18 <sub>13,5</sub> 37/2 ← 17 <sub>13,4</sub> 35/2	14028.7279	0	0.025
18 <sub>7,11</sub> 37/2 ← 17 <sub>7,10</sub> 35/2	14057.3284	-1.5	0.025	18 <sub>13,5</sub> 39/2 ← 17 <sub>13,4</sub> 37/2	14047.7131	1	0.025
18 <sub>7,11</sub> 39/2 ← 17 <sub>7,10</sub> 37/2	14066.5602	0	0.025	18 <sub>13,5</sub> 41/2 ← 17 <sub>13,4</sub> 39/2	14098.9809	-5.6	0.025
18 <sub>7,11</sub> 41/2 ← 17 <sub>7,10</sub> 39/2	14089.6347	0.5	0.025	19 <sub>6,13</sub> 33/2 ← 17 <sub>7,10</sub> 31/2	13688.4654	4.4	0.002
18 <sub>8,10</sub> 31/2 ← 17 <sub>8,9</sub> 29/2	14080.5267	-4.8	0.025	18 <sub>5,14</sub> 37/2 ← 18 <sub>4,15</sub> 37/2	10632.5076	0.6	0.002
18 <sub>8,10</sub> 33/2 ← 17 <sub>8,9</sub> 31/2	14065.65	-4.8	0.025	18 <sub>5,14</sub> 39/2 ← 18 <sub>4,15</sub> 39/2	10633.0604	0.8	0.002
18 <sub>8,10</sub> 35/2 ← 17 <sub>8,9</sub> 33/2	14055.6222	-1.7	0.025	18 <sub>7,11</sub> 33/2 ← 18 <sub>6,12</sub> 31/2	15232.5155	-4.9	0.002
18 <sub>8,10</sub> 37/2 ← 17 <sub>8,9</sub> 35/2	14053.2311	-0.7	0.025	18 <sub>7,11</sub> 33/2 ← 18 <sub>6,12</sub> 33/2	15408.421	-7	0.002
18 <sub>8,10</sub> 39/2 ← 17 <sub>8,9</sub> 37/2	14061.0145	0.3	0.025	19 <sub>0,19</sub> 33/2 ← 18 <sub>0,18</sub> 31/2	14705.2244	-0.2	0.025
18 <sub>8,10</sub> 41/2 ← 17 <sub>8,9</sub> 39/2	14081.5032	-1.2	0.025	19 <sub>0,19</sub> 39/2 ← 18 <sub>0,18</sub> 37/2	14704.3694	0.6	0.025
18 <sub>9,9</sub> 31/2 ← 17 <sub>9,8</sub> 29/2	14084.5696	-5.9	0.025	19 <sub>0,19</sub> 41/2 ← 18 <sub>0,18</sub> 39/2	14706.28	0.2	0.025
18 <sub>9,9</sub> 33/2 ← 17 <sub>9,8</sub> 31/2	14064.5223	-10.3	0.025	19 <sub>0,19</sub> 43/2 ← 18 <sub>0,18</sub> 41/2	14707.4806	0.6	0.025



(Table 9 continued)

Transition	Frequency (MHz)	Obs-Calc (kHz)	Uncertainty (MHz)	Transition	Frequency (MHz)	Obs-Calc (kHz)	Uncertainty (MHz)
19 <sub>1,18</sub> 33/2 ← 18 <sub>1,17</sub> 31/2	14939.1319	-3.2	0.025	19 <sub>4,15</sub> 35/2 ← 18 <sub>4,14</sub> 33/2	14855.1828	-4.6	0.025
19 <sub>1,18</sub> 39/2 ← 18 <sub>1,17</sub> 37/2	14938.5268	-3.1	0.025	19 <sub>4,15</sub> 39/2 ← 18 <sub>4,14</sub> 37/2	14854.7231	-8.9	0.025
19 <sub>1,18</sub> 41/2 ← 18 <sub>1,17</sub> 39/2	14940.0807	-1.3	0.025	19 <sub>4,15</sub> 43/2 ← 18 <sub>4,14</sub> 41/2	14861.391	0.2	0.025
19 <sub>1,18</sub> 43/2 ← 18 <sub>1,17</sub> 41/2	14941.2554	-1	0.025	19 <sub>4,16</sub> 33/2 ← 18 <sub>4,15</sub> 31/2	14857.5945	-0.7	0.025
19 <sub>1,19</sub> 33/2 ← 18 <sub>1,18</sub> 31/2	14660.1973	4	0.025	19 <sub>4,16</sub> 37/2 ← 18 <sub>4,15</sub> 35/2	14853.2612	-1.5	0.025
19 <sub>1,19</sub> 35/2 ← 18 <sub>1,18</sub> 33/2	14658.5252	1.9	0.025	19 <sub>4,16</sub> 39/2 ← 18 <sub>4,15</sub> 37/2	14853.8564	-7.9	0.025
19 <sub>1,19</sub> 37/2 ← 18 <sub>1,18</sub> 35/2	14659.1179	5.2	0.025	19 <sub>4,16</sub> 41/2 ← 18 <sub>4,15</sub> 39/2	14855.6625	-1.5	0.025
19 <sub>1,19</sub> 39/2 ← 18 <sub>1,18</sub> 37/2	14660.8347	4.1	0.025	19 <sub>4,16</sub> 43/2 ← 18 <sub>4,15</sub> 41/2	14860.2758	6.6	0.025
19 <sub>1,19</sub> 41/2 ← 18 <sub>1,18</sub> 39/2	14662.4212	3.8	0.025	19 <sub>5,15</sub> 33/2 ← 18 <sub>5,14</sub> 31/2	14851.7843	0.8	0.025
19 <sub>1,19</sub> 43/2 ← 18 <sub>1,18</sub> 41/2	14662.572	5.2	0.025	19 <sub>5,15</sub> 39/2 ← 18 <sub>5,14</sub> 37/2	14846.7238	5.9	0.025
19 <sub>2,17</sub> 33/2 ← 18 <sub>2,16</sub> 31/2	14952.7456	-1	0.025	19 <sub>5,15</sub> 43/2 ← 18 <sub>5,14</sub> 41/2	14858.2097	6.4	0.025
19 <sub>2,17</sub> 35/2 ← 18 <sub>2,16</sub> 33/2	14952.2666	-3.1	0.025	19 <sub>6,13</sub> 33/2 ← 18 <sub>6,12</sub> 31/2	14827.4223	5.3	0.002
19 <sub>2,17</sub> 37/2 ← 18 <sub>2,16</sub> 35/2	14953.2861	-2.8	0.025	19 <sub>6,13</sub> 37/2 ← 18 <sub>6,12</sub> 35/2	14844.9454	-7.7	0.025
19 <sub>2,17</sub> 39/2 ← 18 <sub>2,16</sub> 37/2	14954.6278	-2.6	0.025	19 <sub>6,13</sub> 39/2 ← 18 <sub>6,12</sub> 37/2	14840.1899	-7	0.025
19 <sub>2,18</sub> 33/2 ← 18 <sub>2,17</sub> 31/2	14819.5688	-5.1	0.025	19 <sub>6,13</sub> 43/2 ← 18 <sub>6,12</sub> 41/2	14860.1717	-11.2	0.025
19 <sub>2,18</sub> 35/2 ← 18 <sub>2,17</sub> 33/2	14814.2539	-2.8	0.025	19 <sub>6,14</sub> 33/2 ← 18 <sub>6,13</sub> 31/2	14827.4196	2.8	0.025
19 <sub>2,18</sub> 37/2 ← 18 <sub>2,17</sub> 35/2	14813.8586	-1.7	0.025	19 <sub>6,14</sub> 35/2 ← 18 <sub>6,13</sub> 33/2	14838.1024	-20.1	0.025
19 <sub>2,18</sub> 39/2 ← 18 <sub>2,17</sub> 37/2	14815.3346	-5.9	0.025	19 <sub>6,14</sub> 43/2 ← 18 <sub>6,13</sub> 41/2	14860.1017	-6.9	0.025
19 <sub>2,18</sub> 41/2 ← 18 <sub>2,17</sub> 39/2	14817.3715	-2.8	0.025	19 <sub>7,12</sub> 33/2 ← 18 <sub>7,11</sub> 31/2	14856.4722	-0.3	0.025
19 <sub>2,18</sub> 43/2 ← 18 <sub>2,17</sub> 41/2	14818.0703	2.5	0.025	19 <sub>7,13</sub> 33/2 ← 18 <sub>7,12</sub> 33/2	14959.3974	11.3	0.002
19 <sub>3,16</sub> 33/2 ← 18 <sub>3,15</sub> 31/2	14876.5272	-0.2	0.025	19 <sub>7,13</sub> 37/2 ← 18 <sub>7,12</sub> 35/2	14800.558	9.7	0.025
19 <sub>3,16</sub> 35/2 ← 18 <sub>3,15</sub> 33/2	14874.7331	-0.6	0.025	19 <sub>7,13</sub> 41/2 ← 18 <sub>7,12</sub> 39/2	14817.7221	-8.5	0.002
19 <sub>3,16</sub> 37/2 ← 18 <sub>3,15</sub> 35/2	14874.8999	-2.4	0.025	19 <sub>7,13</sub> 43/2 ← 18 <sub>7,12</sub> 41/2	14753.1815	-12.5	0.025
19 <sub>3,16</sub> 39/2 ← 18 <sub>3,15</sub> 37/2	14876.0564	-2.3	0.025	19 <sub>8,11</sub> 33/2 ← 18 <sub>8,10</sub> 31/2	14859.7229	-8.5	0.025
19 <sub>3,16</sub> 41/2 ← 18 <sub>3,15</sub> 39/2	14877.4346	2.8	0.025	19 <sub>8,11</sub> 35/2 ← 18 <sub>8,10</sub> 33/2	14848.2811	-9.3	0.025
19 <sub>3,16</sub> 43/2 ← 18 <sub>3,15</sub> 41/2	14878.8734	4.4	0.025	19 <sub>8,11</sub> 37/2 ← 18 <sub>8,10</sub> 35/2	14839.3053	-4.8	0.025
19 <sub>3,17</sub> 33/2 ← 18 <sub>3,16</sub> 31/2	14858.4515	-11.1	0.025	19 <sub>8,11</sub> 39/2 ← 18 <sub>8,10</sub> 37/2	14836.877	-6.2	0.025
19 <sub>3,17</sub> 35/2 ← 18 <sub>3,16</sub> 33/2	14856.0579	-4	0.025	19 <sub>8,11</sub> 41/2 ← 18 <sub>8,10</sub> 39/2	14843.8339	-3	0.025
19 <sub>3,17</sub> 37/2 ← 18 <sub>3,16</sub> 35/2	14855.8716	-5	0.025	19 <sub>8,11</sub> 43/2 ← 18 <sub>8,10</sub> 41/2	14861.8467	-2.8	0.025
19 <sub>3,17</sub> 39/2 ← 18 <sub>3,16</sub> 37/2	14856.9684	-6.6	0.025	19 <sub>9,10</sub> 35/2 ← 18 <sub>9,9</sub> 33/2	14846.1454	-10.6	0.025
19 <sub>3,17</sub> 41/2 ← 18 <sub>3,16</sub> 39/2	14858.6278	-1.9	0.025	19 <sub>9,10</sub> 41/2 ← 18 <sub>9,9</sub> 39/2	14841.5945	-5.7	0.025
19 <sub>3,17</sub> 43/2 ← 18 <sub>3,16</sub> 41/2	14860.7386	-7.9	0.025	19 <sub>10,9</sub> 35/2 ← 18 <sub>10,8</sub> 33/2	14845.5272	-14.7	0.025
19 <sub>4,15</sub> 33/2 ← 18 <sub>4,14</sub> 31/2	14858.3795	-8.2	0.025	19 <sub>10,9</sub> 39/2 ← 18 <sub>10,8</sub> 37/2	14829.6462	11.9	0.025

(Table 9 continued)

Transition	Frequency (MHz)	Obs-Calc (kHz)	Uncertainty (MHz)	Transition	Frequency (MHz)	Obs-Calc (kHz)	Uncertainty (MHz)
19 <sub>10,9</sub> 41/2 ← 18 <sub>10,8</sub> 39/2	14839.6186	0	0.025	20 <sub>1,20</sub> 43/2 ← 19 <sub>1,19</sub> 41/2	15430.8223	1	0.025
19 <sub>10,9</sub> 43/2 ← 18 <sub>10,8</sub> 41/2	14865.6806	-2.7	0.025	20 <sub>1,20</sub> 45/2 ← 19 <sub>1,19</sub> 43/2	15430.9869	3	0.025
19 <sub>11,8</sub> 33/2 ← 18 <sub>11,7</sub> 31/2	14866.871	-10.7	0.025	20 <sub>2,18</sub> 35/2 ← 19 <sub>2,17</sub> 33/2	15745.8827	0.8	0.025
19 <sub>11,8</sub> 37/2 ← 18 <sub>11,7</sub> 35/2	14824.5508	6.7	0.025	20 <sub>2,18</sub> 37/2 ← 19 <sub>2,17</sub> 35/2	15745.443	-2.5	0.025
19 <sub>11,8</sub> 39/2 ← 18 <sub>11,7</sub> 37/2	14824.7127	-1.8	0.025	20 <sub>2,18</sub> 39/2 ← 19 <sub>2,17</sub> 37/2	15746.3204	-2.3	0.025
19 <sub>11,8</sub> 43/2 ← 18 <sub>11,7</sub> 41/2	14868.9475	-3.2	0.025	20 <sub>2,18</sub> 41/2 ← 19 <sub>2,17</sub> 39/2	15747.5818	-0.6	0.025
19 <sub>12,7</sub> 37/2 ← 18 <sub>12,6</sub> 35/2	14825.294	-5.3	0.025	20 <sub>2,18</sub> 43/2 ← 19 <sub>2,17</sub> 41/2	15748.333	-1.3	0.025
19 <sub>12,7</sub> 39/2 ← 18 <sub>12,6</sub> 37/2	14820.9627	3.9	0.025	20 <sub>2,18</sub> 45/2 ← 19 <sub>2,17</sub> 43/2	15747.9237	1.2	0.025
19 <sub>12,7</sub> 43/2 ← 18 <sub>12,6</sub> 41/2	14872.6675	-2.7	0.025	20 <sub>2,19</sub> 35/2 ← 19 <sub>2,18</sub> 33/2	15592.2964	-10	0.025
19 <sub>13,6</sub> 33/2 ← 18 <sub>13,5</sub> 31/2	14881.7677	-8.1	0.025	20 <sub>2,19</sub> 37/2 ← 19 <sub>2,18</sub> 35/2	15590.3964	-8.9	0.025
19 <sub>13,6</sub> 37/2 ← 18 <sub>13,5</sub> 35/2	14822.6563	0.3	0.025	20 <sub>2,19</sub> 39/2 ← 19 <sub>2,18</sub> 37/2	15590.5368	-10	0.025
19 <sub>13,6</sub> 43/2 ← 18 <sub>13,5</sub> 41/2	14876.932	2.9	0.025	20 <sub>2,19</sub> 41/2 ← 19 <sub>2,18</sub> 39/2	15591.7202	-11.1	0.025
20 <sub>6,15</sub> 35/2 ← 18 <sub>7,12</sub> 33/2	15305.6898	-5.2	0.002	20 <sub>2,19</sub> 43/2 ← 19 <sub>2,18</sub> 41/2	15593.0075	-7.1	0.025
20 <sub>6,15</sub> 37/2 ← 18 <sub>7,12</sub> 35/2	15210.7676	-6.3	0.025	20 <sub>2,19</sub> 45/2 ← 19 <sub>2,18</sub> 43/2	15594.3992	-7.9	0.025
20 <sub>6,15</sub> 41/2 ← 18 <sub>7,12</sub> 39/2	15047.9181	-0.5	0.025	20 <sub>3,17</sub> 37/2 ← 19 <sub>3,16</sub> 35/2	15662.641	-3.9	0.025
19 <sub>7,12</sub> 35/2 ← 19 <sub>6,13</sub> 33/2	15177.9921	5.6	0.025	20 <sub>3,17</sub> 39/2 ← 19 <sub>3,16</sub> 37/2	15662.9224	-2.4	0.025
19 <sub>7,12</sub> 37/2 ← 19 <sub>6,13</sub> 35/2	15261.7576	4	0.025	20 <sub>3,17</sub> 43/2 ← 19 <sub>3,16</sub> 41/2	15665.1994	-1.5	0.025
19 <sub>7,13</sub> 41/2 ← 19 <sub>6,14</sub> 39/2	15423.9985	-3.8	0.025	20 <sub>3,17</sub> 45/2 ← 19 <sub>3,16</sub> 43/2	15666.1765	4.3	0.025
19 <sub>7,13</sub> 41/2 ← 19 <sub>6,14</sub> 41/2	15358.4309	3.2	0.002	20 <sub>3,18</sub> 35/2 ← 19 <sub>3,17</sub> 33/2	15640.8797	-3.9	0.025
20 <sub>0,20</sub> 35/2 ← 19 <sub>0,19</sub> 33/2	15469.7685	3.5	0.025	20 <sub>3,18</sub> 37/2 ← 19 <sub>3,17</sub> 35/2	15638.7656	-4.5	0.025
20 <sub>0,20</sub> 37/2 ← 19 <sub>0,19</sub> 35/2	15467.4576	-13.9	0.025	20 <sub>3,18</sub> 39/2 ← 19 <sub>3,17</sub> 37/2	15638.641	-6.5	0.025
20 <sub>0,20</sub> 39/2 ← 19 <sub>0,19</sub> 37/2	15467.5158	15	0.025	20 <sub>3,18</sub> 41/2 ← 19 <sub>3,17</sub> 39/2	15639.6753	-5	0.025
20 <sub>0,20</sub> 41/2 ← 19 <sub>0,19</sub> 39/2	15468.9164	0.9	0.025	20 <sub>3,18</sub> 43/2 ← 19 <sub>3,17</sub> 41/2	15641.1797	-4.1	0.025
20 <sub>0,20</sub> 43/2 ← 19 <sub>0,19</sub> 41/2	15470.6849	3.8	0.025	20 <sub>3,18</sub> 45/2 ← 19 <sub>3,17</sub> 43/2	15642.9292	-3	0.025
20 <sub>0,20</sub> 45/2 ← 19 <sub>0,19</sub> 43/2	15471.8102	4.9	0.025	20 <sub>4,16</sub> 35/2 ← 19 <sub>4,15</sub> 33/2	15641.655	-3	0.025
20 <sub>1,19</sub> 35/2 ← 19 <sub>1,18</sub> 33/2	15718.1522	-3.8	0.025	20 <sub>4,16</sub> 37/2 ← 19 <sub>4,15</sub> 35/2	15637.837	-2.6	0.025
20 <sub>1,19</sub> 41/2 ← 19 <sub>1,18</sub> 39/2	15717.4083	-2.5	0.025	20 <sub>4,16</sub> 39/2 ← 19 <sub>4,15</sub> 37/2	15637.2038	-3.1	0.025
20 <sub>1,19</sub> 43/2 ← 19 <sub>1,18</sub> 41/2	15718.8699	-1.4	0.025	20 <sub>4,16</sub> 41/2 ← 19 <sub>4,15</sub> 39/2	15638.382	-3.4	0.025
20 <sub>1,19</sub> 45/2 ← 19 <sub>1,18</sub> 43/2	15720.1704	-0.4	0.025	20 <sub>4,16</sub> 43/2 ← 19 <sub>4,15</sub> 41/2	15640.7219	-1.2	0.025
20 <sub>1,20</sub> 35/2 ← 19 <sub>1,19</sub> 33/2	15428.8435	1.4	0.025	20 <sub>4,16</sub> 45/2 ← 19 <sub>4,15</sub> 43/2	15644.558	-0.6	0.025
20 <sub>1,20</sub> 37/2 ← 19 <sub>1,19</sub> 35/2	15427.2999	1.2	0.025	20 <sub>4,17</sub> 35/2 ← 19 <sub>4,16</sub> 33/2	15640.5128	-4.3	0.025
20 <sub>1,20</sub> 39/2 ← 19 <sub>1,19</sub> 37/2	15427.8182	0.5	0.025	20 <sub>4,17</sub> 39/2 ← 19 <sub>4,16</sub> 37/2	15636.7244	-6	0.025
20 <sub>1,20</sub> 41/2 ← 19 <sub>1,19</sub> 39/2	15429.3708	0.5	0.025	20 <sub>4,17</sub> 43/2 ← 19 <sub>4,16</sub> 41/2	15639.1141	-3.7	0.025

(Table 9 continued)

Transition	Frequency (MHz)	Obs-Calc (kHz)	Uncertainty (MHz)	Transition	Frequency (MHz)	Obs-Calc (kHz)	Uncertainty (MHz)
20 <sub>6,14</sub> 43/2 ← 19 <sub>6,13</sub> 41/2	15736.2895	8.8	0.025	20 <sub>11,9</sub> 39/2 ← 19 <sub>11,8</sub> 37/2	15612.9471	-11.6	0.025
20 <sub>6,15</sub> 35/2 ← 19 <sub>6,14</sub> 33/2	15710.7832	-15.6	0.002	20 <sub>11,9</sub> 41/2 ← 19 <sub>11,8</sub> 39/2	15610.1759	-4.7	0.025
20 <sub>6,15</sub> 39/2 ← 19 <sub>6,14</sub> 37/2	15629.5924	-7.5	0.025	20 <sub>11,9</sub> 43/2 ← 19 <sub>11,8</sub> 41/2	15620.624	-5.8	0.025
20 <sub>6,15</sub> 41/2 ← 19 <sub>6,14</sub> 39/2	15654.1964	6	0.025	20 <sub>11,9</sub> 45/2 ← 19 <sub>11,8</sub> 43/2	15647.4368	-3.8	0.025
20 <sub>7,13</sub> 35/2 ← 19 <sub>7,12</sub> 33/2	15635.8748	-4.1	0.025	20 <sub>12,8</sub> 37/2 ← 19 <sub>12,7</sub> 35/2	15628.2968	-7.5	0.025
20 <sub>7,13</sub> 37/2 ← 19 <sub>7,12</sub> 35/2	15646.3558	-7.7	0.025	20 <sub>12,8</sub> 39/2 ← 19 <sub>12,7</sub> 37/2	15612.1177	-6.5	0.025
20 <sub>7,13</sub> 39/2 ← 19 <sub>7,12</sub> 37/2	15638.1766	-8.6	0.025	20 <sub>12,8</sub> 41/2 ← 19 <sub>12,7</sub> 39/2	15607.932	-9.1	0.025
20 <sub>7,13</sub> 41/2 ← 19 <sub>7,12</sub> 39/2	15623.9273	-8.5	0.025	20 <sub>12,8</sub> 45/2 ← 19 <sub>12,7</sub> 43/2	15650.5635	-3.9	0.025
20 <sub>7,13</sub> 43/2 ← 19 <sub>7,12</sub> 41/2	15642.2229	-12	0.025	20 <sub>13,7</sub> 35/2 ← 19 <sub>13,6</sub> 33/2	15657.6243	-9.1	0.025
20 <sub>8,12</sub> 35/2 ← 19 <sub>8,11</sub> 33/2	15639.4079	-4.9	0.025	20 <sub>13,7</sub> 39/2 ← 19 <sub>13,6</sub> 37/2	15606.8245	-9.9	0.025
20 <sub>8,12</sub> 37/2 ← 19 <sub>8,11</sub> 35/2	15633.1395	-7.1	0.025	20 <sub>13,7</sub> 41/2 ← 19 <sub>13,6</sub> 39/2	15602.6588	-6.5	0.025
20 <sub>8,12</sub> 39/2 ← 19 <sub>8,11</sub> 37/2	15623.6266	-6.4	0.025	20 <sub>13,7</sub> 43/2 ← 19 <sub>13,6</sub> 41/2	15617.1142	-5.9	0.025
20 <sub>8,12</sub> 41/2 ← 19 <sub>8,11</sub> 39/2	15620.19	-6	0.025	20 <sub>7,13</sub> 43/2 ← 20 <sub>6,14</sub> 41/2	15412.042	-4.2	0.025
20 <sub>8,12</sub> 43/2 ← 19 <sub>8,11</sub> 41/2	15626.7816	-3.2	0.025	22 <sub>0,22</sub> 41/2 ← 21 <sub>0,21</sub> 39/2	16996.1002	3.7	0.002
20 <sub>8,12</sub> 45/2 ← 19 <sub>8,11</sub> 43/2	15643.6534	-0.3	0.025	22 <sub>0,22</sub> 43/2 ← 21 <sub>0,21</sub> 41/2	16996.1159	4.5	0.002
20 <sub>9,11</sub> 37/2 ← 19 <sub>9,10</sub> 35/2	15627.9579	-7.4	0.025	22 <sub>0,22</sub> 45/2 ← 21 <sub>0,21</sub> 43/2	16997.3052	3.8	0.002
20 <sub>9,11</sub> 41/2 ← 19 <sub>9,10</sub> 39/2	15616.9901	-6.8	0.025	32 <sub>7,25</sub> 67/2 ← 32 <sub>6,26</sub> 67/2	15305.3044	-0.7	0.002
20 <sub>9,11</sub> 43/2 ← 19 <sub>9,10</sub> 41/2	15624.2403	-4	0.025	35 <sub>5,30</sub> 65/2 ← 35 <sub>4,31</sub> 65/2	10233.1328	1.4	0.002
20 <sub>10,10</sub> 35/2 ← 19 <sub>10,9</sub> 33/2	15645.3378	-6	0.025	35 <sub>5,30</sub> 67/2 ← 35 <sub>4,31</sub> 67/2	10233.4638	0.8	0.002
20 <sub>10,10</sub> 37/2 ← 19 <sub>10,9</sub> 35/2	15627.0879	-7.9	0.025	35 <sub>5,30</sub> 69/2 ← 35 <sub>4,31</sub> 69/2	10233.7214	0.3	0.002
20 <sub>10,10</sub> 39/2 ← 19 <sub>10,9</sub> 37/2	15615.9566	-6.2	0.025	35 <sub>5,30</sub> 73/2 ← 35 <sub>4,31</sub> 73/2	10233.6428	-3.6	0.002
20 <sub>10,10</sub> 41/2 ← 19 <sub>10,9</sub> 39/2	15613.6934	-7.1	0.025	35 <sub>5,30</sub> 75/2 ← 35 <sub>4,31</sub> 75/2	10233.1399	-3.5	0.002
20 <sub>10,10</sub> 43/2 ← 19 <sub>10,9</sub> 41/2	15622.3995	-5.6	0.025	40 <sub>6,35</sub> 83/2 ← 40 <sub>5,36</sub> 83/2	12790.0619	11.7	0.002
20 <sub>10,10</sub> 45/2 ← 19 <sub>10,9</sub> 43/2	15644.7467	-4.4	0.025	50 <sub>6,45</sub> 95/2 ← 50 <sub>5,46</sub> 95/2	12614.386	-3.9	0.002
20 <sub>11,9</sub> 35/2 ← 19 <sub>11,8</sub> 33/2	15648.9019	-8.2	0.025				
20 <sub>11,9</sub> 37/2 ← 19 <sub>11,8</sub> 35/2	15626.5374	-8.9	0.025				

Table 10. Observed Transitions For C(1) Isotopologue of Trans-1-iodoperfluoropropane,  $\text{CF}_3\text{CF}_2^{13}\text{CF}_2\text{I}$

Transition	Frequency (MHz)	Obs-Calc (kHz)	Uncertainty (MHz)
$13_{1,12}23/2 \leftarrow 12_{1,11}21/2$	10238.2082	-1.5	0.002
$13_{1,12}27/2 \leftarrow 12_{1,11}25/2$	10241.969	-1.3	0.002
$13_{1,12}29/2 \leftarrow 12_{1,11}27/2$	10244.3795	-5.5	0.002
$13_{1,12}31/2 \leftarrow 12_{1,11}29/2$	10245.6724	-1.1	0.002
$13_{1,13}23/2 \leftarrow 12_{1,12}21/2$	10036.5243	-3.7	0.002
$13_{1,13}25/2 \leftarrow 12_{1,12}23/2$	10036.7588	1.6	0.002
$13_{1,13}27/2 \leftarrow 12_{1,12}25/2$	10040.3354	0	0.002
$13_{1,13}29/2 \leftarrow 12_{1,12}27/2$	10043.4511	1.4	0.002
$13_{1,13}31/2 \leftarrow 12_{1,12}29/2$	10043.7791	-0.9	0.002
$14_{0,14}27/2 \leftarrow 13_{0,13}25/2$	10868.0816	-0.2	0.002
$14_{1,13}23/2 \leftarrow 13_{1,12}21/2$	11026.2375	1.6	0.002
$14_{1,13}25/2 \leftarrow 13_{1,12}23/2$	11023.6794	-1	0.002
$14_{1,13}31/2 \leftarrow 13_{1,12}29/2$	11029.1245	1.4	0.002
$14_{1,13}33/2 \leftarrow 13_{1,12}31/2$	11030.1565	0.9	0.002
$14_{1,14}29/2 \leftarrow 13_{1,13}27/2$	10810.9902	-0.9	0.002
$14_{1,14}31/2 \leftarrow 13_{1,13}29/2$	10814.0319	0	0.002
$14_{1,14}33/2 \leftarrow 13_{1,13}31/2$	10813.7707	-0.4	0.002
$14_{3,11}29/2 \leftarrow 14_{0,14}27/2$	10925.9982	0	0.002
$15_{0,15}25/2 \leftarrow 14_{0,14}23/2$	11637.9106	5.7	0.002
$15_{0,15}27/2 \leftarrow 14_{0,14}25/2$	11634.4052	-6.1	0.002
$15_{0,15}31/2 \leftarrow 14_{0,14}29/2$	11638.7599	2.2	0.002
$15_{0,15}33/2 \leftarrow 14_{0,14}31/2$	11642.9052	-2.3	0.002
$15_{1,14}25/2 \leftarrow 14_{1,13}23/2$	11810.5416	-0.2	0.002
$15_{1,14}27/2 \leftarrow 14_{1,13}25/2$	11808.1962	2	0.002
$15_{1,14}29/2 \leftarrow 14_{1,13}27/2$	11808.8038	4.1	0.002
$15_{1,14}31/2 \leftarrow 14_{1,13}29/2$	11810.8889	3.5	0.002
$15_{1,14}33/2 \leftarrow 14_{1,13}31/2$	11812.9497	3.9	0.002
$15_{1,14}35/2 \leftarrow 14_{1,13}33/2$	11813.9408	3.3	0.002
$15_{1,15}27/2 \leftarrow 14_{1,14}25/2$	11577.157	0.5	0.002
$15_{1,15}29/2 \leftarrow 14_{1,14}27/2$	11578.1963	1.9	0.002
$15_{1,15}33/2 \leftarrow 14_{1,14}31/2$	11583.2358	-2.3	0.002
$17_{2,15}37/2 \leftarrow 16_{2,14}35/2$	13369.6166	-6.9	0.002

Table 11. Observed Transitions For C(2) Isotopologue of Trans-1-iodoperfluoropropane,  $\text{CF}_3^{13}\text{CF}_2\text{CF}_2\text{I}$

Transition	Frequency (MHz)	Obs-Calc (kHz)	Uncertainty (MHz)
$13_{0,13}21/2 \leftarrow 12_{0,12}19/2$	10093.1127	-0.8	0.002
$13_{0,13}25/2 \leftarrow 12_{0,12}23/2$	10090.4799	1.4	0.002
$13_{0,13}27/2 \leftarrow 12_{0,12}25/2$	10093.7865	-1.8	0.002
$13_{0,13}29/2 \leftarrow 12_{0,12}27/2$	10097.028	-1.1	0.002
$13_{0,13}31/2 \leftarrow 12_{0,12}29/2$	10098.1716	4.5	0.002
$13_{1,12}21/2 \leftarrow 12_{1,11}19/2$	10232.692	0	0.002
$13_{1,12}23/2 \leftarrow 12_{1,11}21/2$	10229.866	0	0.002
$13_{1,12}27/2 \leftarrow 12_{1,11}25/2$	10233.6238	-1.4	0.002
$13_{1,12}29/2 \leftarrow 12_{1,11}27/2$	10236.0138	0.6	0.002
$13_{1,12}31/2 \leftarrow 12_{1,11}29/2$	10237.3301	2.3	0.002
$13_{1,13}21/2 \leftarrow 12_{1,12}19/2$	10032.3933	-0.9	0.002
$13_{1,13}23/2 \leftarrow 12_{1,12}21/2$	10029.6146	0.8	0.002
$13_{1,13}25/2 \leftarrow 12_{1,12}23/2$	10029.5146	0.1	0.002
$13_{1,13}27/2 \leftarrow 12_{1,12}25/2$	10033.0867	-0.3	0.002
$13_{1,13}29/2 \leftarrow 12_{1,12}27/2$	10036.1988	-1.6	0.002
$13_{1,13}31/2 \leftarrow 12_{1,12}29/2$	10036.5241	0.6	0.002
$14_{0,14}23/2 \leftarrow 13_{0,13}21/2$	10863.7801	2.2	0.002
$14_{0,14}25/2 \leftarrow 13_{0,13}23/2$	10860.3542	2.7	0.002
$14_{0,14}27/2 \leftarrow 13_{0,13}25/2$	10857.1097	7.9	0.002
$14_{0,14}29/2 \leftarrow 13_{0,13}27/2$	10861.9842	-1	0.002
$14_{0,14}31/2 \leftarrow 13_{0,13}29/2$	10864.4856	-3.5	0.002
$14_{0,14}33/2 \leftarrow 13_{0,13}31/2$	10866.5272	0.2	0.002
$14_{1,13}23/2 \leftarrow 13_{1,12}21/2$	11017.2924	0.3	0.002
$14_{1,13}27/2 \leftarrow 13_{1,12}25/2$	11015.5239	0.7	0.002
$14_{1,13}29/2 \leftarrow 13_{1,12}27/2$	11017.9181	-0.7	0.002
$14_{1,13}31/2 \leftarrow 13_{1,12}29/2$	11020.1795	-1.3	0.002
$14_{1,13}33/2 \leftarrow 13_{1,12}31/2$	11021.2132	2.2	0.002
$14_{1,14}23/2 \leftarrow 13_{1,13}21/2$	10801.1062	-0.9	0.002
$14_{1,14}25/2 \leftarrow 13_{1,13}23/2$	10797.5991	-1.3	0.002
$14_{1,14}27/2 \leftarrow 13_{1,13}25/2$	10799.9975	-0.1	0.002
$14_{1,14}29/2 \leftarrow 13_{1,13}27/2$	10803.1984	-0.5	0.002
$14_{1,14}31/2 \leftarrow 13_{1,13}29/2$	10806.2477	-1.3	0.002
$14_{1,14}33/2 \leftarrow 13_{1,13}31/2$	10805.979	0.6	0.002
$14_{3,11}29/2 \leftarrow 14_{0,14}27/2$	10941.6351	-6.5	0.002
$15_{0,15}25/2 \leftarrow 14_{0,14}23/2$	11629.5365	-2.2	0.002
$15_{0,15}27/2 \leftarrow 14_{0,14}25/2$	11625.9571	-1.5	0.002
$15_{0,15}29/2 \leftarrow 14_{0,14}27/2$	11629.7786	-6.1	0.002
$15_{0,15}31/2 \leftarrow 14_{0,14}29/2$	11630.3701	1.5	0.002
$15_{0,15}33/2 \leftarrow 14_{0,14}31/2$	11634.5115	4.6	0.002
$15_{0,15}35/2 \leftarrow 14_{0,14}33/2$	11633.7339	-0.1	0.002
$15_{1,14}25/2 \leftarrow 14_{1,13}23/2$	11801.0081	-3	0.002
$15_{1,14}27/2 \leftarrow 14_{1,13}25/2$	11798.6695	-0.1	0.002
$15_{1,14}29/2 \leftarrow 14_{1,13}27/2$	11799.2789	1.3	0.002
$15_{1,14}31/2 \leftarrow 14_{1,13}29/2$	11801.3617	-0.1	0.002
$15_{1,14}33/2 \leftarrow 14_{1,13}31/2$	11803.4191	1	0.002
$15_{1,14}35/2 \leftarrow 14_{1,13}33/2$	11804.4067	1.3	0.002
$15_{1,15}25/2 \leftarrow 14_{1,14}23/2$	11571.2958	-0.5	0.002
$15_{1,15}27/2 \leftarrow 14_{1,14}25/2$	11568.8341	2	0.002
$15_{1,15}29/2 \leftarrow 14_{1,14}27/2$	11569.8726	0.2	0.002
$15_{1,15}31/2 \leftarrow 14_{1,14}29/2$	11572.577	-0.9	0.002
$15_{1,15}33/2 \leftarrow 14_{1,14}31/2$	11574.9008	-0.1	0.002
$15_{1,15}35/2 \leftarrow 14_{1,14}33/2$	11575.1599	0.4	0.002
$17_{2,15}29/2 \leftarrow 16_{2,14}27/2$	13354.8663	-1.1	0.002
$17_{2,15}31/2 \leftarrow 16_{2,14}29/2$	13354.3067	-1.1	0.002
$17_{2,15}37/2 \leftarrow 16_{2,14}35/2$	13358.3056	-0.1	0.002
$17_{2,15}39/2 \leftarrow 16_{2,14}37/2$	13358.0585	2.1	0.002
$17_{3,14}37/2 \leftarrow 16_{3,13}35/2$	13292.5698	-0.9	0.002
$18_{2,16}41/2 \leftarrow 17_{2,15}39/2$	14150.1854	1.5	0.002

Table 12. Observed Transitions For C(3) Isotopologue of Trans-1-iodoperfluoropropane,  $^{13}\text{CF}_3\text{CF}_2\text{CF}_2\text{I}$

Transition	Frequency (MHz)	Obs-Calc (kHz)	Uncertainty (MHz)
$13_{0,13}21/2 \leftarrow 12_{0,12}19/2$	10053.5224	0.6	0.002
$13_{0,13}23/2 \leftarrow 12_{0,12}21/2$	10049.9188	1.7	0.002
$13_{0,13}25/2 \leftarrow 12_{0,12}23/2$	10050.8727	1.1	0.002
$13_{0,13}27/2 \leftarrow 12_{0,12}25/2$	10054.084	-0.4	0.002
$13_{0,13}29/2 \leftarrow 12_{0,12}27/2$	10057.4284	-1.9	0.002
$13_{0,13}31/2 \leftarrow 12_{0,12}29/2$	10058.5349	1.4	0.002
$13_{1,12}21/2 \leftarrow 12_{1,11}19/2$	10190.8901	0.1	0.002
$13_{1,12}23/2 \leftarrow 12_{1,11}21/2$	10188.079	-0.2	0.002
$13_{1,12}27/2 \leftarrow 12_{1,11}25/2$	10191.8434	0	0.002
$13_{1,12}29/2 \leftarrow 12_{1,11}27/2$	10194.1461	-0.1	0.002
$13_{1,12}31/2 \leftarrow 12_{1,11}29/2$	10195.5571	0.4	0.002
$13_{1,13}25/2 \leftarrow 12_{1,12}23/2$	9990.1527	2.1	0.002
$13_{1,13}27/2 \leftarrow 12_{1,12}25/2$	9993.7253	1.3	0.002
$13_{1,13}29/2 \leftarrow 12_{1,12}27/2$	9996.8412	-0.5	0.002
$13_{1,13}31/2 \leftarrow 12_{1,12}29/2$	9997.1429	1.2	0.002
$14_{0,14}23/2 \leftarrow 13_{0,13}21/2$	10821.4499	-0.9	0.002
$14_{0,14}25/2 \leftarrow 13_{0,13}23/2$	10818.7181	-1.1	0.002
$14_{0,14}27/2 \leftarrow 13_{0,13}25/2$	10816.8556	1.4	0.002
$14_{0,14}29/2 \leftarrow 13_{0,13}27/2$	10819.7368	2.5	0.002
$14_{0,14}31/2 \leftarrow 13_{0,13}29/2$	10822.2128	-1	0.002
$14_{0,14}33/2 \leftarrow 13_{0,13}31/2$	10824.0117	-0.4	0.002
$14_{1,13}25/2 \leftarrow 13_{1,12}23/2$	10969.8437	-2.8	0.002
$14_{1,13}27/2 \leftarrow 13_{1,12}25/2$	10970.6416	3.2	0.002
$14_{1,13}31/2 \leftarrow 13_{1,12}29/2$	10975.2914	0	0.002
$14_{1,13}33/2 \leftarrow 13_{1,12}31/2$	10976.3143	0.6	0.002
$14_{1,14}23/2 \leftarrow 13_{1,13}21/2$	10758.4904	2.3	0.002
$14_{1,14}27/2 \leftarrow 13_{1,13}25/2$	10757.6204	0.7	0.002
$14_{1,14}29/2 \leftarrow 13_{1,13}27/2$	10760.8316	-0.2	0.002
$14_{1,14}31/2 \leftarrow 13_{1,13}29/2$	10763.9097	-0.1	0.002
$14_{1,14}33/2 \leftarrow 13_{1,13}31/2$	10763.6109	-1.5	0.002
$14_{3,11}29/2 \leftarrow 14_{0,14}27/2$	10955.0951	0.1	0.002
$15_{0,15}25/2 \leftarrow 14_{0,14}23/2$	11583.9107	-0.1	0.002
$15_{0,15}29/2 \leftarrow 14_{0,14}27/2$	11582.1751	-2.5	0.002
$15_{0,15}31/2 \leftarrow 14_{0,14}29/2$	11584.8776	-5.2	0.002
$15_{0,15}33/2 \leftarrow 14_{0,14}31/2$	11589.0139	0.3	0.002
$15_{0,15}35/2 \leftarrow 14_{0,14}33/2$	11588.3511	0.5	0.002
$15_{1,14}31/2 \leftarrow 14_{1,13}29/2$	11753.3788	-2.9	0.002
$15_{1,14}33/2 \leftarrow 14_{1,13}31/2$	11755.4296	-1.4	0.002
$15_{1,14}35/2 \leftarrow 14_{1,13}33/2$	11756.4042	-0.9	0.002
$15_{1,15}27/2 \leftarrow 14_{1,14}25/2$	11523.4832	-0.1	0.002
$15_{1,15}29/2 \leftarrow 14_{1,14}27/2$	11524.5337	0.5	0.002
$15_{1,15}31/2 \leftarrow 14_{1,14}29/2$	11527.2353	0.1	0.002
$15_{1,15}33/2 \leftarrow 14_{1,14}31/2$	11529.5194	0	0.002
$15_{1,15}35/2 \leftarrow 14_{1,14}33/2$	11529.817	0.5	0.002
$17_{2,15}29/2 \leftarrow 16_{2,14}27/2$	13299.5612	-1.1	0.002
$17_{2,15}31/2 \leftarrow 16_{2,14}29/2$	13298.9017	-2.8	0.002
$17_{2,15}39/2 \leftarrow 16_{2,14}37/2$	13302.6384	-0.9	0.002
$17_{3,14}37/2 \leftarrow 16_{3,13}35/2$	13238.3409	-0.9	0.002
$17_{3,14}39/2 \leftarrow 16_{3,13}37/2$	13241.1818	2.2	0.002
$18_{2,16}41/2 \leftarrow 17_{2,15}39/2$	14091.4547	6.9	0.002
$18_{4,14}39/2 \leftarrow 17_{4,13}37/2$	14003.0065	-1.2	0.002

## n-Butyronitrile<sup>18</sup>

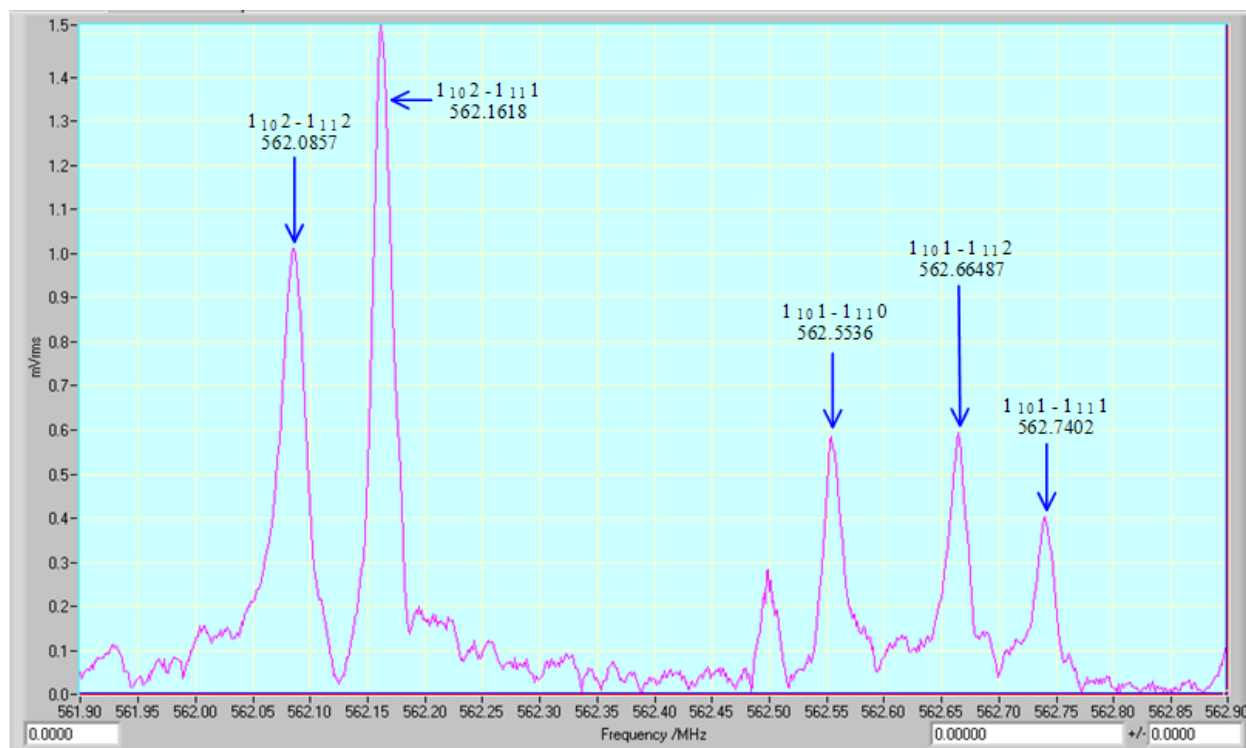


Figure 28. Spectrum of gauche n-butyronitrile while tuned to 562.4 MHz after 12000 cycles.

n-Butyronitrile helps demonstrate the usefulness of the ELF-FTMW. The lower J level transitions were able to be observed which allowed the hyperfine terms to become more precisely defined. The resolution was possible because hyperfine splitting is largest at these lower energy levels. In fact, the ELF-FTMW observed the lowest FTMW transition to date at 562 MHz. The spectrum is shown in Figure 28.

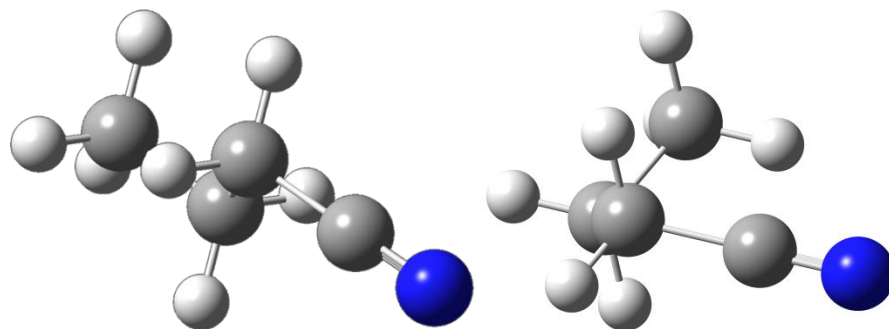


Figure 29. Depiction of anti-butyronitrile (left) and gauche-butyronitrile (right).

## Introduction

Interstellar chemistry requires that molecules be formed despite matter being vastly dispersed and the lack of a medium to transfer energy. Surprisingly, over a 150 molecules have been discovered to exist in the interstellar medium and circumstellar envelopes within the last 40 years. Among these new discoveries are molecules that consist of up to 13 atoms which is rather complex given the conditions. In order to find these molecules laboratory research must be conducted to give astrochemists a frequency region for interstellar candidates and to confirm their findings. n-Butyronitrile is a 12 atom interstellar candidate that was discovered in the hot dense core, Sagittarius B2(N), ~100 pc from the galactic center.<sup>32</sup>

n-Butyronitrile has been previously studied by 6 other research groups. Hirota first assigned  $\mu_a$  and  $\mu_b$  transitions for both the anti and gauche-confirmers. Then, the centrifugal distortion constants for the gauche-symmetry were analyzed by Kaushik. Demaison and Dreizler observed the  $^{14}\text{N}$  quadrupole hyperfine structure using a Fourier transform microwave spectrometer. The centrifugal distortion constants were refined by the work of Wlodarczak et al. with the aid of millimeter wave spectra. Wlodarczak et al. measured the dipole moments and energy difference between the anti and gauche-confirmers. Vormann and Dreizler contributed with refinement of the quadrupole coupling constants and determining the methyl internal rotation parameter by performing a double resonance experiment with a Fourier transform microwave spectrometer. Belloche et al. scanned for several molecules in the Sagittarius B2(N) region of space and greatly refined the rotational and centrifugal constants without taking into account the quadrupole splitting of  $^{14}\text{N}$  or the methyl internal rotation because it is unlikely to be observed in the interstellar n-butyronitrile spectrum.<sup>32, 33</sup>



n-Butyronitrile is a four carbon chain that has anti and gauche-conformers. These two conformers can be essentially treated as two different molecules in microwave spectroscopy and have various physical property differences. One difference is Ray's asymmetry parameter,  $\kappa$ , as defined by Equation 16.

$$\kappa = \frac{2B - A - C}{A - C}$$

Equation 16

Ray's asymmetry parameter is a numerical representation of the symmetry of a molecule, where  $\kappa = -1$  is an ideal prolate symmetric top,  $\kappa = 1$  is an ideal oblate symmetric top and  $\kappa$  values in between the other two are asymmetric tops. The lower energy, anti-symmetry form on n-butyronitrile is a symmetric prolate top with a  $\kappa$  value of  $-0.9893$ . Its counterpart, the gauche-form, is higher in energy having a more asymmetric character with a  $\kappa$  value of  $-0.8471$ . The dipole moments of the anti-conformer are  $\mu_a = 3.60$  D and  $\mu_b = 0.98$  D, while the gauche-conformer has  $\mu_a = 3.27$  D and  $\mu_b = 2.14$  D. The spectrometer used to study this molecule is dependent on the dipole moment for transition intensity. Based strictly on the dipole moments the a-type transition of the anti-form should be the strongest, followed by the gauche's a-type and b-type transitions, and ending with the b-type transitions of the anti-form to be the least intense.<sup>6, 32</sup>

### Experimental Method

The study of this molecule was done with the ELF-FTMW, which proved useful in observing low frequency rotational transitions. Our sample of n-butyronitrile was obtained from Acros Organics with 98% purity and no other purification was necessary. Roughly 2 ml of n-Butyronitrile was loaded in 6.35 mm diameter Teflon tube about 150 cm away from the nozzle. A backing gas of 1300 torr of argon was bubbled through the sample before entering the vacuum

chamber by way of a solenoid nozzle. The  $7 \times 10^{-7}$  torr vacuum on the chamber allowed two nozzle pulses per second to be optimal for obtaining spectra.

## Results

Constants from Vormann and Dreizler's work were used to create a line prediction at the beginning of this research. The fit for the molecular constants was updated as lines were measured on the ELF-FTMW spectrometer, allowing new lines to be predicted and then observed. After obtaining a reasonable fit for the rotational and centrifugal distortion constants, a refinement of the quadrupole coupling constants was pursued. In total, 104 transitions were recorded for the anti-symmetry and 107 transitions for the gauche-symmetry form of n-butyronitrile, which are shown in Table 15 and Table 16, respectively. Table 13 and Table 14 show the constants from this work's fits and compare them with Belloche's, Vormann's, and Dreizler's works.<sup>32-34</sup>

Table 13. Parameters of Anti n-butyronitrile Compared With Previous Work

Parameter	This Work	( 32)	( 33)	( 34)
A/MHz	23668.272 (12)	23668.31931 (143)	23668.320 (7)	23668.06
B/MHz	2268.1422 (11)	2268.14892 (147)	2268.1467 (8)	2268.16
C/MHz	2152.9557 (11)	2152.963946 (168)	2152.9610 (7)	2152.95
$\Delta_J$ /kHz	0.39591 (49)	0.398674 (69)	0.3952 (19)	
$\Delta_{JK}$ /kHz	-10.8209 (65)	-10.82631 (92)	-10.905 (56)	
$\Delta_K$ /kHz	239.83 (54)	240.653 (29)	241.28 (66)	
$\delta_J$ /kHz	-0.04833 (30)	-0.046637 (42)	0.04627 (14)	
$\delta_K$ /kHz	-0.000456 (41)	-0.0005901 (59)	0.835 (49)	
$\Phi_J$ /Hz	-0.000013 (79)	0.000353 (11)		
$\Phi_{JK}$ /Hz	-0.0189 (14)	0.02067 (20)		
$\Phi_{KJ}$ /Hz	0.363 (17)	0.3724 (24)		
$\Phi_K$ /Hz	3 (11)	2.5		
$\phi_J$ /Hz	0.00059 (10)	0.000117 (14)		
$\alpha$ /MHz			-0.989293	
$\sigma$ /Hz			21	
$\chi_{aa'}$ /MHz	-2.61 (13)		-3.440 (4)	
$\chi_{bb'}$ /MHz	0.36 (13)		1.385 (5)	
$\chi_{cc'}$ /MHz	2.250 (70)		2.056 (5)	

Table 14. Parameters of Gauche n-butyronitrile Compared With Previous Work.

Parameter	This Work	( 32)	( 33)	( 34)
A/MHz	10060.41102 ( 60)	10060.41649 (108)	10060.416 (3)	10060.37
B/MHz	3267.660863 (193)	3267.662408 (301)	3267.6793 (8)	3267.63
C/MHz	2705.457727 (178)	2705.459572 (290)	2705.4433 (7)	2705.49
$\Delta_J$ /kHz	3.193967 (170)	3.195064 (207)	3.34948 (52)	
$\Delta_{JK}$ /kHz	-18.25536 (149)	-18.26470 (117)	-19.1862 (18)	
$\Delta_K$ /kHz	60.1712( 37)	60.235 (6)	60.998 (34)	
$\delta_J$ /kHz	-1.0372085(280)	-1.037470 (55)	1.0386 (22)	
$\delta_K$ /kHz	-0.0773157(162)	-0.0771864 (183)	7.779 (10)	
$\Phi_J$ /Hz	0.004249( 55)		0.00579 (16)	
$\Phi_{JK}$ /Hz	0.01928(154)		0.0250 (48)	
$\Phi_{KJ}$ /Hz	-0.5334( 43)		- 0.564 (17)	
$\Phi_K$ /Hz	1.6607(128)		1.80 (13)	
$\varphi_J$ /Hz	0.0023273(164)		0.003088 (90)	
$\varphi_{JK}$ /Hz			-0.0217 (49)	
$\varphi_K$ /Hz			0.380 (92)	
$\alpha$ /MHz			-0.847114	
$\sigma$ /kHz			52	
$\chi_{aa}$ /MHz	-1.6825 (27)		-1.683 (4)	
$\chi_{bb}$ /MHz	-0.2490 (27)		-0.252 (5)	
$\chi_{cc}$ /MHz	1.9315 (26)		1.935 (5)	
$\chi_{ab}$ /MHz	-3.12 (30)			
$\chi_{ac}$ /MHz	-0.70 (17)			

## Discussion

All of the diagonal components of the  $^{14}\text{N}$  quadrupole coupling tensor and two of the off diagonal components were determined from the transitions that were observed. The bottom of Table 14 demonstrates the improved precision of the diagonal components of the quadrupole tensor over Vormann and Dreizler's work. Also, the data recorded by the ELF-FTMW allowed for the calculation of  $\chi_{ab}$  and  $\chi_{ac}$ .

## Conclusion

The pure rotational spectrum of n-butyronitrile below 4 GHz was recorded for the first time. Transitions observed had splitting due to the  $^{14}\text{N}$  quadrupole coupling tensor and internal rotation of the methyl rotor. The diagonal components of the quadrupole tensor were refined to greater precision and two off diagonal terms,  $\chi_{ab}$  and  $\chi_{ac}$ , were determined for both the anti and gauche-confirmers.

Table 11. Observed Transitions of The Anti-symmetry of n-butyronitrile

Transition	Frequency (MHz)	Obs-Calc (kHz)	Uncertainty (MHz)
1 <sub>0,1</sub> 0 ← 0 <sub>0,0</sub> 1	4422.83	421.7	0.002
1 <sub>0,1</sub> 1 ← 0 <sub>0,0</sub> 1	4420.25	-192.2	0.002
1 <sub>0,1</sub> 2 ← 0 <sub>0,0</sub> 1	4421.28	52.6	0.002
2 <sub>0,2</sub> 2 ← 1 <sub>0,1</sub> 1	8841.75	26.76	0.002
2 <sub>0,2</sub> 3 ← 1 <sub>0,1</sub> 2	8841.81	38.77	0.002
2 <sub>1,1</sub> 1 ← 1 <sub>1,0</sub> 0	8958.81	177.25	0.002
2 <sub>1,1</sub> 2 ← 1 <sub>1,0</sub> 1	8956.57	-183.28	0.002
2 <sub>1,1</sub> 3 ← 1 <sub>1,0</sub> 2	8957.64	85.32	0.002
2 <sub>1,2</sub> 1 ← 1 <sub>1,1</sub> 0	8728.27	485.95	0.002
2 <sub>1,2</sub> 2 ← 1 <sub>1,1</sub> 1	8726.21	-177.6	0.002
2 <sub>1,2</sub> 2 ← 1 <sub>1,1</sub> 1	8726.22	-169.6	0.002
2 <sub>1,2</sub> 2 ← 1 <sub>1,1</sub> 1	8727.24	852.49	0.002
2 <sub>1,2</sub> 2 ← 1 <sub>1,1</sub> 2	8726.63	128.37	0.002
2 <sub>1,2</sub> 2 ← 1 <sub>1,1</sub> 2	8727.25	755.47	0.002
2 <sub>1,2</sub> 3 ← 1 <sub>1,1</sub> 2	8727.28	63.57	0.002
2 <sub>1,2</sub> 3 ← 1 <sub>1,1</sub> 2	8727.29	67.37	0.002
1 <sub>1,1</sub> 1 ← 2 <sub>0,2</sub> 2	12559.4	446.36	0.002
1 <sub>1,1</sub> 1 ← 2 <sub>0,2</sub> 2	12559.5	513.86	0.002
3 <sub>0,3</sub> 2 ← 2 <sub>0,2</sub> 1	13261.3	-2.62	0.002
3 <sub>0,3</sub> 2 ← 2 <sub>0,2</sub> 2	13262.7	114.8	0.002
3 <sub>0,3</sub> 3 ← 2 <sub>0,2</sub> 2	13261.4	36.78	0.002
3 <sub>0,3</sub> 4 ← 2 <sub>0,2</sub> 3	13261.5	50.45	0.002
3 <sub>1,2</sub> 2 ← 2 <sub>1,1</sub> 1	13435.9	23.03	0.002
3 <sub>1,2</sub> 3 ← 2 <sub>1,1</sub> 2	13435.6	-18.11	0.002
3 <sub>1,2</sub> 3 ← 2 <sub>1,1</sub> 3	13435.2	-346.69	0.002
3 <sub>1,2</sub> 4 ← 2 <sub>1,1</sub> 3	13435.9	62.25	0.002
3 <sub>1,3</sub> 2 ← 2 <sub>1,2</sub> 1	13090.4	89.77	0.002
3 <sub>1,3</sub> 3 ← 2 <sub>1,2</sub> 2	13090.1	-6.83	0.002
3 <sub>1,3</sub> 4 ← 2 <sub>1,2</sub> 3	13090.4	59.83	0.002
3 <sub>2,1</sub> 2 ← 2 <sub>2,0</sub> 1	13266.3	244.77	0.002
3 <sub>2,1</sub> 3 ← 2 <sub>2,0</sub> 2	13264.5	-170.16	0.002
3 <sub>2,1</sub> 4 ← 2 <sub>2,0</sub> 3	13265.7	99.38	0.002
3 <sub>2,2</sub> 2 ← 2 <sub>2,1</sub> 1	13264	-180.26	0.002
3 <sub>2,2</sub> 3 ← 2 <sub>2,1</sub> 2	13263	124.95	0.002
3 <sub>2,2</sub> 4 ← 2 <sub>2,1</sub> 3	13263.8	99.91	0.002
2 <sub>1,2</sub> 1 ← 3 <sub>0,3</sub> 2	8023.77	-102	0.002
2 <sub>1,2</sub> 2 ← 3 <sub>0,3</sub> 2	8023.64	894.9	0.002
2 <sub>1,2</sub> 2 ← 3 <sub>0,3</sub> 3	8023.79	-146.3	0.002
2 <sub>1,2</sub> 3 ← 3 <sub>0,3</sub> 3	8024.16	-494.2	0.002
2 <sub>1,2</sub> 3 ← 3 <sub>0,3</sub> 4	8023.68	-99.2	0.002
3 <sub>1,2</sub> 2 ← 3 <sub>1,3</sub> 2	690.698	-29.3	0.007
3 <sub>1,2</sub> 4 ← 3 <sub>1,3</sub> 4	691.18	232.9	0.007
4 <sub>0,4</sub> 3 ← 3 <sub>0,3</sub> 2	17679.6	27.53	0.002
4 <sub>0,4</sub> 4 ← 3 <sub>0,3</sub> 3	17679.7	52.49	0.002
4 <sub>0,4</sub> 4 ← 3 <sub>0,3</sub> 4	17678.6	-219.21	0.002
4 <sub>0,4</sub> 5 ← 3 <sub>0,3</sub> 4	17679.7	58.24	0.002
4 <sub>2,3</sub> 3 ← 3 <sub>2,2</sub> 2	17684.4	-15.62	0.002
4 <sub>2,3</sub> 3 ← 3 <sub>2,2</sub> 3	17684.6	113.9	0.002
4 <sub>2,3</sub> 4 ← 3 <sub>2,2</sub> 3	17684	-34.52	0.002
4 <sub>2,3</sub> 3 ← 3 <sub>2,2</sub> 4	17684.6	166.28	0.002
4 <sub>2,3</sub> 5 ← 3 <sub>2,2</sub> 4	17684	-327.9	0.002
3 <sub>1,3</sub> 2 ← 4 <sub>0,4</sub> 3	3434.6	56.7	0.002
3 <sub>1,3</sub> 3 ← 4 <sub>0,4</sub> 3	3434.34	1097.5	0.002
3 <sub>1,3</sub> 3 ← 4 <sub>0,4</sub> 4	3434.4	31.6	0.002
3 <sub>1,3</sub> 4 ← 4 <sub>0,4</sub> 5	3434.53	96	0.002
4 <sub>1,3</sub> 3 ← 4 <sub>1,4</sub> 3	1151.25	-236.5	0.002
4 <sub>1,3</sub> 5 ← 4 <sub>1,4</sub> 5	1151.39	-260.2	0.002
5 <sub>0,5</sub> 4 ← 4 <sub>0,4</sub> 3	22096	56.06	0.002
5 <sub>0,5</sub> 5 ← 4 <sub>0,4</sub> 4	22096.1	69.37	0.002
5 <sub>0,5</sub> 6 ← 4 <sub>0,4</sub> 5	22096.1	68.58	0.002
5 <sub>0,5</sub> 4 ← 4 <sub>1,4</sub> 3	1207.98	-388.6	0.002
5 <sub>0,5</sub> 4 ← 4 <sub>1,4</sub> 3	1208.42	52.4	0.002
5 <sub>0,5</sub> 5 ← 4 <sub>1,4</sub> 4	1208.55	-73.7	0.002
5 <sub>0,5</sub> 5 ← 4 <sub>1,4</sub> 4	1208.56	-61.8	0.002

(Table 11 continued)

Transition	Frequency (MHz)	Obs-Calc (kHz)	Uncertainty (MHz)
5 <sub>0,5</sub> 5 ← 4 <sub>1,4</sub> 4	1208.56	-60.3	0.002
5 <sub>0,5</sub> 5 ← 4 <sub>1,4</sub> 5	1208.23	689.6	0.002
5 <sub>0,5</sub> 6 ← 4 <sub>1,4</sub> 5	1208.5	40.3	0.002
5 <sub>0,5</sub> 6 ← 4 <sub>1,4</sub> 5	1208.51	53.5	0.002
5 <sub>3,3</sub> 4 ← 4 <sub>3,2</sub> 3	22108.1	11.11	0.002
5 <sub>3,3</sub> 5 ← 4 <sub>3,2</sub> 4	22107.5	-17.75	0.002
5 <sub>1,4</sub> 5 ← 5 <sub>1,5</sub> 5	1727.8	-348.5	0.002
5 <sub>1,4</sub> 6 ← 5 <sub>1,5</sub> 6	1727.57	73.7	0.002
6 <sub>1,5</sub> 5 ← 6 <sub>1,6</sub> 5	2418.47	117.5	0.005
6 <sub>1,5</sub> 6 ← 6 <sub>1,6</sub> 6	2418.76	-362.5	0.002
6 <sub>1,5</sub> 7 ← 6 <sub>1,6</sub> 7	2418.52	64.9	0.002
7 <sub>1,6</sub> 6 ← 7 <sub>1,7</sub> 6	3224.47	80.5	0.003
7 <sub>1,6</sub> 7 ← 7 <sub>1,7</sub> 7	3224.77	-376.8	0.005
7 <sub>1,6</sub> 8 ← 7 <sub>1,7</sub> 8	3224.53	49.5	0.003
8 <sub>0,8</sub> 7 ← 7 <sub>1,7</sub> 6	15437.9	50.78	0.002
8 <sub>0,8</sub> 8 ← 7 <sub>1,7</sub> 7	15438.1	-92.12	0.002
8 <sub>0,8</sub> 9 ← 7 <sub>1,7</sub> 8	15438	93.81	0.002
8 <sub>1,7</sub> 7 ← 8 <sub>1,8</sub> 7	4145.48	86.7	0.002
8 <sub>1,7</sub> 8 ← 8 <sub>1,8</sub> 8	4145.75	-398.1	0.002
8 <sub>1,7</sub> 9 ← 8 <sub>1,8</sub> 9	4145.51	33.3	0.002

Transition	Frequency (MHz)	Obs-Calc (kHz)	Uncertainty (MHz)
9 <sub>1,8</sub> 8 ← 9 <sub>1,9</sub> 8	5181.32	65.4	0.005
9 <sub>1,8</sub> 10 ← 9 <sub>1,9</sub> 10	5181.57	236.7	0.005
10 <sub>1,9</sub> 9 ← 10 <sub>1,10</sub> 9	6331.83	10.6	0.07
10 <sub>1,9</sub> 10 ← 10 <sub>1,10</sub> 10	6332.11	-450.2	0.07
10 <sub>1,9</sub> 11 ← 10 <sub>1,10</sub> 11	6331.87	-18.9	0.07
11 <sub>1,10</sub> 10 ← 11 <sub>1,11</sub> 10	7596.73	-125.1	0.002
11 <sub>1,10</sub> 11 ← 11 <sub>1,11</sub> 11	7597.13	-466.7	0.002
11 <sub>1,10</sub> 12 ← 11 <sub>1,11</sub> 12	7596.9	-25.8	0.002
11 <sub>2,10</sub> 10 ← 12 <sub>1,11</sub> 11	6898.06	89.8	0.002
11 <sub>2,10</sub> 11 ← 12 <sub>1,11</sub> 12	6897.91	222.8	0.002
11 <sub>2,10</sub> 12 ← 12 <sub>1,11</sub> 13	6898.02	77.5	0.002
12 <sub>2,10</sub> 11 ← 13 <sub>1,13</sub> 12	12683.2	-123.52	0.002
12 <sub>2,10</sub> 12 ← 13 <sub>1,13</sub> 13	12683.6	-224.75	0.002
12 <sub>2,10</sub> 13 ← 13 <sub>1,13</sub> 14	12683.3	22.46	0.002
14 <sub>2,12</sub> 13 ← 15 <sub>1,15</sub> 14	5937.25	-170.7	0.01
14 <sub>2,12</sub> 14 ← 15 <sub>1,15</sub> 15	5937.42	-513.6	0.002
14 <sub>2,12</sub> 15 ← 15 <sub>1,15</sub> 16	5937.27	-177.3	0.01
Unassigned	13264.3		0.002

Table 12. Observed Transitions of The Gauche-symmetry of n-butyronitrile

Transition	Frequency (MHz)	Obs-Calc (kHz)	Uncertainty (MHz)	Transition	Frequency (MHz)	Obs-Calc (kHz)	Uncertainty (MHz)
1 <sub>0,1</sub> 0 ← 0 <sub>0,0</sub> 1	5973.94992	3.2	0.002	2 <sub>1,1</sub> 1 ← 2 <sub>0,2</sub> 1	7950.1368	2.7	0.002
1 <sub>0,1</sub> 1 ← 0 <sub>0,0</sub> 1	5972.68696	1.7	0.002	2 <sub>1,1</sub> 2 ← 2 <sub>0,2</sub> 1	7950.26082	2.2	0.002
1 <sub>0,1</sub> 2 ← 0 <sub>0,0</sub> 1	5973.1933	3.4	0.002	2 <sub>1,1</sub> 1 ← 2 <sub>0,2</sub> 2	7951.02306	6.4	0.002
1 <sub>1,1</sub> 0 ← 0 <sub>0,0</sub> 1	12765.96309	1.7	0.002	2 <sub>1,1</sub> 2 ← 2 <sub>0,2</sub> 2	7951.14523	4	0.002
1 <sub>1,1</sub> 1 ← 0 <sub>0,0</sub> 1	12765.78142	7.2	0.002	2 <sub>1,1</sub> 2 ← 2 <sub>0,2</sub> 3	7950.58702	12.9	0.002
1 <sub>1,1</sub> 2 ← 0 <sub>0,0</sub> 1	12765.85693	8	0.002	2 <sub>1,1</sub> 3 ← 2 <sub>0,2</sub> 3	7950.49782	3.8	0.002
1 <sub>1,0</sub> 1 ← 1 <sub>0,1</sub> 0	7354.57057	3.4	0.002	2 <sub>1,1</sub> 1 ← 2 <sub>1,2</sub> 1	1685.99181	2.3	0.002
1 <sub>1,0</sub> 0 ← 1 <sub>0,1</sub> 1	7354.37392	-6.5	0.002	2 <sub>1,1</sub> 2 ← 2 <sub>1,2</sub> 1	1686.11444	0.4	0.002
1 <sub>1,0</sub> 2 ← 1 <sub>0,1</sub> 1	7355.24468	-4.7	0.002	2 <sub>1,1</sub> 2 ← 2 <sub>1,2</sub> 2	1687.0811	1.3	0.002
1 <sub>1,0</sub> 1 ← 1 <sub>0,1</sub> 2	7355.31898	-5	0.002	2 <sub>1,1</sub> 3 ← 2 <sub>1,2</sub> 3	1686.3794	0.5	0.002
1 <sub>1,0</sub> 2 ← 1 <sub>0,1</sub> 2	7354.74784	3	0.002	3 <sub>0,3</sub> 3 ← 2 <sub>0,2</sub> 3	17785.356	20.7	0.01
1 <sub>1,0</sub> 1 ← 1 <sub>1,1</sub> 0	562.55355	1.1	0.002	3 <sub>0,3</sub> 4 ← 2 <sub>0,2</sub> 3	17785.949	-15.1	0.01
1 <sub>1,0</sub> 0 ← 1 <sub>1,1</sub> 1	561.29019	-1.3	0.002	3 <sub>1,3</sub> 3 ← 2 <sub>1,2</sub> 2	17055.466	-21.2	0.005
1 <sub>1,0</sub> 1 ← 1 <sub>1,1</sub> 1	562.74019	0.5	0.002	3 <sub>1,3</sub> 4 ← 2 <sub>1,2</sub> 3	17055.664	5.4	0.005
1 <sub>1,0</sub> 2 ← 1 <sub>1,1</sub> 1	562.16183	1.3	0.002	2 <sub>2,1</sub> 1 ← 3 <sub>1,2</sub> 2	1636.51586	-3.4	0.002
1 <sub>1,0</sub> 1 ← 1 <sub>1,1</sub> 2	562.66487	-0.1	0.002	2 <sub>2,1</sub> 2 ← 3 <sub>1,2</sub> 3	1637.45188	2.4	0.002
1 <sub>1,0</sub> 2 ← 1 <sub>1,1</sub> 2	562.08574	-0.1	0.002	2 <sub>2,1</sub> 3 ← 3 <sub>1,2</sub> 3	1636.93081	22	0.002
2 <sub>0,2</sub> 2 ← 1 <sub>0,1</sub> 1	11912.623	-22.1	0.01	2 <sub>2,1</sub> 3 ← 3 <sub>1,2</sub> 4	1636.84427	1.7	0.002
2 <sub>0,2</sub> 3 ← 1 <sub>0,1</sub> 2	11912.707	-0.5	0.01	3 <sub>1,2</sub> 2 ← 3 <sub>1,3</sub> 2	3371.2345	-2.3	0.002
2 <sub>1,2</sub> 3 ← 1 <sub>0,1</sub> 2	18176.781	-41.6	0.005	3 <sub>1,2</sub> 3 ← 3 <sub>1,3</sub> 3	3372.21332	-3.9	0.002
2 <sub>0,2</sub> 1 ← 1 <sub>1,1</sub> 0	5120.4407	189.3	0.002	3 <sub>1,2</sub> 4 ← 3 <sub>1,3</sub> 4	3371.48806	-3	0.002
2 <sub>0,2</sub> 2 ← 1 <sub>1,1</sub> 1	5120.05255	496.5	0.002	3 <sub>3,1</sub> 2 ← 4 <sub>2,2</sub> 3	11025.93962	-4.4	0.005
2 <sub>0,2</sub> 3 ← 1 <sub>1,1</sub> 2	5120.25567	207.2	0.002	3 <sub>3,1</sub> 3 ← 4 <sub>2,2</sub> 4	11027.04654	2.9	0.005
2 <sub>1,1</sub> 1 ← 1 <sub>1,0</sub> 0	12509.28805	6.7	0.002	3 <sub>3,1</sub> 4 ← 4 <sub>2,2</sub> 5	11026.22226	1	0.005
2 <sub>1,1</sub> 2 ← 1 <sub>1,0</sub> 1	12507.958	0.4	0.01	4 <sub>1,3</sub> 3 ← 4 <sub>0,4</sub> 3	10286.3	-7.4	0.005
2 <sub>1,1</sub> 3 ← 1 <sub>1,0</sub> 2	12508.451	-5.7	0.01	4 <sub>1,3</sub> 4 ← 4 <sub>0,4</sub> 4	10287.013	5.8	0.005
2 <sub>1,2</sub> 1 ← 1 <sub>1,1</sub> 0	11384.40348	7.5	0.002	4 <sub>1,3</sub> 5 ← 4 <sub>0,4</sub> 5	10286.458	7.5	0.005
2 <sub>1,2</sub> 1 ← 1 <sub>1,1</sub> 1	11384.58777	4.5	0.002	4 <sub>1,3</sub> 3 ← 4 <sub>1,4</sub> 3	5612.10899	6	0.002
2 <sub>1,2</sub> 2 ← 1 <sub>1,1</sub> 1	11383.627	9.5	0.01	4 <sub>1,3</sub> 4 ← 4 <sub>1,4</sub> 4	5613.03115	-1.3	0.002
2 <sub>1,2</sub> 1 ← 1 <sub>1,1</sub> 2	11384.52171	13.1	0.002	4 <sub>1,3</sub> 5 ← 4 <sub>1,4</sub> 5	5612.29351	2	0.002
2 <sub>1,2</sub> 3 ← 1 <sub>1,1</sub> 2	11384.169	5.5	0.01	5 <sub>1,5</sub> 4 ← 4 <sub>2,2</sub> 3	3741.61085	4.7	0.002
2 <sub>1,2</sub> 3 ← 1 <sub>1,1</sub> 2	11384.17144	7.9	0.002	5 <sub>1,5</sub> 5 ← 4 <sub>2,2</sub> 4	3740.62686	6.7	0.002



(Table 12 continued)

Transition	Frequency (MHz)	Obs-Calc (kHz)	Uncertainty (MHz)
5 <sub>1,5</sub> 6 ← 4 <sub>2,2</sub> 5	3741.44863	4.3	0.002
4 <sub>3,2</sub> 3 ← 5 <sub>2,3</sub> 4	4556.53517	3.5	0.002
4 <sub>3,2</sub> 4 ← 5 <sub>2,3</sub> 4	4556.81741	7.5	0.002
4 <sub>3,2</sub> 4 ← 5 <sub>2,3</sub> 5	4557.02493	-1.6	0.002
4 <sub>3,2</sub> 5 ← 5 <sub>2,3</sub> 6	4556.62475	-0.4	0.002
4 <sub>3,1</sub> 3 ← 5 <sub>2,4</sub> 4	5694.84735	-0.8	0.002
4 <sub>3,1</sub> 4 ← 5 <sub>2,4</sub> 5	5695.57511	3.3	0.002
4 <sub>3,1</sub> 5 ← 5 <sub>2,4</sub> 6	5694.9802	-0.4	0.002
5 <sub>1,4</sub> 4 ← 5 <sub>0,5</sub> 4	12167.59346	1.3	0.002
5 <sub>1,4</sub> 5 ← 5 <sub>0,5</sub> 5	12168.291	3.2	0.005
5 <sub>1,4</sub> 5 ← 5 <sub>0,5</sub> 6	12167.36272	-156.1	0.002
5 <sub>1,4</sub> 6 ← 5 <sub>0,5</sub> 6	12167.70993	-0.1	0.002
5 <sub>1,4</sub> 4 ← 5 <sub>1,5</sub> 4	8396.10985	-4	0.002
5 <sub>1,4</sub> 5 ← 5 <sub>1,5</sub> 5	8397.00777	-4.3	0.002
5 <sub>1,4</sub> 6 ← 5 <sub>1,5</sub> 6	8396.25875	-7.2	0.002
5 <sub>2,3</sub> 4 ← 5 <sub>2,4</sub> 4	1129.60449	-1	0.002
5 <sub>2,3</sub> 5 ← 5 <sub>2,4</sub> 5	1129.82952	-0.7	0.002
5 <sub>2,3</sub> 6 ← 5 <sub>2,4</sub> 6	1129.64294	-0.7	0.002
6 <sub>2,4</sub> 5 ← 5 <sub>3,3</sub> 4	2219.46573	2.4	0.002
6 <sub>2,4</sub> 6 ← 5 <sub>3,3</sub> 5	2219.28224	5.7	0.002
6 <sub>2,4</sub> 7 ← 5 <sub>3,3</sub> 6	2219.44052	-1.6	0.002
6 <sub>1,5</sub> 5 ← 6 <sub>0,6</sub> 5	14609.108	-21.7	0.005
6 <sub>1,5</sub> 6 ← 6 <sub>0,6</sub> 6	14609.842	3.7	0.005

Transition	Frequency (MHz)	Obs-Calc (kHz)	Uncertainty (MHz)
6 <sub>1,5</sub> 7 ← 6 <sub>0,6</sub> 7	14609.234	1.9	0.005
6 <sub>2,4</sub> 5 ← 6 <sub>2,5</sub> 5	2187.01622	2.6	0.002
6 <sub>2,4</sub> 6 ← 6 <sub>2,5</sub> 6	2187.3195	5.1	0.002
6 <sub>2,4</sub> 7 ← 6 <sub>2,5</sub> 7	2187.06823	1.1	0.002
7 <sub>2,5</sub> 6 ← 7 <sub>1,6</sub> 6	17681.37547	10.2	0.002
7 <sub>2,5</sub> 6 ← 7 <sub>1,6</sub> 7	17682.01126	322.1	0.002
7 <sub>2,5</sub> 7 ← 7 <sub>1,6</sub> 7	17681.51241	46.9	0.01
7 <sub>2,5</sub> 8 ← 7 <sub>1,6</sub> 7	17681.4624	-198.5	0.007
7 <sub>2,5</sub> 7 ← 7 <sub>1,6</sub> 8	17681.17886	-3.5	0.002
7 <sub>2,5</sub> 8 ← 7 <sub>1,6</sub> 8	17681.38941	11.5	0.002
7 <sub>2,5</sub> 6 ← 7 <sub>2,6</sub> 6	3759.69796	-11.1	0.002
7 <sub>2,5</sub> 7 ← 7 <sub>2,6</sub> 7	3760.06536	-7.9	0.002
7 <sub>2,5</sub> 8 ← 7 <sub>2,6</sub> 8	3759.7499	-5.1	0.002
7 <sub>4,3</sub> 7 ← 7 <sub>3,6</sub> 8	1315.22109	-2.4	0.002
7 <sub>4,3</sub> 6 ← 8 <sub>3,6</sub> 7	1314.91252	-2.4	0.002
7 <sub>4,3</sub> 8 ← 8 <sub>3,6</sub> 9	1314.94464	-4.1	0.002
8 <sub>2,6</sub> 8 ← 8 <sub>2,7</sub> 8	5906.39757	-6	0.002
8 <sub>2,6</sub> 9 ← 8 <sub>2,7</sub> 9	5906.0287	0.2	0.002
9 <sub>3,6</sub> 8 ← 9 <sub>3,7</sub> 8	1077.39799	-2.9	0.002
9 <sub>3,6</sub> 9 ← 9 <sub>3,7</sub> 9	1077.50101	0.7	0.002
9 <sub>3,6</sub> 10 ← 9 <sub>3,7</sub> 10	1077.4119	1	0.002

## Difluoroiodomethane<sup>35</sup>

Difluoroiodomethane is a good demonstration of the advantages of the chirped pulse spectrometer. The entire spectrum of 8-16 GHz of this molecule was able to be observed and recorded in a mere 14 hours. The 260 transitions recorded with this spectrometer are each of the nature of having correct relative intensity. This allowed for the spectral patterns to be more easily recognized which aided in obtaining a quick fit for the rotational parameters.

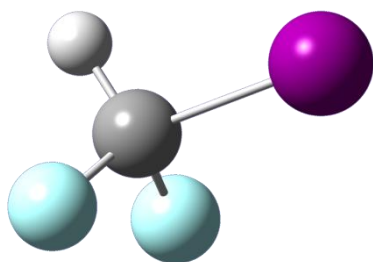


Figure 30. Depiction of difluoroiodomethane.

### Introduction

Many variously fluorinated species have been studied due to their potential use as refrigerants. Difluoroiodomethane has yet to be studied spectroscopically, most likely due to its low boiling point and propensity to disproportionate. This molecule is of interest in that it may allow for relatively strong forbidden transitions like other fluorinated alkyl halides. Also, this molecule will help complete the series of  $\text{CH}_{3-n}\text{F}_n\text{X}$  where  $n = 0, 1, 2, 3$  and  $\text{X} = \text{Cl}, \text{Br}, \text{I}$ .

### Experimental Method

Two spectrometers were used in this study of difluoroiodomethane where each spectrometer's strength could be capitalized upon. The main instrument used was the chirped pulse spectrometer in order to observe 2 GHz of spectra at a time that was averaged for 10000 cycles to cover a range of 8-16 GHz. The ELF-FTMW was used to observe about 25 transitions below 5 GHz and a handful of other transitions.

The sample was prepared by making a 2% gas mixture of difluoroiodomethane mixed with Argon. The 97% purity of difluoroiodomethane was purchased from Synquest Labs, Inc. where no further purification was necessary for these experiments. The backing gas pressure was typically between 2280 - 3800 Torr.

## Results

Over 300 transitions were assigned for difluoroiodomethane and are listed on Table 20. The transitions observed with the chirped pulse spectrometer typically had line widths of 80 kHz but the assigned uncertainty of the line centers is 6 kHz. For the ELF-FTMW an uncertainty of 2 kHz was assigned. The a type R branch transitions were assigned first by using the data obtained by the chirped pulse spectrometer. A Watson S reduction was used with the SPFIT program to generate a rough fit. Then, c type transitions were assigned until the fit was good enough to assign the Q branch transitions. Table 17 shows the final parameters obtained with this study of difluoroiodomethane.

Table 17. Parameters For Difluoroiodomethane

Parameter	Value
A/MHz	10139.33825(41)
B/MHz	2089.441128(90)
C/MHz	1791.825937(76)
$\Delta_J$ /kHz	0.3786(10)
$\Delta_{JK}$ /kHz	2.391(11)
$\Delta_K$ /kHz	8.300(30)
$\delta_1$ /kHz	-0.06088(15)
$\delta_2$ /kHz	-0.01080(12)
$\chi_{aa'}$ /MHz	-1817.9143(34)
$\chi_{bb} - \chi_{cc}$ /MHz	114.3036(56)
$\chi_{ac}$ /MHz	570.2057(81)
$M_{aa'}$ /kHz	5.22(34)
$M_{bb'}$ /kHz	7.77(11)
$M_{cc'}$ /kHz	7.419(93)
N	304
$\sigma$ /kHz	5.65

Numbers in parenthesis indicate one standard deviation in units of the least significant figure. N is the number of observed transitions used in the fit.  $\sigma$  is the standard deviation of the fit,

$$\sqrt{\left(\sum \left[(\text{obs}-\text{calc})^2\right] / N_{\text{lines}}\right)}.$$

### Discussion

The iodine nuclear quadrupole coupling tensor components have been determined and are shown on Table 18 for both the inertial and principal quadrupolar axis.

Table 18. Parameters For The Components of The Iodine Inertial and Principal Nuclear Quadrupole Tensor in Difluoriodomethane

Parameter	Value
$\chi_{aa}/\text{MHz}$	-1817.9153(33)
$\chi_{cc}/\text{MHz}$	851.8060(32)
$\chi_{ac}/\text{MHz}$	520.2074(78)
$\chi_{zz}/\text{MHz}$	-1915.6986(42)
$\chi_{xx}/\text{MHz}$	949.5893(42)
$\chi_{yy} = \chi_{bb}/\text{MHz}$	966.1092(32)
$H_{KJ}$	0.0086234(28)
$\theta_{za}$	10.6457(1) $^\circ$
$\theta_{\text{Cl,a}}$	11.1 $^\circ$

Numbers in parenthesis indicate one standard deviation in units of the least significant figure.  $\theta_{za}$  is the angle between the a-axis of the principal inertial tensor and the z-axis of the principal nuclear quadrupole coupling tensor.  $\theta_{\text{Cl,a}}$  is the angle between the a-axis and the C-I bond.  $\eta$  is the nuclear quadrupole asymmetry parameter,  $\eta = \frac{(\chi_{xx} - \chi_{yy})}{\chi_{zz}}$ .

It should be mentioned that  $\chi_{ac}$  is rather large which aided in the observation of forbidden transitions. Similarly to trans-1-iodoperfluoropropane, the large off diagonal component of the quadrupole coupling tensor allows for a mixing of rotational states. For the  $6_{3,3} \frac{11}{2} \leftarrow 8_{1,8} \frac{13}{2}$  transition, the  $8_{1,8} \frac{13}{2}$  state is mixed with the  $7_{2,5} \frac{13}{2}$  state that is 99 MHz lower. When compared to varying degrees of fluorination of methyl halides, shown on Table 19, the magnitude of  $\chi_{zz}$  has the trend of decreasing for  $-\text{CF}_3 > -\text{CH}_3 > -\text{CHF}_2 > -\text{CH}_2\text{F}$ . This indicates that electron charge around the halogen is the most distributed in  $-\text{CF}_3$  and most localized in  $-\text{CH}_2\text{F}$ . Further supporting this trend, an ab initio calculation, MP2/aug-cc-pVTZ, resulted in the partial charge

of iodine to be decreasing for  $\text{I-CF}_3 > \text{I-CH}_3 > \text{I-CHF}_2 > \text{I-CH}_2\text{F}$  with values of +0.115, +0.068, +0.059, and +0.047, respectively.<sup>36</sup>

Table 19. Comparison of The Nuclear Quadrupole Coupling Tensor Component,  $zz$ , in Varying Degrees of Fluorinated Methyl Halides

Molecule	<sup>35</sup> Cl	<sup>79</sup> Br	I
CH <sub>3</sub> X	-74.753(2) <sup>37</sup>	577.1088(57) <sup>38</sup>	-1934.080(10) <sup>26</sup>
CH <sub>2</sub> FX	-70.48 <sup>39</sup>	554.389 <sup>40</sup>	-1879.832 <sup>41</sup>
CHF <sub>2</sub> X	-71.78 <sup>42</sup>	564.7(23) <sup>43</sup>	-1915.6986(42) <sup>This work</sup>
CF <sub>3</sub> X	-77.902(30) <sup>44</sup>	618.264(15) <sup>45</sup>	-2145.207(3) <sup>46</sup>

Numbers in parenthesis indicate one standard deviation in units of the least significant figure. CH<sub>2</sub>F<sup>35</sup>Cl was approximated by assuming the C-Cl bond is coincident with the z principal axis.

## Conclusion

This is the first time for the spectroscopic constants to be determined for the ground state of difluoroiodomethane. Several forbidden transitions were observed due to the large off diagonal quadrupole coupling tensor component of the iodine nucleus. Lastly, the trend of decreasing magnitude of  $\chi_{zz}$  for  $\text{X-CF}_3 > \text{X-CH}_3 > \text{X-CHF}_2 > \text{X-CH}_2\text{F}$  was upheld.

Table 13. Observed Transitions of Difluoriodopropane

Transition	Frequency (MHz)	Obs-Calc (kHz)	Uncertainty (MHz)	Transition	Frequency (MHz)	Obs-Calc (kHz)	Uncertainty (MHz)
1 <sub>0,1</sub> 3/2← 0 <sub>0,0</sub> 5/2	4144.42625	-1.5	0.002	2 <sub>1,1</sub> 5/2← 1 <sub>1,0</sub> 7/2	8045.4733	-4.06	0.006
1 <sub>0,1</sub> 7/2← 0 <sub>0,0</sub> 5/2	3977.32115	0.53	0.002	2 <sub>1,1</sub> 7/2← 1 <sub>1,0</sub> 7/2	8000.7186	-8.76	0.006
1 <sub>1,0</sub> 3/2← 0 <sub>0,0</sub> 5/2	12105.5148	4.61	0.006	2 <sub>1,1</sub> 9/2← 1 <sub>1,0</sub> 7/2	8177.2679	0.56	0.006
1 <sub>1,0</sub> 5/2← 0 <sub>0,0</sub> 5/2	12369.5584	-3.32	0.006	3 <sub>0,3</sub> 3/2← 1 <sub>1,1</sub> 3/2	11558.0756	-4.19	0.006
1 <sub>1,0</sub> 7/2← 0 <sub>0,0</sub> 5/2	12185.2596	-0.33	0.006	3 <sub>0,3</sub> 5/2← 1 <sub>1,1</sub> 3/2	11348.4635	-2.65	0.006
1 <sub>1,1</sub> 3/2← 1 <sub>0,1</sub> 3/2	7757.76	3.81	0.006	3 <sub>0,3</sub> 9/2← 1 <sub>1,1</sub> 7/2	11178.2365	-4.95	0.006
1 <sub>1,1</sub> 5/2← 1 <sub>0,1</sub> 3/2	7952.5825	0.8	0.006	2 <sub>1,2</sub> 1/2← 2 <sub>0,2</sub> 3/2	7907.0046	1.06	0.006
1 <sub>1,1</sub> 3/2← 1 <sub>0,1</sub> 5/2	8305.7898	-0.04	0.006	2 <sub>1,2</sub> 3/2← 2 <sub>0,2</sub> 3/2	7809.62	1.12	0.006
1 <sub>1,1</sub> 5/2← 1 <sub>0,1</sub> 5/2	8500.6145	-0.85	0.006	2 <sub>1,2</sub> 3/2← 2 <sub>0,2</sub> 5/2	7958.7244	-0.67	0.006
1 <sub>1,1</sub> 7/2← 1 <sub>0,1</sub> 5/2	8301.7509	2.66	0.006	2 <sub>1,2</sub> 5/2← 2 <sub>0,2</sub> 5/2	7827.0137	2.34	0.006
1 <sub>1,1</sub> 5/2← 1 <sub>0,1</sub> 7/2	8119.6872	-1.63	0.006	2 <sub>1,2</sub> 7/2← 2 <sub>0,2</sub> 5/2	7790.3346	-0.43	0.006
1 <sub>1,1</sub> 7/2← 1 <sub>0,1</sub> 7/2	7920.8256	3.89	0.006	2 <sub>1,2</sub> 5/2← 2 <sub>0,2</sub> 7/2	7937.3386	2.61	0.006
2 <sub>0,2</sub> 1/2← 1 <sub>0,1</sub> 3/2	7864.3252	0.93	0.006	2 <sub>1,2</sub> 7/2← 2 <sub>0,2</sub> 7/2	7900.6612	1.54	0.006
2 <sub>0,2</sub> 3/2← 1 <sub>0,1</sub> 5/2	8070.966	-3.73	0.006	2 <sub>1,2</sub> 9/2← 2 <sub>0,2</sub> 7/2	8052.1515	3.94	0.006
2 <sub>0,2</sub> 5/2← 1 <sub>0,1</sub> 5/2	7921.8622	-1.34	0.006	3 <sub>0,3</sub> 1/2← 2 <sub>0,2</sub> 1/2	11611.9601	-1.29	0.006
2 <sub>0,2</sub> 7/2← 1 <sub>0,1</sub> 5/2	7811.5378	-1.12	0.006	3 <sub>0,3</sub> 3/2← 2 <sub>0,2</sub> 1/2	11451.5085	-3.21	0.006
2 <sub>0,2</sub> 9/2← 1 <sub>0,1</sub> 7/2	7795.1712	-2.02	0.006	3 <sub>0,3</sub> 1/2← 2 <sub>0,2</sub> 3/2	11953.3694	19.82	0.006
2 <sub>1,1</sub> 1/2← 1 <sub>0,1</sub> 3/2	16346.7598	4.25	0.002	3 <sub>0,3</sub> 3/2← 2 <sub>0,2</sub> 3/2	11792.895	-4.9	0.006
2 <sub>1,1</sub> 3/2← 1 <sub>0,1</sub> 3/2	16231.62	13.49	0.006	3 <sub>0,3</sub> 5/2← 2 <sub>0,2</sub> 3/2	11583.2894	3.14	0.006
2 <sub>1,1</sub> 3/2← 1 <sub>0,1</sub> 3/2	16231.6108	4.29	0.002	3 <sub>0,3</sub> 5/2← 2 <sub>0,2</sub> 5/2	11732.3936	1.15	0.006
2 <sub>1,1</sub> 5/2← 1 <sub>0,1</sub> 3/2	16086.316	6.46	0.006	3 <sub>0,3</sub> 7/2← 2 <sub>0,2</sub> 5/2	11562.1519	-0.06	0.006
2 <sub>1,1</sub> 5/2← 1 <sub>0,1</sub> 3/2	16086.311	1.46	0.002	3 <sub>0,3</sub> 5/2← 2 <sub>0,2</sub> 7/2	11842.7242	7.13	0.006
2 <sub>1,1</sub> 3/2← 1 <sub>0,1</sub> 5/2	16779.6406	0.44	0.002	3 <sub>0,3</sub> 7/2← 2 <sub>0,2</sub> 7/2	11672.4789	2.31	0.006
2 <sub>1,1</sub> 5/2← 1 <sub>0,1</sub> 5/2	16634.3438	0.61	0.002	3 <sub>0,3</sub> 9/2← 2 <sub>0,2</sub> 7/2	11668.4554	4.63	0.006
2 <sub>1,1</sub> 7/2← 1 <sub>0,1</sub> 5/2	16589.5958	2.62	0.002	3 <sub>0,3</sub> 7/2← 2 <sub>0,2</sub> 9/2	11307.8997	-16.06	0.006
2 <sub>1,1</sub> 5/2← 1 <sub>0,1</sub> 7/2	16253.4175	0.83	0.002	3 <sub>0,3</sub> 9/2← 2 <sub>0,2</sub> 9/2	11303.8898	-0.14	0.006
2 <sub>1,1</sub> 7/2← 1 <sub>0,1</sub> 7/2	16208.6699	3.24	0.006	3 <sub>0,3</sub> 11/2← 2 <sub>0,2</sub> 9/2	11633.6408	2.11	0.006
2 <sub>1,1</sub> 7/2← 1 <sub>0,1</sub> 7/2	16208.668	1.34	0.002	3 <sub>0,3</sub> 3/2← 2 <sub>1,1</sub> 1/2	2969.07726	-3.17	0.002
2 <sub>1,1</sub> 9/2← 1 <sub>0,1</sub> 7/2	16385.2129	6.25	0.002	3 <sub>0,3</sub> 3/2← 2 <sub>1,1</sub> 3/2	3084.23099	1.51	0.002
2 <sub>1,1</sub> 1/2← 1 <sub>1,0</sub> 3/2	8385.6723	-0.81	0.006	3 <sub>0,3</sub> 5/2← 2 <sub>1,1</sub> 3/2	2874.6149	-0.93	0.002
2 <sub>1,1</sub> 3/2← 1 <sub>1,0</sub> 3/2	8270.5218	-2.26	0.006	3 <sub>0,3</sub> 5/2← 2 <sub>1,1</sub> 5/2	3019.9131	0.3	0.002
2 <sub>1,1</sub> 5/2← 1 <sub>1,0</sub> 3/2	8125.2225	-4.6	0.006	3 <sub>0,3</sub> 7/2← 2 <sub>1,1</sub> 5/2	2849.67452	2.21	0.002
2 <sub>1,1</sub> 3/2← 1 <sub>1,0</sub> 5/2	8006.4786	6.06	0.006	3 <sub>0,3</sub> 9/2← 2 <sub>1,1</sub> 9/2	2713.85567	-0.84	0.002
2 <sub>1,1</sub> 7/2← 1 <sub>1,0</sub> 5/2	7816.4386	13.03	0.006	3 <sub>1,2</sub> 1/2← 2 <sub>1,1</sub> 1/2	12178.3665	-2.74	0.006

(Table 13 continued)

Transition	Frequency (MHz)	Obs-Calc (kHz)	Uncertainty (MHz)	Transition	Frequency (MHz)	Obs-Calc (kHz)	Uncertainty (MHz)
3 <sub>1,2</sub> 3/2←2 <sub>1,1</sub> 3/2	12166.5464	-0.12	0.006	3 <sub>2,2</sub> 9/2←2 <sub>2,1</sub> 9/2	11787.2283	-3.5	0.006
3 <sub>1,2</sub> 5/2←2 <sub>1,1</sub> 3/2	12001.2556	-0.86	0.006	3 <sub>2,2</sub> 11/2←2 <sub>2,1</sub> 9/2	11777.0596	0.57	0.006
3 <sub>1,2</sub> 3/2←2 <sub>1,1</sub> 5/2	12311.8389	-4.59	0.006	2 <sub>2,0</sub> 1/2←3 <sub>1,2</sub> 3/2	11548.9106	8.77	0.006
3 <sub>1,2</sub> 5/2←2 <sub>1,1</sub> 5/2	12146.554	0.57	0.006	2 <sub>2,0</sub> 3/2←3 <sub>1,2</sub> 3/2	11776.7885	2.93	0.006
3 <sub>1,2</sub> 7/2←2 <sub>1,1</sub> 5/2	12013.2814	2.64	0.006	2 <sub>2,0</sub> 5/2←3 <sub>1,2</sub> 5/2	12202.8186	4.02	0.006
3 <sub>1,2</sub> 5/2←2 <sub>1,1</sub> 7/2	12191.3132	9.76	0.006	2 <sub>2,0</sub> 5/2←3 <sub>1,2</sub> 7/2	12336.0879	-1.35	0.006
3 <sub>1,2</sub> 7/2←2 <sub>1,1</sub> 7/2	12058.027	-1.77	0.006	2 <sub>2,0</sub> 7/2←3 <sub>1,2</sub> 7/2	12432.2649	-8.56	0.006
3 <sub>1,2</sub> 9/2←2 <sub>1,1</sub> 7/2	12056.4604	-7.73	0.006	2 <sub>2,0</sub> 7/2←3 <sub>1,2</sub> 9/2	12433.8348	0.7	0.006
3 <sub>1,2</sub> 7/2←2 <sub>1,1</sub> 9/2	11881.4914	2.62	0.006	2 <sub>2,0</sub> 9/2←3 <sub>1,2</sub> 9/2	12077.0006	0.92	0.006
3 <sub>1,2</sub> 11/2←2 <sub>1,1</sub> 9/2	12136.7093	-0.31	0.006	2 <sub>2,1</sub> 1/2←3 <sub>1,3</sub> 3/2	13337.2535	1.23	0.006
3 <sub>1,3</sub> 1/2←2 <sub>1,2</sub> 1/2	11287.1929	-0.61	0.006	2 <sub>2,1</sub> 3/2←3 <sub>1,3</sub> 3/2	13565.5766	-0.32	0.006
3 <sub>1,3</sub> 3/2←2 <sub>1,2</sub> 1/2	11171.193	-2.3	0.006	2 <sub>2,1</sub> 3/2←3 <sub>1,3</sub> 5/2	13718.0197	0.46	0.006
3 <sub>1,3</sub> 1/2←2 <sub>1,2</sub> 3/2	11384.576	-2.17	0.006	2 <sub>2,1</sub> 5/2←3 <sub>1,3</sub> 5/2	13978.9103	-2.46	0.006
3 <sub>1,3</sub> 3/2←2 <sub>1,2</sub> 3/2	11268.5771	-2.86	0.006	2 <sub>2,1</sub> 5/2←3 <sub>1,3</sub> 7/2	14102.4265	-4.19	0.006
3 <sub>1,3</sub> 5/2←2 <sub>1,2</sub> 3/2	11116.1354	-2.24	0.006	2 <sub>2,1</sub> 7/2←3 <sub>1,3</sub> 9/2	14198.2994	1.42	0.006
3 <sub>1,3</sub> 3/2←2 <sub>1,2</sub> 5/2	11400.2963	2.63	0.006	2 <sub>2,1</sub> 9/2←3 <sub>1,3</sub> 9/2	13841.2649	7.19	0.006
3 <sub>1,3</sub> 5/2←2 <sub>1,2</sub> 5/2	11247.8492	-2.15	0.006	2 <sub>2,1</sub> 9/2←3 <sub>1,3</sub> 11/2	13607.1946	0.14	0.006
3 <sub>1,3</sub> 7/2←2 <sub>1,2</sub> 5/2	11124.3328	-0.62	0.006	3 <sub>1,2</sub> 11/2←3 <sub>1,3</sub> 11/2	1795.65937	-0.19	0.002
3 <sub>1,3</sub> 5/2←2 <sub>1,2</sub> 7/2	11284.5303	2.62	0.006	4 <sub>0,4</sub> 3/2←3 <sub>0,3</sub> 1/2	15404.7482	-3.89	0.006
3 <sub>1,3</sub> 9/2←2 <sub>1,2</sub> 7/2	11160.918	-3.4	0.006	4 <sub>0,4</sub> 3/2←3 <sub>0,3</sub> 3/2	15565.21	8.22	0.006
3 <sub>1,3</sub> 9/2←2 <sub>1,2</sub> 9/2	11009.4359	2.4	0.006	4 <sub>0,4</sub> 5/2←3 <sub>0,3</sub> 3/2	15373.2966	-2.3	0.006
3 <sub>1,3</sub> 11/2←2 <sub>1,2</sub> 9/2	11243.4981	1.35	0.006	4 <sub>0,4</sub> 5/2←3 <sub>0,3</sub> 5/2	15582.9113	-1.24	0.006
3 <sub>2,1</sub> 5/2←2 <sub>2,0</sub> 3/2	11815.8148	0.68	0.006	4 <sub>0,4</sub> 7/2←3 <sub>0,3</sub> 5/2	15386.5765	2.8	0.006
3 <sub>2,1</sub> 5/2←2 <sub>2,0</sub> 5/2	11555.0746	-0.57	0.006	4 <sub>0,4</sub> 7/2←3 <sub>0,3</sub> 7/2	15556.8143	0.11	0.006
3 <sub>2,1</sub> 7/2←2 <sub>2,0</sub> 5/2	11549.8414	-1.02	0.006	4 <sub>0,4</sub> 9/2←3 <sub>0,3</sub> 7/2	15428.9604	-0.96	0.006
3 <sub>2,1</sub> 7/2←2 <sub>2,0</sub> 7/2	11453.6496	-8.61	0.006	4 <sub>0,4</sub> 9/2←3 <sub>0,3</sub> 9/2	15432.9834	-3.78	0.006
3 <sub>2,1</sub> 9/2←2 <sub>2,0</sub> 7/2	11461.3309	-4.06	0.006	4 <sub>0,4</sub> 11/2←3 <sub>0,3</sub> 9/2	15468.8112	-1	0.006
3 <sub>2,1</sub> 9/2←2 <sub>2,0</sub> 9/2	11818.1525	-16.87	0.006	4 <sub>0,4</sub> 11/2←3 <sub>0,3</sub> 11/2	15139.055	-8.46	0.006
3 <sub>2,1</sub> 11/2←2 <sub>2,0</sub> 9/2	11809.1287	0.7	0.006	4 <sub>0,4</sub> 13/2←3 <sub>0,3</sub> 11/2	15458.1005	0.71	0.006
3 <sub>2,2</sub> 3/2←2 <sub>2,1</sub> 3/2	11787.433	4.06	0.006	4 <sub>1,3</sub> 11/2←3 <sub>1,2</sub> 9/2	16106.0194	-4.72	0.006
3 <sub>2,2</sub> 5/2←2 <sub>2,1</sub> 3/2	11783.9982	-4.5	0.006	4 <sub>1,3</sub> 11/2←3 <sub>1,2</sub> 11/2	15849.2209	-21.75	0.006
3 <sub>2,2</sub> 5/2←2 <sub>2,1</sub> 5/2	11523.1112	2.02	0.006	4 <sub>1,3</sub> 13/2←3 <sub>1,2</sub> 11/2	16131.8718	3.28	0.006
3 <sub>2,2</sub> 7/2←2 <sub>2,1</sub> 5/2	11518.3456	-2.59	0.006	4 <sub>1,4</sub> 3/2←3 <sub>1,3</sub> 1/2	14918.2326	1.6	0.006
3 <sub>2,2</sub> 9/2←2 <sub>2,1</sub> 7/2	11430.1747	-16.84	0.006	4 <sub>1,4</sub> 3/2←3 <sub>1,3</sub> 3/2	15034.2268	-2.4	0.006



(Table 13 continued)

Transition	Frequency (MHz)	Obs-Calc (kHz)	Uncertainty (MHz)	Transition	Frequency (MHz)	Obs-Calc (kHz)	Uncertainty (MHz)
4 <sub>1,4</sub> 5/2←3 <sub>1,3</sub> 3/2	14875.7946	2.01	0.006	5 <sub>0,5</sub> 5/2←4 <sub>1,3</sub> 3/2	9474.163	-2.71	0.006
4 <sub>1,4</sub> 5/2←3 <sub>1,3</sub> 5/2	15028.2336	-1.31	0.006	5 <sub>0,5</sub> 5/2←4 <sub>1,3</sub> 5/2	9645.1822	0.29	0.006
4 <sub>1,4</sub> 7/2←3 <sub>1,3</sub> 5/2	14866.6432	-0.12	0.006	5 <sub>0,5</sub> 7/2←4 <sub>1,3</sub> 5/2	9436.5541	-0.53	0.006
4 <sub>1,4</sub> 7/2←3 <sub>1,3</sub> 7/2	14990.1561	-5.15	0.006	5 <sub>0,5</sub> 7/2←4 <sub>1,3</sub> 7/2	9610.415	2.06	0.006
4 <sub>1,4</sub> 9/2←3 <sub>1,3</sub> 7/2	14884.8379	1.29	0.006	5 <sub>0,5</sub> 9/2←4 <sub>1,3</sub> 7/2	9423.9464	-2.62	0.006
4 <sub>1,4</sub> 11/2←3 <sub>1,3</sub> 9/2	14914.6655	0.33	0.006	5 <sub>0,5</sub> 9/2←4 <sub>1,3</sub> 9/2	9536.634	1.15	0.006
4 <sub>1,4</sub> 13/2←3 <sub>1,3</sub> 11/2	14941.61	-1.25	0.006	5 <sub>0,5</sub> 11/2←4 <sub>1,3</sub> 9/2	9434.0171	1.11	0.006
4 <sub>2,2</sub> 5/2←3 <sub>2,1</sub> 3/2	15649.1675	-16.04	0.006	5 <sub>0,5</sub> 11/2←4 <sub>1,3</sub> 11/2	9402.4837	2.26	0.006
4 <sub>2,2</sub> 7/2←3 <sub>2,1</sub> 5/2	15570.6659	-2.3	0.006	5 <sub>0,5</sub> 13/2←4 <sub>1,3</sub> 11/2	9460.1845	0.59	0.006
4 <sub>2,2</sub> 9/2←3 <sub>2,1</sub> 7/2	15522.5787	-0.95	0.006	5 <sub>0,5</sub> 13/2←4 <sub>1,3</sub> 13/2	9177.5547	-3.35	0.006
4 <sub>2,2</sub> 11/2←3 <sub>2,1</sub> 9/2	15533.3401	2.25	0.006	5 <sub>0,5</sub> 15/2←4 <sub>1,3</sub> 13/2	9488.2152	-0.78	0.006
4 <sub>2,2</sub> 13/2←3 <sub>2,1</sub> 11/2	15667.9962	2.1	0.006	5 <sub>1,4</sub> 15/2←5 <sub>1,5</sub> 15/2	4471.52474	-2.44	0.002
4 <sub>2,3</sub> 5/2←3 <sub>2,2</sub> 3/2	15569.3838	16.36	0.006	6 <sub>0,6</sub> 7/2←5 <sub>1,4</sub> 5/2	12361.5704	-2.63	0.006
4 <sub>2,3</sub> 7/2←3 <sub>2,2</sub> 5/2	15491.3084	-10.29	0.006	6 <sub>0,6</sub> 7/2←5 <sub>1,4</sub> 7/2	12558.13	4.97	0.006
4 <sub>2,3</sub> 9/2←3 <sub>2,2</sub> 7/2	15442.8202	-3.41	0.006	6 <sub>0,6</sub> 9/2←5 <sub>1,4</sub> 7/2	12339.3404	-2.95	0.006
4 <sub>2,3</sub> 11/2←3 <sub>2,2</sub> 9/2	15453.1262	-0.21	0.006	6 <sub>0,6</sub> 9/2←5 <sub>1,4</sub> 9/2	12513.4187	-8.75	0.006
4 <sub>2,3</sub> 13/2←3 <sub>2,2</sub> 11/2	15587.5208	2.98	0.006	6 <sub>0,6</sub> 11/2←5 <sub>1,4</sub> 9/2	12334.5107	-0.62	0.006
4 <sub>3,1</sub> 9/2←3 <sub>3,0</sub> 7/2	15383.5372	-7.18	0.006	6 <sub>0,6</sub> 11/2←5 <sub>1,4</sub> 11/2	12430.1668	3.29	0.006
4 <sub>3,1</sub> 13/2←3 <sub>3,0</sub> 11/2	15673.8753	5.55	0.006	6 <sub>0,6</sub> 13/2←5 <sub>1,4</sub> 11/2	12344.5019	-1.98	0.006
4 <sub>3,2</sub> 9/2←3 <sub>3,1</sub> 7/2	15382.6613	10.58	0.006	6 <sub>0,6</sub> 13/2←5 <sub>1,4</sub> 13/2	12291.6112	0.06	0.006
4 <sub>3,2</sub> 11/2←3 <sub>3,1</sub> 9/2	15372.3796	-4	0.006	6 <sub>0,6</sub> 15/2←5 <sub>1,4</sub> 13/2	12363.0998	-0.37	0.006
3 <sub>2,1</sub> 7/2←4 <sub>1,3</sub> 9/2	7812.9941	-8.64	0.006	6 <sub>0,6</sub> 15/2←5 <sub>1,4</sub> 15/2	12069.9657	-2.87	0.006
3 <sub>2,1</sub> 9/2←4 <sub>1,3</sub> 11/2	7789.1431	-1.84	0.006	6 <sub>0,6</sub> 17/2←5 <sub>1,4</sub> 15/2	12373.9201	-2.67	0.006
3 <sub>2,2</sub> 1/2←4 <sub>1,4</sub> 3/2	10316.5132	6.36	0.006	5 <sub>2,4</sub> 7/2←6 <sub>1,6</sub> 9/2	4518.95939	2.81	0.002
3 <sub>2,2</sub> 3/2←4 <sub>1,4</sub> 3/2	10318.7776	0.94	0.006	5 <sub>2,4</sub> 9/2←6 <sub>1,6</sub> 11/2	4566.96687	2.62	0.002
3 <sub>2,2</sub> 3/2←4 <sub>1,4</sub> 5/2	10477.2156	2.33	0.006	5 <sub>2,4</sub> 11/2←6 <sub>1,6</sub> 13/2	4584.14855	-2.34	0.002
3 <sub>2,2</sub> 5/2←4 <sub>1,4</sub> 5/2	10473.7821	-4.93	0.006	5 <sub>2,4</sub> 15/2←6 <sub>1,6</sub> 17/2	4463.09811	-0.61	0.002
3 <sub>2,2</sub> 5/2←4 <sub>1,4</sub> 7/2	10635.3787	0.08	0.006	6 <sub>1,6</sub> 17/2←6 <sub>0,6</sub> 17/2	5499.50476	2.26	0.002
3 <sub>2,2</sub> 7/2←4 <sub>1,4</sub> 7/2	10630.615	-2.63	0.006	7 <sub>0,7</sub> 9/2←6 <sub>1,5</sub> 7/2	14973.6028	-3.94	0.006
3 <sub>2,2</sub> 7/2←4 <sub>1,4</sub> 9/2	10735.94	-2.27	0.006	7 <sub>0,7</sub> 9/2←6 <sub>1,5</sub> 9/2	15186.5539	3.08	0.006
3 <sub>2,2</sub> 9/2←4 <sub>1,4</sub> 9/2	10743.5611	-3.46	0.006	7 <sub>0,7</sub> 11/2←6 <sub>1,5</sub> 9/2	14961.2579	-3.84	0.006
3 <sub>2,2</sub> 9/2←4 <sub>1,4</sub> 11/2	10713.8194	-4.95	0.006	7 <sub>0,7</sub> 11/2←6 <sub>1,5</sub> 11/2	15136.701	8.02	0.006
3 <sub>2,2</sub> 11/2←4 <sub>1,4</sub> 11/2	10703.6526	1.03	0.006	7 <sub>0,7</sub> 13/2←6 <sub>1,5</sub> 11/2	14963.8833	-3.78	0.006
3 <sub>2,2</sub> 11/2←4 <sub>1,4</sub> 13/2	10442.6461	3.85	0.006	7 <sub>0,7</sub> 13/2←6 <sub>1,5</sub> 13/2	15047.2707	2.25	0.006

(Table 13 continued)

Transition	Frequency (MHz)	Obs-Calc (kHz)	Uncertainty (MHz)	Transition	Frequency (MHz)	Obs-Calc (kHz)	Uncertainty (MHz)
7 <sub>0,7</sub> 15/2← 6 <sub>1,5</sub> 13/2	14973.8178	-2.92	0.006	6 <sub>3,3</sub> 11/2← 8 <sub>1,8</sub> 13/2	13062.4955	9.24	0.006
7 <sub>0,7</sub> 15/2← 6 <sub>1,5</sub> 15/2	14901.3433	-1.55	0.006	7 <sub>3,4</sub> 9/2← 8 <sub>2,6</sub> 11/2	8627.7564	2.42	0.006
7 <sub>0,7</sub> 17/2← 6 <sub>1,5</sub> 15/2	14982.0528	-2.54	0.006	7 <sub>3,4</sub> 11/2← 8 <sub>2,6</sub> 13/2	8710.1399	3.44	0.006
7 <sub>0,7</sub> 19/2← 6 <sub>1,5</sub> 17/2	14988.4923	-2.05	0.006	7 <sub>3,4</sub> 13/2← 8 <sub>2,6</sub> 15/2	8763.9193	-3.47	0.006
6 <sub>3,3</sub> 7/2← 7 <sub>2,5</sub> 9/2	12935.4911	3.27	0.006	7 <sub>3,4</sub> 15/2← 8 <sub>2,6</sub> 17/2	8780.3273	-3.17	0.006
6 <sub>3,3</sub> 9/2← 7 <sub>2,5</sub> 11/2	13068.6591	-8.31	0.006	7 <sub>3,4</sub> 17/2← 8 <sub>2,6</sub> 19/2	8748.2906	-1.45	0.006
6 <sub>3,3</sub> 11/2← 7 <sub>2,5</sub> 13/2	13161.4003	-23.15	0.006	7 <sub>3,4</sub> 19/2← 8 <sub>2,6</sub> 21/2	8649.0387	11.79	0.006
6 <sub>3,3</sub> 13/2← 7 <sub>2,5</sub> 15/2	13139.3838	-4.65	0.006	7 <sub>3,5</sub> 9/2← 8 <sub>2,7</sub> 11/2	10233.1771	3	0.006
6 <sub>3,3</sub> 15/2← 7 <sub>2,5</sub> 17/2	13103.1192	-11.42	0.006	7 <sub>3,5</sub> 11/2← 8 <sub>2,7</sub> 13/2	10325.2692	-3.38	0.006
6 <sub>3,3</sub> 17/2← 7 <sub>2,5</sub> 19/2	12960.0258	-5.5	0.006	7 <sub>3,5</sub> 13/2← 8 <sub>2,7</sub> 15/2	10326.3368	-14.33	0.006
6 <sub>3,4</sub> 7/2← 7 <sub>2,6</sub> 9/2	13922.6321	7.8	0.006	7 <sub>3,5</sub> 15/2← 8 <sub>2,7</sub> 17/2	10372.6539	-6.64	0.006
6 <sub>3,4</sub> 11/2← 7 <sub>2,6</sub> 13/2	14093.2361	-6.07	0.006	7 <sub>3,5</sub> 17/2← 8 <sub>2,7</sub> 19/2	10342.8232	-8.18	0.006
6 <sub>3,4</sub> 13/2← 7 <sub>2,6</sub> 15/2	14120.8737	-8.57	0.006	7 <sub>3,5</sub> 19/2← 8 <sub>2,7</sub> 21/2	10246.7691	-0.6	0.006
6 <sub>3,4</sub> 15/2← 7 <sub>2,6</sub> 17/2	14084.2836	10.5	0.006	8 <sub>1,8</sub> 11/2← 8 <sub>0,8</sub> 11/2	4126.93917	-4.63	0.002
6 <sub>3,4</sub> 17/2← 7 <sub>2,6</sub> 19/2	13953.7695	-0.08	0.006	8 <sub>1,8</sub> 17/2← 8 <sub>0,8</sub> 17/2	4119.98434	-2.77	0.002
7 <sub>1,7</sub> 9/2← 7 <sub>0,7</sub> 9/2	4791.43365	4.22	0.002	8 <sub>1,8</sub> 19/2← 8 <sub>0,8</sub> 19/2	4109.39007	-4.43	0.002
7 <sub>1,7</sub> 11/2← 7 <sub>0,7</sub> 11/2	4807.24377	1.54	0.002	8 <sub>1,7</sub> 13/2← 8 <sub>1,8</sub> 11/2	10405.8738	4.01	0.006
7 <sub>1,7</sub> 13/2← 7 <sub>0,7</sub> 11/2	4647.44653	-0.57	0.002	8 <sub>1,7</sub> 15/2← 8 <sub>1,8</sub> 13/2	10436.1155	10.92	0.006
7 <sub>1,7</sub> 11/2← 7 <sub>0,7</sub> 13/2	4980.0515	3.38	0.002	8 <sub>1,7</sub> 17/2← 8 <sub>1,8</sub> 15/2	10581.4167	-14.01	0.006
7 <sub>1,7</sub> 13/2← 7 <sub>0,7</sub> 13/2	4820.25277	-0.23	0.002	9 <sub>1,8</sub> 15/2← 8 <sub>2,6</sub> 13/2	14934.0863	-0.65	0.006
7 <sub>1,7</sub> 15/2← 7 <sub>0,7</sub> 13/2	4752.14929	-1.22	0.002	9 <sub>1,8</sub> 17/2← 8 <sub>2,6</sub> 15/2	14913.9218	-1.08	0.006
7 <sub>1,7</sub> 13/2← 7 <sub>0,7</sub> 15/2	4893.70133	0.6	0.002	9 <sub>1,8</sub> 19/2← 8 <sub>2,6</sub> 17/2	14911.1199	1.19	0.006
7 <sub>1,7</sub> 15/2← 7 <sub>0,7</sub> 15/2	4825.59607	-2.17	0.002	9 <sub>1,8</sub> 21/2← 8 <sub>2,6</sub> 19/2	14928.9591	1.73	0.006
7 <sub>1,7</sub> 17/2← 7 <sub>0,7</sub> 15/2	4899.67155	2.18	0.002	9 <sub>1,8</sub> 23/2← 8 <sub>2,6</sub> 21/2	14967.9541	-3.82	0.006
7 <sub>1,7</sub> 15/2← 7 <sub>0,7</sub> 17/2	4744.88466	-3.09	0.002	7 <sub>3,5</sub> 13/2← 9 <sub>0,9</sub> 15/2	10395.9926	-9.87	0.006
7 <sub>1,7</sub> 17/2← 7 <sub>0,7</sub> 17/2	4818.95715	-1.73	0.002	10 <sub>4,6</sub> 25/2← 11 <sub>3,8</sub> 27/2	13957.8943	-0.39	0.006
7 <sub>1,7</sub> 19/2← 7 <sub>0,7</sub> 19/2	4798.8244	1.07	0.002	11 <sub>2,10</sub> 17/2← 11 <sub>1,10</sub> 17/2	15508.5201	-0.54	0.006
8 <sub>1,7</sub> 11/2← 7 <sub>2,5</sub> 9/2	10561.7321	-7.94	0.006	11 <sub>2,10</sub> 19/2← 11 <sub>1,10</sub> 19/2	15529.1013	-15.02	0.006
8 <sub>1,7</sub> 13/2← 7 <sub>2,5</sub> 11/2	10544.7545	-13.73	0.006	11 <sub>2,10</sub> 21/2← 11 <sub>1,10</sub> 21/2	15536.0553	-18.52	0.006
8 <sub>1,7</sub> 15/2← 7 <sub>2,5</sub> 13/2	10535.0222	-19.57	0.006	11 <sub>2,10</sub> 23/2← 11 <sub>1,10</sub> 23/2	15551.9796	10.55	0.006
8 <sub>1,7</sub> 17/2← 7 <sub>2,5</sub> 15/2	10479.3122	5.32	0.006	11 <sub>2,10</sub> 25/2← 11 <sub>1,10</sub> 25/2	15491.6128	-9.21	0.006
8 <sub>1,7</sub> 17/2← 7 <sub>2,5</sub> 17/2	10414.7081	-9.42	0.006	11 <sub>2,10</sub> 27/2← 11 <sub>1,10</sub> 27/2	15502.3103	4.35	0.006
8 <sub>1,7</sub> 19/2← 7 <sub>2,5</sub> 17/2	10503.1692	-6.33	0.006	12 <sub>1,12</sub> 19/2← 11 <sub>2,10</sub> 17/2	9580.6556	5.43	0.006
8 <sub>1,7</sub> 21/2← 7 <sub>2,5</sub> 19/2	10548.3879	-8.08	0.006	12 <sub>1,12</sub> 23/2← 11 <sub>2,10</sub> 21/2	9574.7873	-10.93	0.006

(Table 13 continued)

Transition	Frequency (MHz)	Obs-Calc (kHz)	Uncertainty (MHz)
12 <sub>1,12</sub> 29/2←11 <sub>2,10</sub> 27/2	9594.1474	-3.77	0.006
12 <sub>2,11</sub> 19/2←12 <sub>1,11</sub> 19/2	14061.1711	14.45	0.006
12 <sub>2,11</sub> 21/2←12 <sub>1,11</sub> 21/2	14079.9973	1.58	0.006
12 <sub>2,11</sub> 23/2←12 <sub>1,11</sub> 23/2	14092.0844	-4.73	0.006
12 <sub>2,11</sub> 25/2←12 <sub>1,11</sub> 25/2	14095.9876	-4.2	0.006
12 <sub>2,11</sub> 27/2←12 <sub>1,11</sub> 27/2	14088.7437	10.69	0.006
12 <sub>2,11</sub> 29/2←12 <sub>1,11</sub> 29/2	14063.8503	6.99	0.006
13 <sub>2,12</sub> 21/2←13 <sub>1,12</sub> 21/2	12595.2218	2.84	0.006
13 <sub>2,12</sub> 23/2←13 <sub>1,12</sub> 23/2	12611.7258	-8.69	0.006
13 <sub>2,12</sub> 25/2←13 <sub>1,12</sub> 25/2	12622.2486	-5.6	0.006
13 <sub>2,12</sub> 27/2←13 <sub>1,12</sub> 27/2	12625.3439	-5.43	0.006
13 <sub>2,12</sub> 29/2←13 <sub>1,12</sub> 29/2	12618.5745	-0.8	0.006
13 <sub>2,12</sub> 31/2←13 <sub>1,12</sub> 31/2	12597.5818	-1.81	0.006
14 <sub>1,14</sub> 33/2←13 <sub>2,12</sub> 31/2	12958.1779	-6.19	0.006
14 <sub>2,13</sub> 23/2←14 <sub>1,13</sub> 23/2	11132.016	15.58	0.006
14 <sub>2,13</sub> 25/2←14 <sub>1,13</sub> 25/2	11145.7931	6.39	0.006

Transition	Frequency (MHz)	Obs-Calc (kHz)	Uncertainty (MHz)
14 <sub>2,13</sub> 27/2←14 <sub>1,13</sub> 27/2	11154.2216	-4.41	0.006
14 <sub>2,13</sub> 29/2←14 <sub>1,13</sub> 29/2	11156.8466	-6.02	0.006
14 <sub>2,13</sub> 31/2←14 <sub>1,13</sub> 31/2	11151.278	-7.22	0.006
14 <sub>2,13</sub> 33/2←14 <sub>1,13</sub> 33/2	11132.644	6.7	0.006
15 <sub>2,14</sub> 25/2←15 <sub>1,14</sub> 25/2	9697.6525	4.13	0.006
15 <sub>2,14</sub> 27/2←15 <sub>1,14</sub> 27/2	9710.2961	0.12	0.006
15 <sub>2,14</sub> 29/2←15 <sub>1,14</sub> 29/2	9718.2937	2.51	0.006
15 <sub>2,14</sub> 31/2←15 <sub>1,14</sub> 31/2	9720.1444	-4.52	0.006
15 <sub>2,14</sub> 33/2←15 <sub>1,14</sub> 33/2	9714.4137	-6.53	0.006
15 <sub>2,14</sub> 35/2←15 <sub>1,14</sub> 35/2	9699.7722	4.23	0.006
16 <sub>2,15</sub> 27/2←16 <sub>1,15</sub> 27/2	8327.7805	4.81	0.006
16 <sub>2,15</sub> 29/2←16 <sub>1,15</sub> 29/2	8338.5685	-0.09	0.006
16 <sub>2,15</sub> 31/2←16 <sub>1,15</sub> 31/2	8345.2793	0.36	0.006
16 <sub>2,15</sub> 33/2←16 <sub>1,15</sub> 33/2	8346.7937	2.82	0.006
16 <sub>2,15</sub> 35/2←16 <sub>1,15</sub> 35/2	8341.9059	3.83	0.006
16 <sub>2,15</sub> 37/2←16 <sub>1,15</sub> 37/2	8329.3556	2.85	0.006

## Strontium Sulfide<sup>47</sup>

Strontium sulfide demonstrates the importance of using a proper gas mix. Through the study of strontium sulfide it was discovered that an OCS precursor gas was far superior to a H<sub>2</sub>S precursor gas. Without this discovery the rotational transitions of the less abundant isotopomers of this molecule would not have been observed.

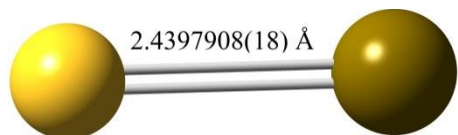


Figure 31. Depiction of strontium sulfide.

### Introduction

Strontium sulfide has been previously studied by two other groups. The study was performed by Pianalto et. al. where rotational analysis of the most abundant isotopomer, <sup>88</sup>Sr<sup>32</sup>S, was achieved. The second study came from Halfen et. al. that reported several observed rotational transitions of <sup>88</sup>Sr<sup>32</sup>S during their investigation of SrSH.<sup>48,49</sup>

The reason for this study is to determine the hyperfine constants of <sup>87</sup>Sr<sup>32</sup>S isotopomer and evaluate the Born-Oppenheimer breakdown parameters for the SrS by observing the minor isotopomers for the first time.

### Experimental Method

Our classic Balle-Flygare FTMW spectrometer was used in this study of SrS. A small chunk of strontium was purchased from Sigma Aldrich and fashioned to be screwed on top of an aluminum mount. This rod was rotated inside a Walker-Gerry ablation nozzle and ablated with a Nd:YAG laser at a wavelength of 1064 nm at 45 mJ to create a plasma at the surface. Then a 0.2% OCS gas mixed with Ar at approximately 760 torr was blown over the freshly ablated Sr surface and carried over into the resonator. Initially, H<sub>2</sub>S was used as the precursor gas but the SrS signals were very weak compared to the OCS gas mix.

## Results

The pure rotational spectra of SrS was observed for  $J = 1 \leftarrow 0$ ,  $J = 2 \leftarrow 1$  and  $J = 3 \leftarrow 2$  in the 6-26 GHz region. For the  $^{88}\text{Sr}^{32}\text{S}$  isotopomer the rotational transitions for the  $v = 0, 1, 2$ , and 3 states were observed. In the beginning of the study, the SrS constants of Halfen et al. were used to locate the  $^{88}\text{Sr}^{32}\text{S}$  transitions. Using these new transitions, the fit for SrS was improved to give good predictions for the transitions of the other three isotopomers. Table 26 shows the observed transitions of the  $^{88}\text{Sr}^{32}\text{S}$ ,  $^{87}\text{Sr}^{32}\text{S}$ ,  $^{86}\text{Sr}^{32}\text{S}$ , and  $^{88}\text{Sr}^{34}\text{S}$  isotopomers.<sup>49</sup>

After improving the fit for  $^{88}\text{Sr}^{32}\text{S}$ , the  $^{87}\text{Sr}^{32}\text{S}$  isotopomer was fit using Pickett's SPFIT program to determine the rotational, centrifugal distortion, and electric quadrupole coupling constants shown on Table 21. The rotational and centrifugal distortion constants were used to determine the hypothetical unsplit transitions for  $^{87}\text{Sr}^{32}\text{S}$ . A Dunham-type, multi-isotopomer, multi-vibrational state fitting routine used these hypothetical unsplit  $^{87}\text{Sr}^{32}\text{S}$  transitional frequencies along with the  $^{88}\text{Sr}^{32}\text{S}$ ,  $^{86}\text{Sr}^{32}\text{S}$ , and  $^{88}\text{Sr}^{34}\text{S}$  data to obtain the mass independent Dunham parameters for SrS found on Table 22.<sup>31, 50-52</sup>

Table 21. Constants For  $^{87}\text{Sr}^{32}\text{S}$

Constant	Value / MHz
$B_0$	3625.2656(13)
$D_0$	0.00136(6)
$eQq(^{87}\text{Sr})$	-21.959(85)

The parentheses denote one standard deviation in units of the last significant figure.

Table 22. Mass Independent Dunham Parameters For SrS

Parameter	Value / MHz
$U_{01}/u$	84906.76(15)
$U_{02}/u^2$	-0.770453(38)
$U_{03}/u^3$	-0.00000106(10)
$U_{11}/u^{3/2}$	-1591.51(10)
$U_{12}/u^{5/2}$	-0.01686(15)
$U_{21}/u^2$	-132.19(31)
$U_{22}/u^3$	-0.00078(25)
$U_{31}/u^{5/2}$	119.39(26)

## Discussion

The mass dependent Dunham parameters derived from the mass independent parameters are shown in Table 23.

Table 23. Mass Dependent Dunham Parameters of SrS Isotopomers

Parameter	$^{88}\text{Sr}^{32}\text{S}$	$^{87}\text{Sr}^{32}\text{S}$	$^{86}\text{Sr}^{32}\text{S}$	$^{88}\text{Sr}^{34}\text{S}$
$Y_{01}$ / MHz	3621.28738	3632.36388	3643.73053	3465.27738
$Y_{02}$ / $10^3$ MHz	-1.4016775	-1.4102655	-1.4191056	-1.2834969
$Y_{03}$ / $10^{11}$ MHz	-8.22	-8.30	-8.38	-7.21
$Y_{11}$ / MHz	-14.0196441	-14.0840177	-14.1501797	-13.1234201
$Y_{12}$ / $10^6$ MHz	-6.3369	-6.3855	-6.4355	-5.6762
$Y_{21}$ / MHz	-0.240489	-0.241962	-0.243479	-0.220213
$Y_{22}$ / $10^8$ MHz	-6.05979	-6.11557	-6.17316	-5.30980
$Y_{31}$ / MHz	0.04486	0.04520	0.04555	0.04018
$r_e$ / Å	2.4397908(18)	2.4397908(18)	2.4397909(18)	2.4397861(18)

$r_e$  values were calculated using  $Y_{01}$  in the equation  $Y_{01} = \frac{h}{8\pi^2\mu r_e^2}$ .

Equation 28, from Bunker, was used to determine the internuclear separation at the bottom of the Born-Oppenheimer potential,  $r_e^{\text{BO}}$

$$U_{01} = \frac{h}{8\pi^2(r_e^{\text{BO}})^2}$$

Equation 28

where  $U_{01}$  is the mass independent ground state rotational constant ( $B_e$ ),  $r_e^{\text{BO}}$  is the internuclear distance between the atoms. The vibration frequency,  $\omega_e$ , and the anharmonicity constant,  $\omega_e\chi_e$ , have been determined through Equation 29 and Equation 30 developed by Kratzer and Pekeris for diatomics

$$Y_{10} = \omega_e = \sqrt{\frac{4Y_{01}^3}{Y_{02}}}$$

Equation 29

where  $Y_{10}$  and  $\omega_e$  are the vibration frequency,  $Y_{01}$  is the mass-dependent ground state rotational constant ( $B_e$ ) and  $Y_{02}$  is the mass-dependent ground state centrifugal distortion constant ( $D_e$ ).

$$Y_{20} = \omega_e\chi_e = Y_{01} \left( \frac{Y_{11}Y_{10}}{6Y_{01}^2} + 1 \right)^2$$

Equation 30

$Y_{20}$  and  $\omega_e\chi_e$  are the anharmonicity constant and  $Y_{11}$  is the mass-dependent rotation-vibration interaction constant ( $\alpha_e$ ). These values were used in Equation 31 to estimate the dissociation energy,  $E_{\text{diss}}$ , for SrS.

$$E_{\text{diss}} = \frac{\omega_e^2}{4\omega_e\chi_e}$$

Equation 31

Table 24 compiles the results of these additional constants.<sup>53-55</sup>

Table 24. Calculated Constants of SrS

Constant	Value
$r_e^{\text{BO}} / \text{\AA}$	2.4397045(22)
$\omega_e / \text{cm}^{-1}$	388(5)
$\omega_e x_e / \text{cm}^{-1}$	1.14(8)
$E_{\text{diss}} / \text{kJ mol}^{-1}$	395

Table 25. Nuclear Quadrupole Coupling Constants For SrO and SrS

Molecule	$eQq(^{87}\text{Sr})$
$^{87}\text{Sr}^{16}\text{O}$	$-42.729(37)^{56}$
$^{87}\text{Sr}^{32}\text{S}$	$-21.959(85)$

The nuclear quadrupole coupling constant,  $eQq(^{87}\text{Sr})$ , in  $^{87}\text{Sr}^{32}\text{S}$  and  $^{87}\text{Sr}^{16}\text{O}$  are shown on Table 25. Both values have the same sign but  $eQq(^{87}\text{Sr})$  of  $^{87}\text{Sr}^{32}\text{S}$  is approximately half the value when compared to the  $^{87}\text{Sr}^{16}\text{O}$ . The ground state configuration of Sr is  $[\text{Kr}] 5s^2$ . This configuration has an electron distribution that is spherically symmetric resulting in a zero  $eQq(^{87}\text{Sr})$  value. It is known that s electrons make only small contributions to  $eQq$  values. The magnitude of the  $eQq$  values of both  $^{87}\text{Sr}^{32}\text{S}$  and  $^{87}\text{Sr}^{16}\text{O}$  are caused by electron cloud distortions about the Sr nucleus due to the presence of the sulfur or oxygen, respectively. The increased charge of the O ion compared to the S ion causes the larger distortion of the electrons of the Sr ion in SrO than in SrS.<sup>36</sup>

The Born-Oppenheimer breakdown terms,  $\Delta_{01}^{\text{Sr}}$  and  $\Delta_{01}^{\text{S}}$ , were determined using Equation 32 - Equation 34 that were derived by Watson for a diatomic molecule AB.

$$|c_A| = \left| \frac{D}{er_e} \right|$$

Equation 32



$C_A$  is the formal charge on atom A,  $D$  is the dipole moment of the diatomic,  $e$  is the charge of an electron, and  $r_e$  is the internuclear distance between the atoms A and B.

$$(\mu g_J)_B = \mu g_J + \frac{2c_A m_p M_A}{(M_A + M_B)}$$

Equation 33

$(\mu g_J)_B$  is the isotopically independent value of  $\mu g_J$  referred to nucleus B as the origin,  $\mu$  is the reduced mass of the diatomic,  $g_J$  is rotational g-factor,  $m_p$  is the mass of a proton,  $M_A$  is the mass of atom A, and  $M_B$  is the mass of atom B.

$$\Delta_{01}^A = (\Delta_{01}^A)^{\text{ad}} + \frac{(\mu g_J)_B}{m_p} + \frac{\mu \Delta Y_{01}^{(D)}}{m_e Y_{01}}$$

Equation 34

$\Delta_{01}^A$  is the Born-Oppenheimer breakdown term for atom A,  $(\Delta_{01}^A)^{\text{ad}}$  is the adiabatic contribution to  $\Delta_{01}^A$ ,  $\Delta Y_{01}^{(D)}$  is the Dunham correction,  $m_e$  is the mass of an electron, and  $Y_{01}$  is the mass-dependent ground state rotational constant ( $B_e$ ). The value of  $\Delta_{01}^{\text{Sr}}$  was -0.78(30) and the value of  $\Delta_{01}^{\text{S}}$  was -3.773(56). Both are fairly “normal” being between 0 and -5. However, the magnitude of  $\Delta_{01}^{\text{Sr}}$  is somewhat smaller than the magnitude of  $\Delta_{01}^{\text{S}}$  with a difference being greater than 1. Non-adiabatic effects are most likely the cause of this large difference in the Born-Oppenheimer breakdown terms.<sup>50-52</sup>

## Conclusion

The pure rotational spectra of the  $^{88}\text{Sr}^{32}\text{S}$ ,  $^{87}\text{Sr}^{32}\text{S}$ ,  $^{86}\text{Sr}^{32}\text{S}$ , and  $^{88}\text{Sr}^{34}\text{S}$  isotopomers were observed for the 6-26 GHz region. Also, the SrS internuclear separation has been determined with significant improvement in precision. The  $eQq(^{87}\text{Sr})$  value in SrS has been measured and compared to the value of SrO. Lastly, the Born-Oppenheimer breakdown terms have been determined for both Strontium and sulfur in SrS.

Table 26. Observed Transitions of SrS

Isotopomer	$J' \leftarrow J''$	$F' \leftarrow F''$	$v$	Transition (MHz)		Obs – Calc (kHz)	
$^{88}\text{Sr}^{32}\text{S}$	1←0		0	7228.4416		1.1	
	1←0		1	7199.7328		2.0	
	1←0		2	7170.8786		1.2	
	2←1		0	14456.8478		0.6	
	2←1		1	14399.4278		0.2	
	2←1		2	14341.6974		-1.6	
	2←1		3	14284.7379		0.0	
	3←2		0	21685.1893		2.8	
	3←2		1	21599.0599		-0.9	
	3←2		2	21512.4599		-3.6	
	$^{87}\text{Sr}^{32}\text{S}$	2←1	11/2←9/2	0	14502.1144		
		2←1	13/2←11/2	0	14501.4882	14501.0188 <sup>a</sup>	-0.4
2←1		5/2←7/2	0	14501.8850			
3←2		15/2←13/2	0	21751.7078			
3←2		9/2←9/2	0	21751.9348	21751.4467 <sup>a</sup>	-2.8	
3←2		13/2←11/2	0	21752.0567			
$^{86}\text{Sr}^{32}\text{S}$	2←1		0	14546.3569		1.4	
	2←1		1	14488.3995		0.5	
	3←2		0	21819.4495		1.5	
$^{88}\text{Sr}^{34}\text{S}$	3←2		0	20751.8549		0.0	

<sup>a</sup> represents hypothetical unsplit frequencies.

## Thorium Oxide<sup>57</sup>

The laser ablation technique is very useful in allowing the ability to study heavy metal containing species. This is demonstrated in the study of ThO where the bond length is determined to a very high precision. The pure rotational spectra of these types of molecules are used to determine the experimental constants that serve as a guideline for theoretical methods to be tested against.

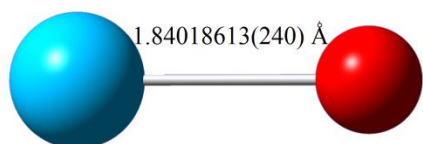


Figure 32. Depiction of Thorium oxide.

### Introduction

An understanding of actinide chemistry is necessary due to interests and uneasiness surrounding these elements to be used as sources of nuclear fuel. Unfortunately, there has been very little experimental research done on actinide compounds due to their inherent danger and the difficulties associated with interpretation of their data.

Overcoming these difficulties, a few groups have done some research on thorium. Edvinsson and Lagerqvist studied the electronic spectra of ThO where several band systems were observed and studied with rotational resolution. Kushto and Andrews used matrix isolation spectroscopy to study the result of ablating thorium in the presence of NO<sub>2</sub>.<sup>58,59</sup>

A larger group of researchers interested in actinide species are computational chemists. This is a much safer and cheaper way to explore chemistry surrounding actinides. ThO serves as a useful guide of an actinide system for testing new computational methodologies.<sup>60-63</sup>

## Experimental Method

The classic Balle-Flygare FTMW spectrometer was used in the study of ThO. A small piece of thorium foil was wrapped around a copper wire and rotated inside a Walker-Gerry ablation nozzle. The thorium was ablated with a Nd:YAG laser at a wavelength of 1064 nm at 37.5 mJ to create a plasma at the surface. Then a 0.1% O<sub>2</sub> gas in a 30:70 He:Ne gas mix at approximately 3700 torr was blown over the freshly ablated Th surface and carried over into the resonator. For the <sup>232</sup>Th<sup>17</sup>O and <sup>232</sup>Th<sup>18</sup>O, isotopically enriched <sup>17</sup>O<sub>2</sub> was obtained from Icon Isotopes Ltd with 10% abundance.

## Results

The pure rotational spectra of ThO was observed for the  $J = 1 \leftarrow 0$  transitions shown on Table 27. These were the only transitions able to be recorded due to the frequency limits of the spectrometer. To determine the constants of this molecule, <sup>232</sup>Th<sup>17</sup>O was fit first to determine the rotational constant, nuclear quadrupole coupling constant and nuclear spin-rotation constant. The constant for each vibrational state were determined independently. Then the rotational constant was doubled to give the hypothetical unsplit  $J = 1 \leftarrow 0$  transitions. A Dunham-type, multi-isotopomer, multi-vibrational state fitting routine used the hypothetical unsplit <sup>232</sup>Th<sup>17</sup>O transitional frequencies along with the <sup>232</sup>Th<sup>16</sup>O and <sup>232</sup>Th<sup>18</sup>O data to obtain the  $r_e^{BO}$  and Dunham Parameters. The results are presented in Table 28.<sup>50, 51</sup>

Table 27. Observed Transitions For Isotopologues of ThO

Isotope	V	F'-F''	Frequency (MHz)	Obs-Calc (kHz)
$^{232}\text{Th}^{16}\text{O}$	0		19904.4756	-5.6
	1		19826.2165	-1.2
	2		19747.7977	1.7
	3		19669.2191	3.1
	4		19590.4795	1.8
	5		19511.5778	-3.3
	6		19432.5218	-4.4
	7		19353.3168	3.8
$^{232}\text{Th}^{17}\text{O}$	0	3/2-5/2	18805.3640	
		7/2-5/2	18805.5492	18805.7266 <sup>a</sup> 4.9
		5/2-5/2	18806.1830	
	1	3/2-5/2	18733.5014	
		7/2-5/2	18733.6890	18733.8641 <sup>a</sup> 4.4
		5/2-5/2	18734.3186	
$^{232}\text{Th}^{18}\text{O}$	0		17833.2850	0.4
	1		17766.9301	-3.6
	2		17700.4537	-1.7

<sup>a</sup> represents hypothetical unsplit frequencies.

Table 28. Parameters For Thorium oxide

Parameter	Value
$Y_{01}/\text{MHz}$	9971.7767(35)
$U_{01}/\text{u MHz}$	149242.742(52)
$Y_{11}/\text{MHz}$	-39.05256(26)
$Y_{21}/\text{MHz}$	-0.039573(33)
$\Delta_{01}^0$	-5.970(11)
$eQq(^{17}\text{O}) v = 0/\text{MHz}$	2.827(9)
$eQq(^{17}\text{O}) v = 1/\text{MHz}$	2.815(9)
$c_I(^{17}\text{O}) v = 0/\text{MHz}$	-0.0108(5)
$c_I(^{17}\text{O}) v = 1/\text{MHz}$	-0.0110(5)
$r_e^{\text{BO}}/\text{\AA}$	1.84018613(240)

Numbers in parenthesis indicate one standard deviation in units of the least significant figure.

### Discussion

The  $eQq(^{17}\text{O})$  value of  $^{12}\text{C}^{17}\text{O}$  has been determined to be 4.3205(7) MHz by Beninati. The comparatively small  $eQq(^{17}\text{O})$  for  $^{232}\text{Th}^{17}\text{O}$  suggest that the ThO bond has a higher ionic nature than the CO bond. This is due to the electron donation of the d-orbitals of Th to the p-orbitals of O being more complete than the electron donation of the p-orbitals of C to the

p-orbitals of O. Pyykkö calculated the charge on Th in ThO to be between +0.5 e and +0.7 e, but given the value of  $eQq(^{17}\text{O})$  the charge on the Th should be on the upper end of this prediction or possibly higher than 0.7 e.<sup>60, 64</sup>

## Conclusion

This is the first pure rotational spectroscopic investigation of any actinide containing compound. The constants for the molecule were determined using solely  $J = 1 \leftarrow 0$  transitions, namely the  $eQq(^{17}\text{O})$ ,  $C_I(^{17}\text{O})$ , and  $r_e^{BO}$ .

## CURRENT WORK

### High Frequency System

A high frequency, 75 - 110 GHz, FTMW spectrometer is in the process of being made at the University of North Texas. There are a few advantages to working in the high frequency region for the purpose of looking at molecules with larger rotational constants. Through frequency multiplier chains, the range of the spectrometer is greatly increased. Also, the components are relatively small which removes the need for a large vacuum chamber. Lastly, many molecules have several transitions at higher frequencies.

This instrument was not designed to scan a large spectral region like the chirped pulse FTMW spectrometer, but this is conceivable with a few more components. When this instrument proves to be successful a chirped pulse version could feasibly start being used to identify unknown molecules with a microwave finger print of previously studied molecules. The small size of the components makes the idea of a portable device conceivable. Ultimately, a portable chirped pulse version could be used to perform onsite identification of dangerous or illegal materials.

### Microwave Region

#### *Horns*

Rather than using an antenna which would have to be extremely small, microwave horns were used for this instrument. Also, horns allow the ability to convert the instrument into a chirped pulse technique later. The horns used in this instrument are A-Info standard gain horn antenna with a 25 dB gain in the 75 – 110 GHz region. To keep the circuit components outside the vacuum chamber the horns are placed flush with Teflon windows on the vacuum chamber. A



new chamber is in the process of being made which is much smaller and has Teflon sides to allow the addition of two high frequency mirrors to be used to increase the path length.

### Nozzle

A Series 9, Parker Hannifin solenoid valve was used. A perpendicular orientation proved to be unsuccessful, while a parallel orientation seemed cumbersome given the small size of the Teflon window for the preliminary test. A slightly off parallel orientation, approximately  $35^\circ$ , showed success. A new Teflon window has been constructed for the Balle-Flygare spectrometer's vacuum chamber, which is shown on Figure 33.

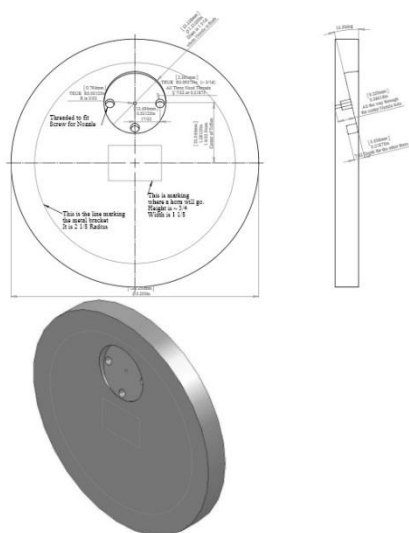


Figure 33. Sketch of the Teflon window constructed for the high frequency FTMW.

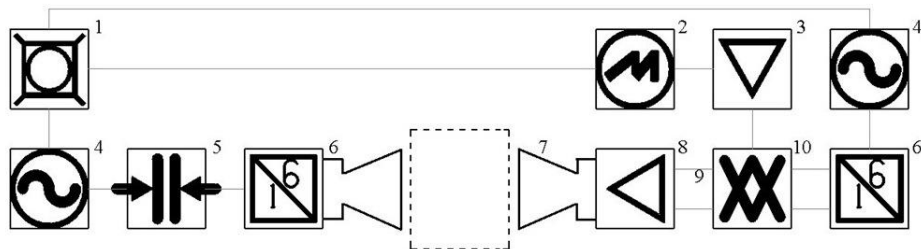
### Vacuum System

Currently, the high frequency FTMW uses the same vacuum chamber as the ELF-FTMW and has the same diffusion and rotatory pumps.

### Circuit

The current circuit is designed to work only in a frequency span of 1-5 MHz per spectral scan. Past experiments proved the components of this instrument can easily over heat while under vacuum, so the entire circuit is outside the vacuum chamber.

80-120 GHz













1	10 MHz Source		SRS FS725 Rubidium Frequency Standard	6	6x Multiplier		Millitech (75 - 110 GHz)
2	Oscilloscope		Tektronix TDS 6124C	7	High Frequency Antenna Horns		A INFOMW JXTXLB-10-25 (gain 25 dB, 75 - 110 GHz)
3	Low Noise Amplifier		Miteq AMF-6F-00100400 (gain 65 dB, noise figure 1.0 dB)	8	High Frequency Low Noise Amplifier		Spacek Labs SLW-15-5 (gain 20dB, 75 - 110 GHz, noise figure 4.5dB)
4	MW Synthesizer		HP 8341A	9	High Frequency Waveguide		10Wal-25
5	SPST Switch		ATM S1517D	10	High Frequency Mixer		Spacek Labs ME-15

Figure 34. Circuit Diagram of the high frequency FTMW spectrometer. The dashed square represents the vacuum chamber. The double lines between components represent waveguide (component 9).

### *Microwave Synthesizer*

Two microwave synthesizers were used in this experiment, HP 8341A. Each had its signal multiplied by a 6x multiplier chain to reach the frequency region required. One was used to create the proper frequency for the molecular transition while the other was used to mix the receiving signal down into the range of the oscilloscope. Typically, the mixing down synthesizer was offset by about 80 MHz below the other synthesizer before multiplication.

### *Oscilloscope*

For this instrument a Tektronix TDS 6124C was used. Due to the oscilloscope being unable to operate in the range of 80 – 120 GHz the signal had to be mixed down below 12 GHz. The offset of the synthesizer was normally around 80 MHz, making the observed transitions come in around 480 MHz.

## Results

### *Carbonyl Sulfide*

To test the high frequency FTMW spectrometer, carbonyl sulfide was chosen due to it being a standard in calibrating microwave spectrometers. Table 29 shows the 3 transitions observed and Figure 35 shows the spectrum of the  $J = 7 \leftarrow 6$  transition.

Table 29. Observed Transitions of OCS Using The High Frequency FTMW

Transition	Frequency / MHz
$7 \leftarrow 6$	85139.0954 (40)
$8 \leftarrow 7$	97301.2109 (40)
$9 \leftarrow 8$	109463.1105 (60)

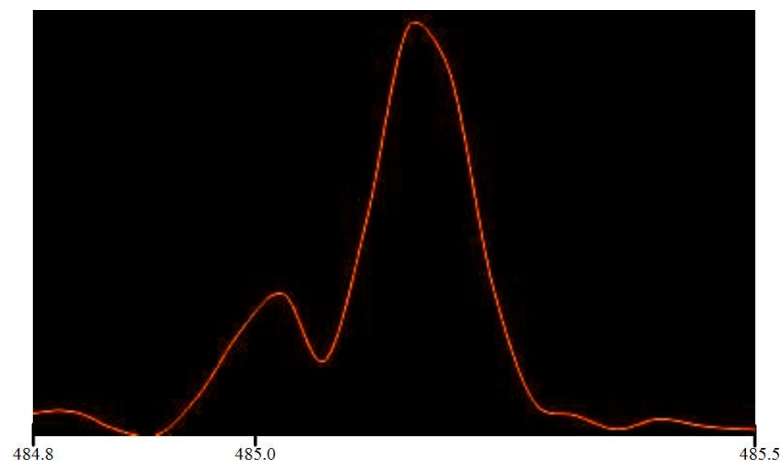


Figure 35. Spectrum of OCS transition of  $J = 7 \leftarrow 6$  transition. The emitting synthesizer was set to 14189.82 MHz while the mixing synthesizer was set to 14109.0 MHz, both prior to the 6x multiplication. The small peak on the left is at 485.0212 MHz and the peak on the right is at 485.1697 MHz.

## CONCLUSION

My research at the University of North Texas has led to the successful construction of several instruments that have helped expand the field of microwave spectroscopy.

### The Classic Balle-Flygare FTMW Spectrometer

The classic Balle-Flygare FTMW spectrometer is modeled after Grabow's COBRA model with two unique differences. The instrument uses two separate antenna sets and two low noise amplifiers to operate in the entire frequency region of 6-26 GHz without having to break vacuum or having to change the components in the circuit. Also, the low noise amplifiers are placed inside the vacuum chamber to allow the receiving signal to be amplified as soon as physically possible to reduce signal loss. This instrument exhibits great sensitivity and yields highly resolved spectra.

### ELF-FTMW Spectrometer

The ELF-FTMW ventured into new territory with the use of highly curved mirrors to contain the beam waist allowing it to become a stable resonator even at low frequencies. This instrument observed the lowest frequency transition of an FTMW spectrometer of 562 MHz. During the instrument's time of operation, further improvements have been made. It was discovered that the signal to noise ratio could be improved by lowering the voltage of the low noise amplifier below its rated value. Another improvement I made to this instrument is a new antenna design that allows the spectra of 1 – 22 GHz to be observed without opening the chamber to air in order to switch classic "L" shaped antennas. The instrument's ability to observe low frequency transitions is essential for increasing the precision of hyperfine structure measurements and studying larger molecular systems.

## Chirped Pulse FTMW Spectrometer

The chirped pulse FTMW spectrometer is able to observe spectra that span 2 GHz versus the standard 1 MHz of a cavity technique. This instrument not only decreases the amount of time to obtain a large spectral region of molecular transitions, but it also gives the correct relative intensities of observable transitions. This instrument's abilities greatly aid in obtaining a good spectra to produce a fit quickly for a molecule.

## Laser Ablation Apparatus

The laser ablation apparatus uses a Nd:YAG laser and Walker-Gerry nozzle head to successfully look at heavy metal containing molecules. This component has been able to work in conjunction with the classic Balle-Flygare FTMW and the chirped pulse FTMW spectrometers. It has allowed microwave spectroscopy studies to be done on a new series of molecules.

## Molecules

The instruments I constructed and the techniques I used have allowed the discovery of further insights into molecular chemistry. I have seen the effects of fluorinating an alkyl halide by determining the geometry of the carbon backbone of trans-1-iodoperfluoropropane and observed the effects of a strong quadrupole coupling constant on a heavy molecule by observing a  $\Delta J = 3$  forbidden transition. The quadrupole coupling tensors of butyronitrile, a molecule observed in space, have been improved. The nuclear quadrupole coupling tensor of difluoroiodomethane was added to a list of variably fluorinated methyl halides where the trend of a decreasing magnitude of  $\chi_{zz}$  for  $X\text{-CF}_3 > X\text{-CH}_3 > X\text{-CHF}_2 > \text{CH}_2\text{F}$  was upheld. The study of SrS led to an improvement in determining the SrS internuclear distance as well the determination of the Born-Oppenheimer breakdown terms. I have also conducted the first pure rotational spectroscopic investigation of an actinide containing molecule, ThO.

## WORKS CITED

1. Cleeton, C. E.; Williams, N. H. Electromagnetic Waves of 1.1 cm Wave-Length and The Absorption Spectrum of Ammonia. *Phys. Rev.* **1934**, *45*, 234-237.
2. Fabry, C.; Pérot, A. On A New Form Of Interferometer. *Astrophysical Journal* **1901**, *13*, 265-273.
3. Balle, T. J.; Campbell, E. J.; Keenan, M. R.; Flygare, W. H. A New Method For Observing The Rotational Spectra of Weak Molecular Complexes: KrHCl. *J. Chem. Phys.* **1979**, *71*, 2723-2724.
4. Balle, T. J.; Flygare, W. H. Fabry-Perót Cavity Pulsed Fourier Transform Microwave Spectrometer with a Pulsed Nozzle Particle Source. *Rev. Sci. Instrum.* **1981**, 33-45.
5. Suenram, R. D.; Lovas, F. J.; Matsumura, K. Laboratory Measurement of The 101-000 Transition and Electric Dipole Moment of SiCl<sub>2</sub>. *Astrophys. J. L.* **1989**, *342*, 103-105.
6. Townes, C. H.; Schawlow, A. L. *Microwave Spectroscopy*; Dover Publications: NY, 1955.
7. Herzberg, L.; Herzberg, G. In *Molecular Spectra: In Fundamental Formula's of Physics*, 2 ed.; Menzel, D., Ed.; Dover Publications: NY, 1960; Vol. 2, 465-479.
8. Campbell, E. J.; Buxton, L. W.; Balle, T. J.; Keenan, M. R.; Flygare, W. H. The Gas Dynamics of a Pulsed Supersonic Nozzle Molecular Source as Observed with a Fabry-Perot Cavity Microwave Spectrometer. *J. Chem. Phys.* **1981**, *74*, 829-840.
9. Self, S. A. Focusing of Spherical Gaussian Beams. *Appl. Opt.* **1983**, *22*, 658-661.
10. Ishii, T. K. *Handbook of Microwave Technology: Components and Devices*; Academic Press: CA, 1995; Vol. 2.
11. Hansen, J. E. In *Spherical Near-field Antenna Measurements*; Pergrinus, P., Ed.; London, England, 1988.
12. Etchison, K. C.; Dewberry, C. T.; Kerr, K. E.; Shoup, D. W.; Cooke, S. A. A Fabry-Perót Type Resonator Tunable Below 2 GHz for Use in Time Domain Rotational Spectroscopy: Application to the Measurement of the Radio Frequency Spectra of Bromobenzene and Iodobenzene. *J. Mol. Spec.* **2007**, *242*, 39-45.
13. Grabow, J. U.; Stahl, W.; Dreizler, H. A Multioctave Coaxially Oriented Beam-Resonator Arrangement Fourier-transform Microwave Spectrometer. *Rev. Sci. Instrum.* **1996**, *67*, 4072-4084.
14. Arunan, E.; Emilsson, T.; Gutowsky, H. S. Rotational Spectra and Structures of Rg-C<sub>6</sub>H<sub>6</sub>-H<sub>2</sub>O Trimers and the Ne-C<sub>6</sub>H<sub>6</sub> Dimer (Rg=Ne, Ar, or Kr). *J. Chem. Phys.* **1994**, *101*, 861.

15. Storm, V.; Dreizler, H.; Consalvo, D.; Grabow, J.; Merke, I. A Newly Designed Molecular Beam Fourier Transform Microwave Spectrometer in the Range of 1-4 GHz. *Rev. Sci. Instrum.* **1996**, *67*, 2714-2719.
16. Sarkozy, L.; Kukolich, S. G. *Construction and Development of a New Low-Frequency Fourier Transform Spectrometer for Operation in the 1-6 GHz Range*, Columbus, Oh, 2010; TC06.
17. Best, S. R. *Electrically Small Antennas*, Vye D. Ed., 2009; <http://event.on24.com>.
18. Dewberry, C. T.; Grubbs II, G. S.; Raphelt, A.; Cooke, S. A. *Measurement of Nitrogen Hyperfine Structure on The 53 cm 562 MHz Butyronitrile Line*, Columbus, OH, 2009; MH13.
19. Brown, G. G.; Dian, B. C.; Douglass, K. O.; Geyer, S. M.; Pate, B. P. The Rotational Spectrum of Epifluorohydrin Measured by Chirped-Pulse Fourier Transform Microwave Spectroscopy. *J. Mol. Spec.* **2006**, No. 238, 200-212.
20. Fox, M. *Optical Properties of Solids*, 2nd ed.; Oxford University Press Inc.: Oxford, NY, 2010; 257-259.
21. Koechner, W. *Solid-State Laser Engineering*, 6th ed.; Springer Science+Business Media, Inc.: New York, NY, 2006; 522-529.
22. Dewberry, C. T.; Grubbs, G. S.; Cooke, S. A. A Molecule with Small Rotational Constants Containing an Atom with a Large Nuclear Quadrupole Moment: The Microwave Spectrum of Trans-1-iodoperfluoropropane. *J. Mol. Spec.* **2009**, No. 257, 66-73.
23. Javan, A. Theory of a Three-Level Maser. *Phys. Rev.* **1957**, *107*, 1579-1589.
24. Oka, T. Observation of  $\Delta J = 3$  'Forbidden' Transition in Ethyl Iodide by The Use of Double Resonance. *J. Chem. Phys.* **1966**, *45*, 752-753.
25. Fujitake, M.; Hayashi, M. Microwave Spectrum of 1-Iodopropane: The Observation of The Forbidden Transitions. *J. Mol. Spec.* **1988**, *127*, 112-124.
26. Wlodarczak, G.; Boucher, D.; Bocquet, R.; Demaison, J. The Rotational Constants of Methyl Iodide. *J. Mol. Spec.* **1987**, *124*, 53-65.
27. Boucher, D.; Dubrulle, A.; Demaison, J. Microwave Spectrum of Ethyl Iodide: Nuclear Quadrupole Interaction and Centrifugal Distortion Analysis. *J. Mol. Spectrosc.* **1980**, *84*, 375-387.
28. Cox, A. P.; Duxbury, G.; Hardy, J. A.; Kawashima, Y. Microwave Spectra of CF<sub>3</sub>Br and CF<sub>3</sub>I. *J. Chem. Soc. Farad. Soc II* **1980**, *76*, 339-350.
29. Grubbs, G. S.; Cooke, S. A. Chirped-Pulse Fourier Transform Microwave Spectroscopy of Perfluoroiodoethane. *J. Mol. Spec.* **2010**, No. 963, 87-91.

30. Kraitchman, J. Determination of Molecular Structure From Microwave Spectroscopic Data. *Am. J. Phys.* **1953**, *21*, 17-24.
31. Pickett, H. M. The Fitting and Prediction of Vibration-Rotation Spectra with Spin Interactions. *J. Mol. Spec.* **1991**, *148*, 371-377.
32. Belloche, A.; Garrod, R. T.; Muller, H. P.; Menten, K. M.; Comito, C.; Schilke, P. Increased Complexity in Interstellar Chemistry: Detection and Chemical Modeling of Ethyl Formate and n-Propyl Cyanide in Sagittarius B2(N). *A&A* **2009**, No. 499, 215-232.
33. Vormann, K.; Dreizler, H. Microwave Spectrum of Butyronitrile: Methyl Internal Rotation and  $^{14}\text{N}$  Quadrupole Coupling. *Z. Naturforsch* **1988**, No. 43a, 338-344.
34. Demaison, J.; Dreizler, H. Quadrupole Coupling in Butyronitrile: An Application of Microwave Fourier Transform Spectroscopy. *Z. Naturforsch* **1982**, No. 37a, 199-200.
35. Dewberry, C. T.; Kisiel, Z.; Cooke, S. A. The Pure Rotational Spectrum of Difluoriodomethane,  $\text{CHF}_2\text{I}$ . *J. Mol. Spec.* **2010**, No. 261, 82-86.
36. Gordy, W.; Cook, R. L. *Microwave Molecular Spectra, Techniques of Chemistry*; John Wiley and Sons: NY, 1984; Vol. XVII.
37. Kukolich, S. G.; Nelson, A. C. Chlorine Quadrupole Coupling in Methyl Chloride: Variation of Quadrupole Coupling Strength with Isotopic Substitution. *J. Am. Chem. Soc.* **1973**, *95*, 680-682.
38. Carocci, S.; Minguzzi, P.; Tonelli, M.; Di Lieto, A. The Electric Dipole and The Nuclear Quadrupole Moment of Methyl Bromide in The Ground Vibrational State. *J. Mol. Spec.* **1993**, *160*, 359-370.
39. Blanco, S.; Lesarri, A.; Lopez, J. C.; Alonso, J. L.; Guarnieri, A. The Rotational Spectrum of Chlorofluoromethane. *J. Mol. Spec.* **1995**, *174*, 397-416.
40. Cazzoli, G.; Puzzarini, C.; Stopkowicz, S.; Gauss, J. The Hyperfine Structure in The Rotational Spectra of Bromofluoromethane: Lamb-dip Technique and Quantum-chemical Calculations. *Mol. Phys.* **2008**, *106*, 1181-1192.
41. Puzzarini, C.; Cazzoli, G.; Lopez, J. C.; Alonso, J. L.; Baldacci, A.; Baldan, A.; Stopkowicz, S.; Cheng, L.; Gauss, J. Spectroscopic Investigation of Fluoriodomethane,  $\text{CH}_2\text{FI}$ : Fourier-Transform Microwave and Millimeter-/Submillimeter-Wave Spectroscopy and Quantum-Chemical Calculations. *J. Chem. Phys.* **2011**, *134*, 174312-174321.
42. Cramb, D. T.; Bos, Y.; Jemson, H. M.; Gerry, M. C. The Microwave Spectrum, Harmonic Force Field and Structure of Chlorodifluoromethane,  $\text{CHF}_2\text{Cl}$ . *J. Mol. Struct.* **1988**, *190*, 387-400.
43. Ogata, T.; Kuwano, S.; Oe, S. Microwave Spectrum, Nuclear Quadrupole Coupling Constants, and Structure of Bromodifluoromethane. *J. Mol. Spec.* **1997**, *185*, 147-152.



44. Carpenter, J. H.; Muse, J. D.; Small, C. E.; Smith, J. G. The Millimeter-Wave Spectrum of CF<sub>3</sub>Cl. *J. Mol. Spec.* **1982**, *93*, 286-306.
45. Harder, H.; Nicolaisen, H. W.; Dreizler, H.; Mader, H. Quadrupole Transitions in CF<sub>3</sub>Br Investigated by Two-Dimensional Fourier Transform Spectroscopy in The Microwave-Radiofrequency Range. *J. Mol. Spec.* **1993**, *160*, 244-252.
46. Walters, S. W.; Whiffen, D. H. Rotational Spectrum of Trifluoriodomethane. *J. Chem. Soc. Faraday Trans. II* **1983**, *79*, 941-949.
47. Etchison, K. C.; Dewberry, C. T.; Cooke, S. A. Born-Oppenheimer Breakdown Effects and Hyperfine Structure in The Rotational Spectrum of Strontium Monosulfide, SrS. *Chem. Phys.* **2007**, *342*, 71-77.
48. Pianalto, F. S.; Brazier, C. R.; O'Brian, L. C.; Bernath, P. F. Rotational Analysis of The A 1 Sigma<sup>+</sup>-X 1 Sigma<sup>+</sup> Transition of SrS. *J. Mol. Spec.* **1988**, *132*, 80-88.
49. Halfen, D. T.; Apponi, A. J.; Thompsen, J. M.; Ziurys, L. M. The Pure Rotational Spectra of SrSH X~2A' and SrS X 1 Sigma<sup>+</sup>: Further Studies in Alkaline-Earth Bonding . *J. Chem. Phys.* **2001**, *115*, 11131-11138.
50. Dunham, J. L. The Energy Levels of a Rotating Vibrator. *Phys. Rev.* **1932**, *41*, 721-731.
51. Watson, J. G. The Isotope Dependence of Diatomic Dunhama Coefficients. *J. Mol. Spectrosc.* **1980**, *80*, 411-421.
52. Watson, J. G. The Isotope Dependence of The Equilibrium Rotational Constants in 1 Sigma States of Diatomic Molecules. *J. Mol. Spec.* **1973**, *45*, 99-113.
53. Bunker, P. R. The Rigid Bender and Semirigid Bender Models for The Rotation-vibration Hamiltonian. *J. Mol. Spec.* **1977**, *67*, 374-385.
54. Kratzer, A. Die Ultraroten Rotationsspektren Der Halogenwasserstoffe. *Z. Phys.* **1920**, *3*, 289-307.
55. Pekeris, C. L. The Rotation-Vibration Coupling in Diatomic Molecules. *Phys. Rev.* **1934**, *45*, 98-103.
56. Blom, C. E.; Hedderich, H. G.; Lovas, F. J.; Suenram, R. D.; Maki, A. G. Infrared and Microwave Spectra of SrO and BaO. *J. Mol. Spec.* **1992**, *152*, 109-118.
57. Dewberry, C. T.; Etchison, K. C.; Cooke, S. A. The Pure Rotational Spectrum of The Actinide-Containing Compound Thorium Monoxide. *Phys. Chem. Chem. Phys.* **2007**, *9*, 4895-4897.
58. Edvinsson, G.; Lagerqvist, A. Two New Band Systems in ThO. *Phys. Scr.* **1990**, *41*, 316-320.

59. Kushto, G. P.; Andrews, L. Infrared Spectroscopic and Density Functional Theoretical Investigation of The Reaction Products of Laser-Ablated Zr, Hf, and Th Atoms with Nitric Oxide. *J. Phys. Chem. A*. **1999**, *103*, 4836-4844.
60. Marian, C. M.; Wahlgren, U.; Gropen, O.; Pyykko, P. Bonding and Electronic Structure in Diatomic ThO: Quasirelativistic Effective Core Potential. *J. Mol. Struct.* **1988**, *169*, 339-354.
61. Watanabe, Y.; Matsuoka, O. All-electron Dirac-Fock-Roothaan Calculations for The ThO Molecule. *J. Chem. Phys.* **1997**, *107*, 3738-3739.
62. Watanabe, Y.; Matsuoka, O. Four-Component Relativistic Configuration-Interaction Calculation Using The Reduced Frozen-Core Approximation. *J. Chem. Phys.* **2002**, *116*, 9585-9590.
63. Paulovic, J.; Nakajima, T.; Hirao, K.; Seijo, L. Third-order Douglas-Kroll Ab Initio Model Potential for Actinide Elements. *J. Chem. Phys.* **2002**, *117*, 3597-3604.
64. Cazzoli, G.; Dore, L.; Puzzarini, C.; Beninati, S. Millimeter- and Submillimeter-wave Spectrum of C17O Rotational Hyperfine Structure Analyzed Using the Lamb-dip Technique. *Phys. Chem. Chem. Phys.* **2002**, *4*, 3575-3577.
65. Mellish, R. G.; Dennis, R. B.; Allwood, R. L. Investigation of Parameters Controlling Stimulated Raman Scattering in InSb Around 5  $\mu\text{m}$ . *Opt. Comm.* **1971**, *4*, 249-254.
66. Wright, N.; Randall, H. M. The Far Infrared Absorption of Ammonia and Phosphine Gases Under High Resolving Power. *Phys. Rev.* **1933**, *44*, 391-398.